

MODELING OF VERTICAL GROUND LOOP HEAT
EXCHANGERS FOR GROUND SOURCE
HEAT PUMP SYSTEMS

By

CENK YAVUZTURK

Diplom Ingenieur

Technical University of Berlin

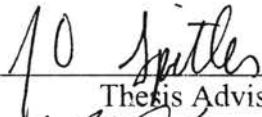
Berlin, Germany

1988

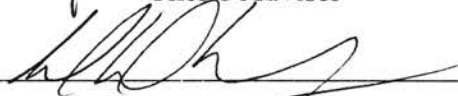
Submitted to the Faculty of the
Graduate College of the
Oklahoma State University
in partial fulfillment of
the requirements for
the Degree of
DOCTOR OF PHILOSOPHY
December, 1999

MODELING OF VERTICAL GROUND LOOP HEAT
EXCHANGERS FOR GROUND SOURCE
HEAT PUMP SYSTEMS

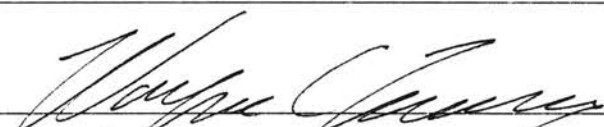
Thesis Approved:

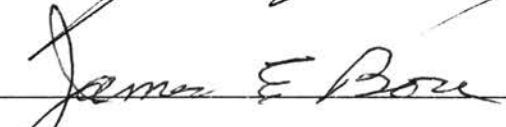


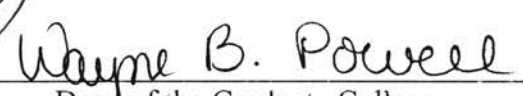
Thesis Adviser











Wayne B. Powell.
Dean of the Graduate College

PREFACE

The ability to predict both the long-term and short-term behavior of ground loop heat exchangers is critical to the design and energy analysis of ground source heat pump systems. For detailed analysis and accurate simulation of the transient heat transfer in vertical ground loop heat exchangers, a numerical model is developed. The model is based on the two-dimensional, fully implicit finite volume formulation and utilizes an automated parametric grid generation algorithm for different pipe sizes, shank spacing and borehole geometry. The numerical method and grid generation techniques have been validated against an analytical model. The numerical model has been developed with two main purposes in mind. The first application is the calculation of non-dimensional temperature response factors for short time scales that can be used in building simulation. The second application is use in a parameter estimation technique used to predict borehole ground formation thermal properties from short time scale test data.

The short-term behavior of ground-coupled heat pump systems is important for the design of ground loop heat exchangers, the energy analysis of ground source heat pump systems, and the design of hybrid ground source systems. Using short time-step response factors, a direct evaluation of system energy consumption and electrical demand in hourly or shorter time intervals becomes possible since a detailed assessment of the ground heat exchanger behavior on an hour-by-hour basis can be performed. This is

important especially when dealing with strong short time-step system fluctuations due to building dynamics and for commercial buildings that have time-of-day electricity rates. The short time-step model is cast as a TRNSYS component model and validated using actual operating field data from an elementary school building located in Lincoln, Nebraska.

Furthermore, a short time-step ground loop heat exchanger model is crucial for analysis of hybrid ground source heat pump systems. Ground source heat pumps for cooling-dominated commercial buildings utilize supplemental heat rejecters such as cooling towers, fluid coolers or surface heat rejecters to reduce system first cost and to improve system performance. The use of supplemental heat rejecters for cooling dominated buildings allows the design of smaller borehole fields. Heat pump performance degradation is avoided by offsetting the annual load imbalance in the borefield and the resulting long-term temperature rise. Utilizing the short time-step model, a parametric study is presented to investigate the advantages and the disadvantages of various system operating and control strategies in a hybrid ground source heat pump application under different climate conditions. An actual office building located in Stillwater, Oklahoma is used as the example building. A preliminary life cycle cost analysis is conducted to compare each operating and control strategy to determine the lowest cost alternative for a given climate.

The numerical model is also used as part of parameter estimation algorithm that is developed to predict borehole ground formation thermal properties from short time scale

test data. Determination of the ground's thermal conductivity is a significant challenge facing designers of Ground Source Heat Pump (GSHP) systems applied in commercial buildings. The number of boreholes and the depth and cost of each borehole are highly dependent on the ground thermal properties. Hence, depending on the geographic location and the local drilling costs, the ground thermal properties strongly influence the initial cost to install a GSHP system. In order to be able to predict ground thermal properties, a parameter estimation technique is employed that minimizes the sum of the squares error between experimentally measured temperature responses and the temperature predictions of the numerical model. An experimental apparatus has been built capable of imposing a heat flux on a test borehole, and measuring its temperature response. The downhill simplex method of Nelder and Mead (1969) in conjunction with the two-dimensional numerical model is used to determine the thermal conductivity of the surrounding ground. In order to validate the procedure, independent measurements of the soil conductivity test results are reported for several test boreholes and a laboratory experiment. A detailed uncertainty analysis of the thermal conductivity prediction is conducted to assess the impact of uncertainty of a series of input parameters.

ACKNOWLEDGEMENTS

I would like to thank my daughter, Eda, for being such a good and understanding girl, day in and day out throughout the years of this research. I know that a lot of this work would not have been possible without her love, quiet smile and her big ‘I missed you daddy’-hugs.

I would like to extend my sincere gratitude and appreciation to my adviser, Dr. Jeffrey D. Spitler, for his continuous support, leadership, constructive guidance, and friendship. I consider myself very fortunate to have had the opportunity to work with a teacher and friend like Dr. Spitler. It was his inspiration, integrity and undying understanding that got many things this far.

My sincere appreciation also extends to the members of my doctoral committee, Drs. Simon J. Rees, James E. Bose, Ronald D. Delahoussaye, Ronald L. Dougherty and Wayne C. Turner for their committed service and support, their ideas, and suggestions that helped improve my work significantly.

Dr. Marvin Smith, Professor in the Division of Engineering Technology at the Oklahoma State University graciously provided experimental data from borehole sample measurements that are used extensively throughout this work. Warren A. Austin III,

currently staff mechanical engineer with EMC Engineers in Denver, CO, designed and fabricated the experimental apparatus and collected experimental data at various test sites. Randy Perry, Development Engineer, with the Division of Engineering Technology provided expert assistance on portions of the design and fabrication.

I would also like to thank to Andrew D. Chiasson for the long hours of discussions, his valuable ideas and suggestions to improve this work.

Support of the U.S. Department of Energy under grant numbers DE-FG48-94R689416 and DE-FG48-97R810627, and of the National Rural Electric Cooperative Association (NRECA) under research project RER 95-6 for various parts of this project is gratefully acknowledged.

Support from ASHRAE in the form of a grant-in-aid during 1996-1997 is also gratefully acknowledged.

TABLE OF CONTENTS

Chapter	Page
1. INTRODUCTION	1
2. BACKGROUND AND LITERATURE REVIEW	8
2.1 Existing Design and Simulation Tools for Ground Loop Heat Exchangers- Analytical	8
2.1.1. Ingersoll’s Approach.....	10
2.1.2. Hart and Couvillion Approach.....	13
2.1.3. IGSHPA Approach	17
2.1.4. Kavanaugh’s Approach.....	21
2.2. Existing Design and Simulation Tools for Ground Loop Heat Exchangers- Numerical.....	26
2.2.1. Eskilson’s Model	27
2.2.2. Hellstrom’s Model	29
2.2.3. Thornton et al. Implementation of Hellstrom’s Model.....	31
2.2.4. Mei and Emerson Model.....	31
2.2.5. Muraya’s Model.....	32
2.2.6. Rottmayer, Beckman and Mitchell Model.....	32
2.2.7. Shonder and Beck Model.....	33
2.3. Currently Available Methods for the Determination of Thermal Conductivity of Ground Formation	34
2.3.1. Steady State Methods.....	36
2.3.2. Transient Methods	36
3. DEFINITION OF THE PROBLEM AND OBJECTIVES	38
4. TRANSIENT, TWO-DIMENSIONAL NUMERICAL MODEL OF THE VERTICAL GROUND HEAT EXCHANGER	42
4.1. Finite Volume Approach.....	43
4.2. Parametric Grid Generation	46
4.3. Pie-Sector Approximation	47
4.4. Boundary Conditions	49
4.5. Convective Resistance Adjustment.....	51
4.6. Model Validation and Error Analysis.....	53

Chapter	Page
4.6.1. Validation Test Cases	55
4.6.1. Sensitivity to Grid Resolution and Time Step	57
4.7. Discussion of the Results	63
5. SHORT TIME-STEP RESPONSE FACTOR MODEL	66
5.1. Eskilson’s Long Time-Step Temperature Response Factors Model.....	66
5.2. Short Time-Step Temperature Response Factors	70
5.2.1. Development of Short Time-Step g-Functions	70
5.2.2. Aggregation of Ground Loads	74
5.3. Component Model for TRNSYS	82
5.4. Example Application for the Component Model.....	85
5.5. Discussion of the Model Results.....	89
6. SHORT TIME-STEP RESPONSE FACTOR MODEL VALIDATION	90
6.1. Description of the Maxey Elementary School Ground Source Heat Pump System.....	90
6.2. Monitored Field Data.....	91
6.3. Comparison of Model Predictions and Field Data.....	94
6.3.1. Adjustments to Field Data	94
6.3.2. Adjustments to the Short Time Step Component Model.....	95
6.3.3. Short Time Step Model Predictions.....	98
6.4. Sensitivity Analysis	102
6.4.1. Power Consumption Sensitivity Analysis based on Maximum Power Consumption.....	103
6.4.2. Power Consumption Sensitivity Analysis based on Total Error in Power Consumption for the Best and Worst Prediction Months.....	105
6.5. Discussion of Model Validation	106
7. EXAMPLE APPLICATION USING A HYBRID GROUND SOURCE SYSTEM ..	109
7.1. Background on Hybrid Ground Source Heat Pump Systems	109
7.2. Review of Literature	112
7.3. Supplemental Heat Rejection.....	117
7.4. Hybrid System Operation Using the Short Time-Step Simulation Model ...	118
7.4.1. Example Hybrid System Description.....	118
7.4.2. Climatic Considerations-Building Loads.....	119
7.4.3. Hybrid System Component Configuration	121
7.4.4. Ground Loop Heat Exchanger and Cooling Tower Sizing	122
7.4.5. Operating and Control Strategies.....	124
7.4.5.1. Base Case-Optimum Design of the Borefield without Supplemental Heat Rejection.....	127

Chapter	Page
7.4.5.2. Case 2-Undersized Design of the Borefield without Supplemental Heat Rejection.....	131
7.4.5.3. Set Point Control for the Heat Pump Entering and Exiting Fluid Temperatures	134
7.4.5.4. Differential Control for the Heat Pump Entering and Exiting Fluid Temperatures	137
7.4.5.5. Scheduled Recharge of the Borefield	144
7.5. Comparison of Control Strategies - Hybrid System Installation and Operating Cost Analysis	149
7.6. Discussion of the Results	155
8. MEASUREMENT OF GROUND’S THERMAL CONDUCTIVITY USING PARAMETER ESTIMATION TECHNIQUES.....	160
8.1. Description of Experimental Apparatus.....	162
8.2. Objective Function.....	165
8.3. Nelder Mead Simplex Optimization	168
8.4. Procedure Validation	172
8.4.1. Cored Borehole	173
8.4.2. Medium-Scale Laboratory Experiment.....	175
8.5. Overview of the Parameter Estimation Results	176
8.6. Sensitivity and Error Analysis	181
8.6.1. Length of In-Situ Testing.....	184
8.6.2. Undisturbed Far-Field Ground Temperature	188
8.6.3. U-Tube Shank Spacing	190
8.6.4. Volumetric Specific Heat of Ground Formation	192
8.6.5. Power Input and Temperature Calibration.....	195
8.6.6. Borehole Geometry	197
8.7. Discussion	199
9. SUMMARY.....	204
BIBLIOGRAPHY	208
APPENDIX A – Discussion of Cooling Tower Sizing Procedure	226

LIST OF TABLES

Table	Page
4.1. Input Data Varied for Model Validation Test Cases	56
4.2. Input Data common to all Validation Test Cases	56
4.3. Relative Error (%) between the Analytical and Numerical Results for each Test Case at 1 and 192 hours Simulated Time (3-min. time steps)	58
6.1 Comparison of Total Error on Maxey Elementary School Power Consumption for the Months August and December 1996.....	106
7.1. System Simulation Summary for Base Case	130
7.2. System Simulation Summary for Case 2	133
7.3. Hybrid System Simulation Summary for Control Strategy 3a	135
7.4. Hybrid System Simulation Summary for Control Strategy 3b	136
7.5. Hybrid System Simulation Summary for Control Strategy 4a	140
7.6. Hybrid System Simulation Summary for Control Strategy 4b	141
7.7. Hybrid System Simulation Summary for Control Strategy 4c	142
7.8. Hybrid System Simulation Summary for Control Strategy 5a	145
7.9. Hybrid System Simulation Summary for Control Strategy 5b	148
7.10. Hybrid System Simulation Summary for Control Strategy 5c	149
7.11. Cost Analysis Summary for each Control Strategy for Houston, TX.....	153
7.12. Cost Analysis Summary for each Control Strategy for Tulsa, OK.....	154

Table	Page
8.1. Thermal Conductivity Estimation for the Cored Borehole and the Simulated Borehole Configuration	179
8.2. Thermal Conductivity Estimations and Associated Errors from the Converged Value for the Okla. State University Site A#1, #1 and Chickasha Test Boreholes.....	186
8.3. Change in Ground Thermal Conductivity BTU/hr-ft-°F (W/m-K) Estimations Based on Changes in Power Input and Temperature Measurements	196
8.4. Summary of Primary Sources of Uncertainties in the Estimation of Thermal Conductivity of the Ground	200

LIST OF FIGURES

Figure	Page
1.1. Schematic of a Typical Vertical Closed-Loop, Ground-Coupled heat Pump System ..3	
2.1. Top View Cross-Section of a Typical Borehole9	
3.1. Objectives41	
4.1. Simplified Representation of the Borehole Region on the Numerical Model Domain using the Pie-Sector Approximation for the U-Tube Pipes42	
4.2. Notation of the Finite Control Volumes44	
4.3. Example Numerical Grid near the Borehole Center47	
4.4. The Pie-Sector Representation of the U-Tube Pipe48	
4.5. Variation of the Relative Error of the Calculated Temperature with Different Grid Resolution at the Pipe Wall (for Test Case #4 with 3-minute Time steps).....58	
4.6. Variation in the Relative Error of the Calculated Temperature with Time Step (Test case #4)59	
4.7. Variation in the Relative Error of the Calculated Temperature with Pie-Sector Position (Test case #4)61	
4.8. Comparison of the Numerical and Analytical Model Temperature Predictions. Test Case #4. Pipe Wall Thickness Approximated with Four Cells. Time Step = 3 minutes ..62	
4.9. Comparison of the Numerical and Analytical Model Temperature Predictions over the First Hour of Simulation. (Test Case #4).....63	

Figure	Page
5.1. Superposition of Piece-Wise Linear Step Heat Inputs in Time. The Step Heat Inputs Q2, Q3, and Q4 are Superimposed in Time on the Basic Heat Pulse Q1	67
5.2. Temperature Response Factors (g-Functions) for Various Multiple Borehole Configurations Compared to the Temperature Response Curve for a Single Borehole	69
5.3. Short Time Step g-Function Curve as an Extension of the Long Time Step g-Functions Plotted for a Single Borehole and 8X8 Borehole Field.....	73
5.4. Comparison of temperature responses based on hourly loads with temperature responses obtained through load aggregation for first week average and first month average loads for a typical Case.....	76
5.5. Hourly history versus aggregated history for a typical case	78
5.6. Comparison of the error in predicted exiting temperatures for various minimum hourly history periods	80
5.7. TRNSYS short time-step component model configuration.....	84
5.8. Annual hourly building load profile for the example building in Tulsa.....	86
5.9. Hourly average borehole temperature profile for the example building in Tulsa, Oklahoma as a result of an annual simulation with TRNSYS.....	87
5.10. Hourly input and output temperatures to the ground during the month of January for the example building in Tulsa, Oklahoma.....	88
5.11. Hourly input and output temperatures to the ground during the month of July for the example building in Tulsa, Oklahoma.....	88
6.1. Heat pump entering fluid temperatures from 12:00am 1/1/1996 to 11:55pm 12/31/1996 plotted hourly.....	92

Figure	Page
6.2. Heat transfer fluid flow rate 12:00am 1/1/1996 to 11:55pm 12/31/1996 plotted hourly (processed to remove flow rates below 50gpm)	92
6.3. Comparison of hourly heat pump entering fluid temperatures. Predicted versus experimental for the month of January 1996	99
6.4. Comparison of hourly heat pump entering fluid temperatures. Predicted versus experimental for the month of March 1996	100
6.5. Comparison of hourly heat pump entering fluid temperatures. Predicted versus experimental for the month of August 1996	100
6.6. Comparison of hourly heat pump entering fluid temperatures. Predicted versus experimental for the month of October 1996.....	101
6.7. Comparison of hourly heat pump entering fluid temperatures. Predicted versus experimental for the month of November 1996.....	101
6.8. Comparison of hourly heat pump entering fluid temperatures. Predicted versus experimental for the month of December 1996	102
6.9. Comparison of hourly heat pump power consumption for the month of August 1996, considering predicted and actual heat pump EFT	104
6.10. Comparison of hourly heat pump power consumption for the month of December 1996, considering predicted and actual heat pump EFT	104
7.1. Annual hourly building loads considering Houston, TX and Tulsa, OK typical climatic conditions	120
7.2. Hybrid ground source heat pump system component configuration diagram	121

Figure	Page
7.3. Hourly entering fluid temperatures to the heat pump considering Houston, TX, and Tulsa, OK typical climatic conditions. Base Case	129
7.4. Hourly entering fluid temperatures to the heat pump for typical Houston, TX and Tulsa, OK climatic conditions. Case 2.....	132
7.5. Hourly entering fluid temperatures to the heat pump and heat rejection in the cooling tower for typical Houston, TX climatic conditions. 2-year simulation - Case 3a	137
7.6. Hourly entering fluid temperatures to the heat pump and heat rejection in the cooling tower for typical Houston, TX climatic conditions. 2-year simulation - Case 4c	143
7.7. Hourly entering fluid temperatures to the heat pump for typical Houston, TX climatic conditions. 20 year simulation - Case 4c	144
7.8. Hourly heat pump entering fluid temperature and heat rejection in the cooling tower for Houston, TX typical weather conditions and using control strategy 5a for the first two years of simulation.....	147
7.9. Cooling tower size required for each control strategy	152
8.1. In-situ thermal conductivity test system schematic	164
8.2. Information flow diagram for the parameter estimation algorithm	171
8.3. Thermal conductivity vs. the cored borehole depth based on the guarded hot plate core experiments for Oklahoma State University site A #6 borehole	174
8.4. Comparison of in-situ experimental temperatures to predicted temperatures using the numerical function evaluation model based on the estimated parameters (k_{soil} and k_{grout}) using the Nelder-Mead simplex minimization. Oklahoma State University site A #6 borehole.....	180

Figure	Page
8.5. Ground thermal conductivity estimation vs. in-situ test duration. Oklahoma State University site A #1 and #2, and Chickasha test boreholes. (Dotted lines indicate logarithmic extrapolations.)	185
8.6. Thermal conductivity estimation vs. duration of in-situ testing. Simulated Borehole	187
8.7. Ground thermal conductivity estimation vs. the undisturbed far-field ground temperature. Oklahoma State University site A #6 borehole	188
8.8. Thermal conductivity estimations vs. the undisturbed far-field temperature. Simulated borehole	190
8.9. Thermal conductivity vs. the shank spacing of the U-tube. Oklahoma State University site A #6 borehole, and the simulated borehole in the medium-scale test unit with dry and saturated sand	191
8.10. Ground thermal conductivity estimation vs. the ground's volumetric specific heat. Oklahoma State University site A #6 borehole	193
8.11. Thermal conductivity estimations vs. the volumetric specific heat. Simulated borehole	194
8.12. Ground thermal conductivity estimation vs. the borehole radius. Cored borehole Oklahoma State University site A#6	198

NOMENCLATURE

α	thermal diffusivity (ft ² /hr [m ² /s])
a	conductance (Btu/hr.°F [W/°C])
adj	adjusted
A	area (ft ² [m ²])
B	boundary
b	borehole.
β	integration variable in the analytical solution
C	specific heat (Btu/lb-F [kJ/kg-K])
D'	diameter (ft [m])
e, E	east
exp	experimental.
EFT	entering fluid temperature to the heat pump
ExFT	exiting fluid temperature from the heat pump
ff	far field
g	g-function.
H	Borehole depth (ft [m]).
h	convective heat transfer coefficient (Btu/hr-ft ² -F[W/m ² -K])
i	index of any time steps.
i,j	cell index
in	inside.
J_0	Bessel Function of first kind zero th order
J_1	Bessel Function of first kind first order
k	conductivity (Btu/hr-ft-°F [W/m-°C]).
L	borehole depth (ft [m])
l	index of hourly time steps.

m	index for the load aggregated time blocks.
n	number of data points.
N	north
num	numerical.
out	outside.
P	current cell
Pr	Prandtl number
Q	Heat transfer rate (Btu/hr-ft [W/m]).
q'	Heat transfer rate for short time-steps (Btu/hr-ft [W/m]).
q	heat flux (Btu/hr-ft ² [W/m ²])
r	radius (ft [m]).
R	thermal resistance (°F per Btu/hr-ft [°C per W/m]).
Re	Reynolds number.
ρ	density (lb/ft ³ [kg/m ³])
s	steady-state.
S	Source term (Btu/hr-ft ³ [W/m ³])
SSE	sum of the squares of the error
T	temperature (°F [°C])
t	time (hr or sec).
θ	angular coordinate
V	volume (ft ³ [m ³])
w, W	west
Y ₀	Bessel Function second kind of zeroth order
Y ₁	Bessel Function second kind of first order

1. INTRODUCTION

The need for alternative low-cost energy sources has given rise to the development of ground-coupled heat pump systems for residential and commercial heating and cooling applications. These systems have been recognized to provide viable, environment-friendly alternatives to conventional unitary systems. They can make significant contributions to reductions in electrical energy usage, and allow for more effective demand-side management schemes. However, compared to air source heat pump systems, ground source systems have not been widely used. This may be attributed to comparatively higher installation costs and ground area requirements, but may also be attributed to the lack of reliable system design and simulation models. Even though the system design process for ground loop heat exchangers has long passed the stage of heuristic models, Cane and Forgas (1991) estimate that current North American practice results in ground loop heat exchanger lengths being oversized by about 10% to 30% - a high enough percentage to make the short-time economics of these applications comparatively unattractive. Nevertheless, tens of thousands of residential systems per year are installed worldwide, and a steadily increasing interest in systems for non-residential applications is observed. The further acceptance of the technology will also clearly depend on the availability of accurate, reliable and fast system design and simulation tools.

In general, there are three common heat sources/sinks for the heat pump - surface water, outdoor air and the ground - of which the ground is widely available and remains

at moderate temperatures year around. In the case of cooling a building, the ground is the system heat sink, and the building to be cooled the system heat source. In the case of heating, these functions are reversed - the ground becomes the heat source and the building the heat sink.

Heat is extracted from or rejected to the ground by means of buried pipes, through which a heat transfer fluid circulates usually water or a water/antifreeze solution. The buried pipes are commonly called ground loop heat exchangers, and are placed in either vertical holes in the ground-boreholes, or horizontal trenches. Ground loop heat exchangers may be installed in a single borehole or a single trench or in interconnected networks of boreholes and trenches depending on the available ground area and the specific application. A schematic of a typical vertical closed loop, ground-source heat pump system is provided in Figure 1.1.

Ground-coupled heat pump systems are a subset of ground-source heat pump systems and typically consist of water-to-air or water-to-water heat pumps linked to a network of closed ground loop heat exchangers. The heat pump unit is most often located indoors with a traditional energy distribution system. Another subset of ground-source heat pump systems is the groundwater heat pump systems that utilize an open loop in which water is pumped from the ground or a reservoir through the heat pump.

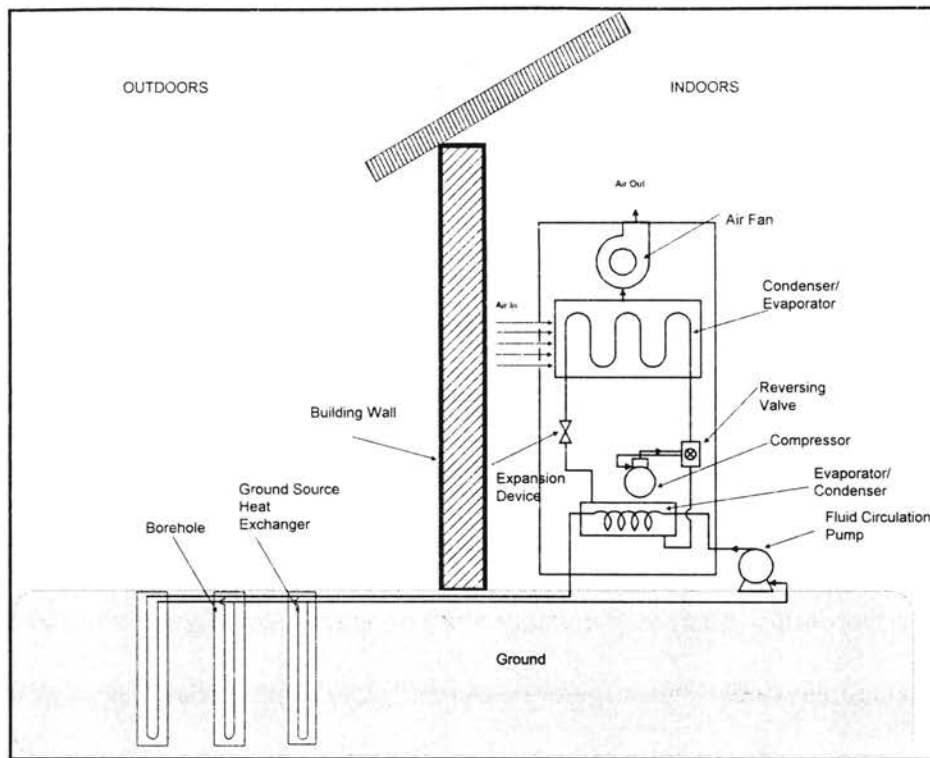


Figure 1.1. *Schematic of a Typical Vertical Closed-Loop, Ground-Coupled Heat Pump System.*

Although ground-source heat pump systems may use horizontal or vertical ground loop heat exchangers, the scope of this research has been limited to vertical, closed loop, ground-coupled systems because the main interest of this research is directed toward commercial applications where these systems are the most common type. Vertical ground loop heat exchangers typically consist of a high-density-polyethylene (HDPE) pipe U-tubes inserted into 100 ft (30 m) to 300 ft (90 m) deep boreholes. The boreholes have typical diameters of 3" (76 mm) to 5" (127 mm) and the pipe diameters in the range from $\frac{3}{4}$ " (19 mm) to 1 $\frac{1}{2}$ " (38 mm). The pipes forming the U-tube are accordingly closely spaced in the borehole. A grout mixture is typically pumped into the borehole to fill the gap between the U-tube and the borehole walls. The purpose of the grout is to improve

the heat transfer between the soil and plastic pipes by providing a better contact surface between them. and also to provide a seal around the U-tube to guard against migration of contaminants into the groundwater system.

The fact that vertical, closed loop, ground-coupled systems require less land area than do horizontal systems, and do not require water-bearing formations means that they are the most universally applicable ground source system configuration for commercial applications. A detailed discussion on the advantages of vertical, ground-coupled, heat exchangers in ground-source heat pump systems is provided in the literature. (Kavanaugh 1992, 1985; Hart and Couvillion 1986; Sauer et al., 1983) However, despite the perceived economic benefits of such systems, there has been almost no work reported on detailed ground loop heat exchanger models suitable for short time-step (hourly or less) energy analysis.

In a ground-coupled heat pump application, the actual heat transfer to and from the ground loop heat exchanger varies continuously due to changing building energy requirements. These changes result in short time-step fluctuations in the supply and return temperatures of the ground loop and can typically vary from 10–18 °F (5.6–10 °C) over a given day. The resulting variations have a direct impact on the coefficient of performance (COP) of the heat pump unit and thus influence the overall system performance in a significant way. In cases where time-of-day electricity rates are applicable, the impact of fluctuating performance on the system economics will be even more significant.

For a detailed building energy analysis, a ground loop heat exchanger simulation model is called for that can reliably and efficiently predict the short term fluctuations of the ground loop heat exchanger return temperature during a given day. This enables the determination of energy consumption and demand information on an hour-by-hour basis. In ground loop heat exchanger design programs, the actual daily load profile is often approximated as a single fixed load with a user-specified duration. A true hourly model of the ground loop heat exchanger can be used to eliminate this approximation.

In addition to building energy analysis and ground loop design applications, the short time-step model can be used for hybrid ground source applications. In some situations, for example, where cooling loads are very dominant, supplemental heat rejecters such as cooling towers are used. Various operating strategies might be utilized in hybrid systems. For example, to reduce heat build-up in the ground by running during the winter, or, by running at night during the summer. In order to quantify the impact of various operating strategies on ground loop heat exchanger size and operating costs, a model that can account for changes in the hourly load profile and interaction between the ground loop heat exchanger and heat rejecter is advantageous.

Another important aspect of ground source heat pump design is the determination of the thermal conductivity of the ground formation surrounding the ground heat exchanger borehole. There are a number of design tools used to size ground loop heat exchangers (Ingersoll 1954, Kavanaugh 1984, Eskilson 1987, Cane 1991, IGSHPA 1991 and Spitler et al. 1996). All of the design tools rely on some estimate of the ground

thermal conductivity and volumetric specific heat. This estimate is critical to the design, yet it is very difficult to make. The required borehole depth or length is highly dependent on the thermal properties of the ground. This in turn strongly influences the cost of the system and its competitiveness with conventional systems.

The traditional approach to estimating the ground thermal properties has been to first ascertain the type (or types) of soil or rock that surrounds the borehole. Once the type of soil or rock is determined, its thermal conductivity can be estimated from tabulated data, such as that contained in the Soil and Rock Classification for the Design of Ground-Coupled Heat Pump Systems Field Manual (EPRI, 1989). For each rock type, a horizontal band is drawn to indicate the range of thermal conductivity expected. Considering one rock type, “Quartzose sandstone, wet”, the thermal conductivity varies from about 1.8 Btu/h-ft-°F (3.1 W/m-K) to about 4.5 Btu/h-ft-°F (7.8 W/m-K). This is a significant variation, and the prudent designer will probably choose the lower value of about 1.8 Btu/h-ft-°F (3.1 W/m-K), even though the extra borehole depth required may not allow the ground loop system to be competitive on either a first cost basis or a life cycle cost basis. A method for more accurately estimating the ground thermal conductivity is therefore highly desirable.

For these purposes, a transient, two-dimensional numerical finite volume model for the vertical ground loop heat exchanger borehole is developed that can be used to develop a short time-step model and be used inside a parameter estimation algorithm to predict the thermal conductivity of the ground formation surrounding the borehole. The

short time-step model developed is an extension of the long time-step model of Eskilson (1987). The numerical model is used to develop non-dimensional temperature response factors for time intervals as small as three minutely. The parameter estimation method utilizes the downhill simplex minimization algorithm of Nelder and Mead (1965) in conjunction with the numerical model of the borehole to estimate the ground thermal conductivity.

2. BACKGROUND AND LITERATURE REVIEW

A review of the literature yields several variations of two analytical methodologies that are used for the design and dimensioning of vertical ground loop heat exchangers: methods based on Kelvin's line source theory, and methods based on the cylinder source solution. Several investigators have also taken numerical, analytical, and combined approaches to simulate the thermal behavior of ground loop heat exchangers. In addition, there are "rule of thumb" approximations, which are discussed by Ball et al. (1983).

A literature review on determining the thermal conductivity of ground formation yielded a multitude of methods that may be divided into steady state and transient methods based on the heat transfer applied to the ground sample. In steady-state methods, the temperature of the sample is in steady state when the measurements are made. In transient methods, the temperature of the sample varies with time.

2.1. EXISTING DESIGN AND SIMULATION TOOLS FOR GROUND LOOP HEAT EXCHANGERS – ANALYTICAL

The viability of a particular ground loop heat exchanger design often depends on its ability to reject or extract heat over a number of years and the avoidance of excessive build up or loss of heat in the borehole field. A model for the design of ground loop heat

exchanger fields therefore has to be computationally efficient enough to allow calculation of transient effects over long time periods. The use of an analytical model is attractive in terms of computational efficiency but the fact that the pipes are not co-axial with the borehole, and a number of different materials are involved, makes the task of finding a suitable analytical model difficult or impossible. (A horizontal plane cross-section of a single borehole is shown in Figure 2.1).

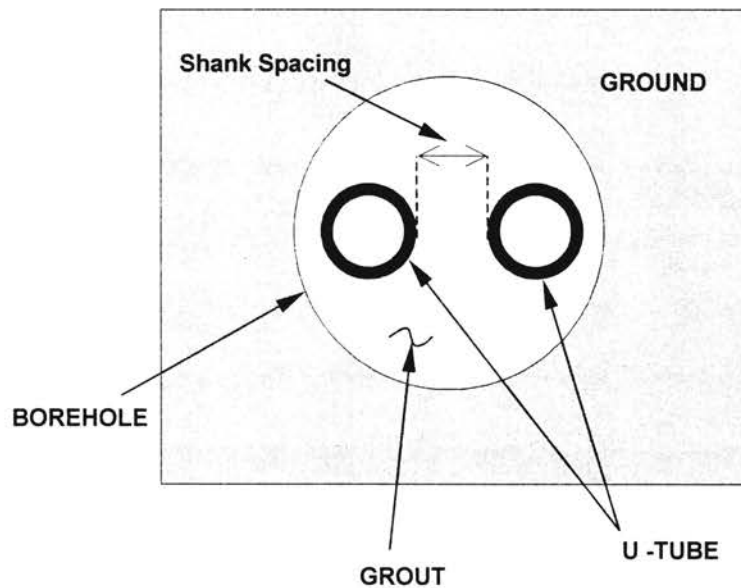


Figure 2.1. *Top view cross-section of a typical borehole.*

Nevertheless, a number of design methods using analytical approaches have been developed, but which make a number of simplifying assumptions. The most significant of these is the assumption of the so-called “equivalent diameter” approximation that treats the two legs of the U-tube as a single pipe co-axial with the borehole so that a solution such as the ‘cylinder source’ solution (Carslaw and Jaeger, 1947) may be applied. The geometry can alternatively be further approximated as an infinitely long

'line source' (Kelvin 1882, Ingersoll 1948, 1954). Cane and Forgas (1991) give a review of a number of these models.

2.1.1. INGERSOLL'S APPROACH

Ingersoll (1948, 1954) provides a practical elaboration to Kelvin's (1861) line source theory to treat the problem of obtaining the temperature at any point in an infinite medium. The medium is assumed to be initially at a uniform temperature, in which an infinitely long line source or sink of heat with a constant heat rate is switched on at time zero. This temperature according to Ingersoll is given by the following equation for a pipe:

$$T - T_0 = \frac{Q'}{2\pi k} \int_x^\infty \frac{e^{-\beta^2}}{\beta} d\beta = \frac{Q'}{2\pi k} I(X) \quad (2.1)$$

where

$$X = \frac{r}{2\sqrt{\alpha t}} \quad (2.2)$$

T = Temperature of ground at any selected distance from the line source in $^{\circ}F$,
(Selecting a distance that is equal to the pipe diameter represents the pipe surface temperature.)

T_0 = Initial temperature of the ground in $^{\circ}F$ [$^{\circ}C$],

Q' = Heat transfer rate over the source in $\frac{BTU}{ft - hr}$ [$\frac{W}{m}$]

r = Distance from center line of pipe, in ft [m],

k = Thermal conductivity of the ground formation, in $\frac{BTU}{hr - ft - ^\circ F}$ [$\frac{W}{m - ^\circ C}$],

α = Thermal diffusivity of the ground formation defined to be $= \frac{k}{\rho c}$,

ρ = Density of the ground formation, in $\frac{lb}{ft^3}$ [$\frac{kg}{m^3}$],

t = Time since the start of the operation, in (hr),

β = Integration variable (Equals to $\frac{r}{2\sqrt{\alpha(t-t')}}$).

For values of $X < 0.2$ the following approximation is provided for the integral term,

$$I(X) = 2.303 \log_{10} \frac{1}{X} + \frac{X^2}{2} - \frac{X^4}{8} - 0.2886 \quad (2.3)$$

For other values, $I(X)$ is tabulated in reference by Ingersoll et al. (1954) .

One of the primary assumptions made in Ingersoll's approach is that the pipe or the line source must be infinitely long so that the heat flow can be considered all normal to the length of the source - radial heat flow. In cases where the radial heat flow from or to the source is not constant but varies from month to month, Ingersoll suggests that the integral term in equation (2.1) be split into parts considering average heat transfer rates for a given time interval. The integration limits are then determined by integrand values corresponding to the beginning and the end of the particular time interval. A perfect

contact between the source and the surrounding ground formation is also stipulated along with constant ground formation properties.

Ingersoll states that the equation (2.1) is exact only for a true line source, but that it can also be applied with negligible error, after a few hours of operation, to small pipes (2 inches [50.8mm] or less) in actual use in most heat pump systems. For pipes that are larger and for periods of operation less than a few days, Ingersoll notes that an error will be involved which can be approximated. The criterion for the error term is that the dimensionless “time-to-pipe” ratio $\frac{\alpha t}{R^2}$ be greater than 20 for small pipes in order for the error to be small for practical purposes.

Ingersoll provides several sample calculations and comparisons based on two different types of soils; wet clay with high thermal conductivity and moist soil of medium low conductivity. In addition, sample calculations are given for short and long pipes for both constant pipe surface temperature and constant heat rejection or extraction rates.

It should be noted here that Ingersoll’s approach provides only rough approximations to the actual heat transfer process, and its applicability to modeling of real-life ground loop heat exchangers is limited without further assumptions and modifications. Ingersoll, in his 1948, paper does make some general statements for use in practical system design applications, but topics that are of interest to system designers such as calculation of heat exchanger lengths, pipe to pipe thermal interference in a borehole, effects of long-time and short-time system operation on the surrounding ground

formation, effects of entering and exiting fluid temperatures and system operational efficiency as a function of soil types, are treated marginally. Ingersoll's approach nevertheless lays the groundwork for more extensive system design methodologies that were developed in the ensuing decades.

2.1.2. HART AND COUVILLION'S APPROACH

Hart and Couvillion (1986) also utilize Kelvin's line source equation of continuous time-dependent heat transfer between a line source and the earth to obtain a time-dependent temperature distribution around a line source. An approximate equation for the far-field radius r_∞ is calculated considering the heat rejected by the line source must be absorbed by the immediate ground formation region surrounding the line source. Hart and Couvillion state that the equation for the far-field radius is approximate because the solution to the Kelvin's line source equation falsely predicts a temperature distribution in the surrounding ground formation at all radii short of infinity any time after the line source is switched on. Based on this, the only correct value of r_∞ is that $r_\infty = \infty$. Hart and Couvillion assume however an "arbitrary" far-field radius of

$$r_\infty = 4\sqrt{\alpha t} \quad (2.4)$$

The ground temperature beyond the far-field radius is assumed to be undisturbed and constant. The line source equation is stated similar to Ingersoll's approach as follows:

$$T - T_o = \frac{Q'}{4\pi k} \int_y^\infty \frac{e^{-\lambda}}{\lambda} d\lambda \quad (2.5)$$

where

$$y = \frac{r^2}{4\alpha t} \quad (2.6)$$

The solution to the integral term in the equation (2.5) is obtained from integral tables to be equal to $\left[y - \ln y - \gamma - \frac{y^2}{2 \times (2!)} + \frac{y^3}{3 \times (3!)} + \dots + \frac{(-1)^{N+1} y^N}{N \times (N!)} \right]$, where γ is the Euler constant ($\gamma \cong 0.5772157$). Assuming that the heat rejected or absorbed by the line source must be equal to the heat rejected or absorbed by the ground formation surrounding ground region and replacing the line source integral, Hart and Couvillion arrive at the following expression for the temperature distribution equation around a line source:

$$T - T_o = \frac{Q'}{2\pi k} \left[\ln \frac{r_\infty}{r} - 0.9818 + \frac{4r^2}{2r_\infty^2} - \frac{1}{4 \times (2!)} \left(\frac{4r^2}{r_\infty^2} \right)^2 + \dots + \frac{(-1)^{N+1}}{2N \times (N!)} \left(\frac{4r^2}{r_\infty^2} \right)^N \right] \quad (2.7)$$

Note that in equation (2.7) r is the radial distance from the line source at which the temperature value is desired. If r is set to be equal to the pipe radius, the approximate pipe surface temperature is obtained.

An important aspect in regards to the Hart and Couvillion implementation of the Kelvin's line source theory is the introduction of the far-field radius r_∞ . This component stipulates a defined region around the line source with a radius of r_∞ where heat exchange between the ground formation and the line source occurs. All ground formation at a distance from the line source greater than r_∞ is assumed to be at the undisturbed far-field temperature, and the value of the far-field radius depends on the length of time the line source has been operating and on the ground's thermal diffusivity. In multiple borehole configurations the analysis of borehole to borehole thermal interference is based on the value of r_∞ so that no thermal interference is assumed to occur when the r_∞ value is less than the distance between the boreholes. Only after r_∞ reaches or exceeds the distance between the boreholes thermal interference is effective, and is estimated using superposition techniques.

Hart and Couvillion also develop time-dependent equations for pipes based on time-dependent equations developed for line sources. According to Hart and Couvillion, the equation (2.7) also applies for pipes as long as the value of $\frac{r_\infty}{R}$ is greater than or equal to 15, where R is the pipe radius. For cases where $\frac{r_\infty}{R} < 15$, it is stated that the calculation of r_∞ becomes more involved. A detailed derivation for the value of r_∞ in such cases is provided. The equation (2.7) contains a power series of N terms. The issue of accuracy in the equation (2.7) is answered by investigating the ratio of $\frac{r_\infty}{R}$. Only two

terms are suggested to be included in the power series as long as $\frac{r_\infty}{R} \geq 3$. For cases where this ratio is less than 3, it is recommended that the number of terms in the power series be increased. However, the question of how many terms should be included for cases where $\frac{r_\infty}{R} < 3$ is not discussed. The authors apparently leave this to system designers to decide based on experimental data and field experience.

System design equations such as the temperature distribution around the heat transfer pipe, the rate of heat rejection or extraction at any radius around the source and all other equations necessary to describe the time-dependent heat transfer process around a line source (or pipe) are developed using the concept of the far-field radius.

Adjustments are suggested to be made in temperature distribution calculations that arise due to overall coupling thermal resistance which consists of earth's thermal

resistance ($R_s = \frac{(T_\infty - T_0)}{Q}$), pipe thermal resistance ($R_p = \frac{\ln \frac{r_o}{r_i}}{2\pi k_p}$), and fluid convective

resistance ($R_c = \frac{1}{2h_{fluid}\pi r_i}$),

where

r_o = inside pipe radius,

r_i = outside pipe radius,

k_p = conductivity of pipe,

h_{fluid} = convective heat transfer coefficient of fluid.

2.1.3. IGSHPA APPROACH

The IGSHPA modeling procedure is also built around Kelvin's line source theory. Bose (1984, 1988) sizes the ground-loop heat exchanger length for the coldest and the hottest month of the year and then calculates the seasonal performance and system energy consumption using the monthly bin method of energy analysis. The IGSHPA approach defines the ground formation resistance of a single vertical heat exchanger as follows:

$$R_s(X) = \frac{I(X_{r_0})}{2\pi k_s} \quad \text{with} \quad X_{r_0} = \frac{r_0}{2\sqrt{\alpha_s t}} \quad (2.8)$$

where

$I(X_{r_0})$ = the exponential integral,

r_0 = outside pipe radius in ft [m],

α_s = diffusivity of the ground formation in $\frac{ft^2}{hr}$ [$\frac{m^2}{hr}$],

k_s = thermal conductivity of the ground formation in $\frac{BTU}{hr - ft - ^\circ F}$ [$\frac{W}{m - ^\circ C}$],

t = time in hr.

An approximation for the exponential integral is given for $0 < X \leq 1$ and for $1 \leq X \leq \infty$ intervals.

For $0 < X \leq 1$

$$I(X) \approx \frac{1}{2}(-\ln X^2 - 0.57721566 + 0.99999193X^2 - 0.24991055X^4 + 0.05519968X^6 - 0.00976004X^8) \quad (2.9)$$

For $1 \leq X \leq \infty$

$$I(X) = \left[\frac{1}{2X^2 e^{X^2}} \right] \frac{A}{B} \quad (2.10)$$

with

$$A = X^8 + 8.5733287X^6 + 18.059017X^4 + 8.637609X^2 + 0.2677737 \quad (2.11)$$

and

$$B = X^8 + 9.5733223X^6 + 25.6329561X^4 + 21.0996531X^2 + 3.9684969 \quad (2.12)$$

The methodology allows for the calculation of ground formation resistance for multiple vertical heat exchangers by superimposing the thermal resistive effects of adjacent heat exchangers and adding the total effect to the ground formation resistance of a single pipe of an equivalent radius. (Bose defines the equivalent diameter as

$$D_{eq} = \sqrt{n}(D_o) \text{ with } n = \text{number of U-tube legs in a borehole.})$$

Underground formation temperatures and maximum and minimum earth temperatures are estimated using Kusuda's (1965) analytical equations. Bose (1984, 1988) provides tables and maps to approximate the mean earth temperature, yearly earth surface temperature swings and phase constants. The annual mean surface temperature is set equal to the minimum and maximum annual earth temperatures.

The pipe resistance to heat flow is determined for single pipes with

$$R_p = \frac{1}{2\pi k_p} \ln \frac{r_o}{r_i} \quad (2.13)$$

For a vertical U-tube, the pipe resistance is given as

$$R_p = \frac{1}{2\pi k_p} \ln \frac{D_{eq}}{D_{eq} - (OD - ID)} \quad (2.14)$$

where OD denotes the pipe outer diameter and ID the pipe inside diameter.

The IGSHPA approach calculates the annual heating and cooling run fractions based on heat pump maximum and minimum entering fluid temperatures. Bose (1984), and Cane and Forgas (1991) recommend that a design minimum entering fluid temperature T_{min} of 30°F to 40°F (-1.1 °C to 4.4 °C) above the coldest outdoor air temperature at a given geographical location and essentially assume 100°F (37.8 °C) as the first approximation for the maximum entering fluid temperature T_{max} . Based on the

selection of T_{\min} and T_{\max} , a ground-source heat pump is selected with a total heating and cooling capacity and coefficients of performance in heating and cooling modes. (COP_H , COP_C)

Design equations to determine the length of heat exchangers are provided as follows:

For Heating,

$$L_H = \frac{(Capacity_{Heating}) \left(\frac{COP_H - 1}{COP_H} \right) (R_p + R_s \cdot RunFraction_{Heating})}{T_{S \min, Annual} - T_{\min}} \quad (2.15)$$

For Cooling,

$$L_C = \frac{(Capacity_{Cooling}) \left(\frac{COP_C - 1}{COP_C} \right) (R_p + R_s \cdot RunFraction_{Cooling})}{T_{\max} - T_{S \max, Annual}} \quad (2.16)$$

A monthly energy analysis is performed based on the monthly bin method. The IGSHPA method requires that the expected ground-loop heat exchanger temperature be estimated during all other months given the first estimate of the length from the coldest and hottest months. The expected average fluid temperature in the ground-loop heat exchanger, also the average borehole temperature, is estimated as follows:

- a) For each month depending on the heating or cooling requirement a T_{\min} or a T_{\max} is assumed with a corresponding heat pump capacity and coefficient of performance.
- b) Heat pump run fractions are calculated for each month using assumed T_{\min} and T_{\max} in the bin method.
- c) Temperature differences ($T_{S,\min,Annual} - T_{\min}$) or ($T_{\max} - T_{S,\max,Annual}$) for each month are determined from equations (2.15) and (2.16).
- d) Assumed values for T_{\min} and T_{\max} are compared to the calculated values. In case the difference between the assumed and calculated values are greater than 0.2 °F (0.1°C), a new set of T_{\min} and T_{\max} values are assumed and the procedure repeated until the desired accuracy is obtained.

2.1.4. KAVANAUGH'S APPROACH

Kavanaugh (1985) approaches the problem of determining the temperature distribution or the heat transfer rate around a buried pipe by using the cylinder source solution as the exact solution. The cylinder source solution, as the line source solution, can produce results for either a constant pipe surface temperature or a constant heat transfer rate to or from the pipe to its surroundings.

Kavanaugh develops the cylindrical source approach considering a single isolated pipe surrounded by an infinite solid with constant properties. It is assumed that the heat transfer process is of the nature of pure conduction in a perfect ground formation /pipe contact. Groundwater movements in the earth and thermal interference between adjacent boreholes are considered to be negligible.

The cylindrical source solution for a constant heat transfer rate is essentially based on Carslaw and Jaeger's (1947) and Ingersoll's (1948, 1954) works:

$$T - T_o = \frac{Q'}{k} G(z, p) \quad (2.17)$$

where

$$z = \frac{\alpha t}{r^2}, \quad p = \frac{r}{r_o}, \quad \text{and} \quad r_o = \text{Outer pipe radius.}$$

The expression $G(z,p)$ is only a function of time and distance from the pipe considering the assumptions made and defined as follows by Carslaw and Jaeger (1947):

$$G(z, p) = \frac{1}{\pi^2} \int_0^{\infty} \frac{e^{-\beta^2 z} - 1}{J_1^2(\beta) + Y_1^2(\beta)} [J_0(p\beta)Y_1(\beta) - J_1(\beta)Y_0(p\beta)] \frac{1}{\beta^2} d\beta \quad (2.18)$$

Kavanaugh provides graphical results for the $G(z,p)$ function where $p=1$. The location $p=1$ is of interest since it represents the surface of the pipe under consideration.

It should also be noted that equations (2.17, 2.18) are derived based on constant heat transfer rates.

An equivalent heat transfer coefficient per unit area from the outer pipe wall to the fluid inside the pipe is given as follows:

$$h_{eq} = \left[\frac{r_o}{r_i h_i} + \frac{r_o}{k} \ln \left(\frac{r_o}{r_i} \right) \right]^{-1} \quad (2.19)$$

where r_i is the inside pipe radius.

The inside convective heat transfer coefficient for turbulent flow in a smooth circular pipe is defined as $h_i = Nu_{D_i} \frac{k_{fluid}}{D_i}$. (Dittus-Boelter relationship is used to determine the Nusselt number with $Nu_{D_i} = 0.023 Re_{D_i}^{0.8} Pr^n$; $n=0.4$ for heating and $n = 0.3$ for cooling) Since the pipe configuration (U-Tube) presents a major deviation from the original line source approach of Kelvin and Ingersoll, the original solution is modified considering an equivalent pipe diameter as suggested by Bose (1984). This equivalent pipe diameter is given to be $D_{eq} = \sqrt{n}(D_o)$ where n is the number of U-tube legs in a borehole. It allows for the U-tube geometry to be treated as a single pipe to approximate a line source.

Correcting for a non-uniform heat flux flow over the surface of closely positioned pipes and the number of U- tubes in question, Kavanaugh provides the following equation for the temperature difference across the U-tube pipes where the correction factors C and N are determined from experiment and simulation:

$$\Delta T_p = \frac{Q'}{CN_i 2\pi r_o h_{eq}} \quad (2.20)$$

where

N_i = Number of U-tubes.

C = The correction factor for non-uniform heat flow. (C= 0.85 when N=2; C=0.6-0.7 when N=4; see Kavanaugh [1985])

The average water temperature is then found by using the sum of temperature drops from the far-field temperature T_o to the inside of the pipe. The average water temperature T_{aw} is stated to be:

$$T_{aw} = T_o + \left[\frac{Q'}{k} G(z, p) \right] + \frac{Q'}{CN_i 2\pi r_o h_{eq}} \quad (2.21)$$

An energy balance on the entire coupling then allows the calculation of the total temperature difference between the inlet and outlet water:

$$T_{wo} - T_{wi} = \frac{Q' L}{m_w c_{pw}} \quad (2.22)$$

with $T_{aw} = \frac{T_{wi} + T_{wo}}{2}$.

The outlet water temperature becomes:

$$T_{wo} = \frac{Q' L}{2m_w c_{pw}} + T_{aw} \quad (2.23)$$

Kavanaugh (1992) implements this model at two test sites and provides experimental data. According to Kavanaugh, the model works well if (1) care is taken in choosing the effective ground formation properties, and (2) initial entering water temperatures are not desired immediately after startup.

The single U-tube pipe introduces a complication since there is short circuit heat transfer within the borehole due to temperature differences between the up-leg and the down-leg of the U-tube. Kavanaugh, as an alternative to calculating the interference of two line sources in a single borehole, considers a single line source with short circuit losses. Kavanaugh suggests two ways to correct for the short circuiting phenomenon. One method, according to Kavanaugh, is to correct the average fluid temperature as stated in (22) by the temperature difference caused by the short circuiting as follows:

$$\Delta T_{sc} = \frac{Q_{sc}' L}{m_w c_{pw}} \quad (2.24).$$

The short circuit heat flux Q_{sc}' defined as $Q_{sc}' = \frac{T_{wi} - T_{wo}}{2R_{sc}}$ where the short circuit resistance R_{sc} is the sum of the pipe inside film resistance, the wall resistance and the ground formation resistance.

The second method that is suggested is based on Kalman's work (1980) that corrects for the short circuiting effect in a general equation for heat transfer from an element of differential length and integrates this equation over the entire length of the coupling. Kavanaugh recommends that the second approach be adapted in situations where the temperature difference between the entering water temperature and exiting water temperature is less than 10°F and short circuiting is less than 10%.

2.2. EXISTING DESIGN AND SIMULATION TOOLS FOR GROUND LOOP HEAT EXCHANGERS – NUMERICAL

As discussed above, when line source and/or cylindrical source models are implemented in actual loop design models further adjustments are necessary to account for the leg-to-leg thermal short-circuiting effects and pipe wall and contact resistances. In the later phases of the life of a borehole field, where the build up of heat in the far field is of much more significance than the heat distribution local to the borehole, these simplifications are correspondingly insignificant. Correspondingly, in the shorter-term

(of the order of hours to weeks) effects local to the borehole, and the influence of the geometry, are important.

Numerical models of conduction around the borehole accordingly have the advantage of being able to account for the complexities of the geometry but the disadvantage of being computationally more expensive and are therefore more suitable for modeling on shorter time scales. A number of ground loop heat exchanger design methods have been devised that combine numerical and analytical methods and some of these are discussed below.

2.2.1. ESKILSON'S MODEL

Eskilson's (1987) approach to the problem of determining the temperature response of a multiple borehole ground loop heat exchanger is based on dimensionless temperature response factors, called g-functions. The response factors are computed with a two step process. First, a two-dimensional (radial-axial) explicit finite-difference simulation of a single borehole is performed to determine the response to a unit step function heat pulse. The borehole in the finite difference model has a finite length and diameter. The borehole (pipe and grout) thermal resistance and capacitance are neglected in the numerical model; the borehole thermal resistance is accounted for separately. Using the spatial temperature distribution of a single borehole, a spatial superposition is formed to determine the response of a pre-defined configuration of boreholes (characterized by their ratio of horizontal spacing to depth) to the unit step function heat

pulse. When the borehole outer wall temperature vs. time response is non-dimensionalized, the resulting dimensionless temperature vs. dimensionless time curve is the g-function. Individual response factors, which give the temperature response to a specific length unit step function heat pulse, are determined by interpolating the g-function.

Once the response factors have been determined, the response of the ground loop heat exchanger to any heat rejection/extraction vs. time profile can be determined by decomposing the heat rejection/extraction vs. time profile into a set of unit step functions. Then, the response of the ground loop heat exchanger to each unit step function can be superimposed to determine the overall response. Additional details, e.g. converting from non-dimensional units to dimensional units, and accounting for the borehole thermal resistance are described by Eskilson (1987). The model is intended to provide the response of the ground to heat rejection/extraction over longer periods of time (up to 25 years) but as the numerical model that provides the g-functions does not account for the local borehole geometry, it cannot accurately provide the shorter term response.

Since the short time step model developed in this study is an extension of Eskilson's long time step model additional details of the model are discussed in section 5.1.

2.2.2. HELLSTROM'S MODEL

Hellstrom (1989, 1991) developed a simulation model for vertical ground heat stores, which are densely packed ground loop heat exchangers used for seasonal thermal energy storage. This type of system may or may not incorporate heat pumps. The model subdivides the ground formation volume with multiple boreholes into two regions. The volume that immediately surrounds a single borehole is described as the 'local' region. The difference between the 'local' average temperature and the average fluid temperature in the borehole for a given time is proportional to the heat rejection/extraction rate for that time via a time-dependent fluid-to-ground formation resistance. This is used to account for heat transfer conditions around individual boreholes due to short-time thermal variations. Over longer time scales, the heat flow field in this region does not change with time. A constant temperature difference is then computed due to the constant heat flux via a constant steady-flux thermal resistance. The second region is concerned with the heat conduction problem between the bulk of the heat store volume (multiple boreholes) and the far field. Hellstrom defines this to be the 'global' problem. The 'global' problem is treated as three components: a steady-state heat loss component, a thermal build-up component and a periodic heat loss component. The steady-state regime for the 'global' problem may be reached after several years (depending on the size of the heat store and heat rejection and extraction rates) during which a transient thermal build-up is assumed to occur around the borehole field where the heat flow gradually approaches a steady-state value.

Hellstrom's model thus represents the total change in the initial ground formation temperature for a time step first by the spatial superposition of three parts: a so-called 'global' temperature difference, a temperature difference from the 'local' solution immediately around the heat store volume, and a temperature difference from the 'local' steady-flux part. The ground formation temperature at any subsequent time is determined by decomposing the time-varying heat transfer profile into a series of individual step heat pulses and superimposing the resulting responses in time. The model is essentially a hybrid model that uses a numerical solution for the 'local' and the 'global' problems and then superimposes them spatially with the analytical solution from the steady-flux part. The numerical model uses a two-dimensional explicit finite difference scheme on the radial-axial coordinate system for the 'global' problem. For the local solution, a one-dimensional radial mesh is used that divides the storage region into several sub-areas. Hellstrom's model is not ideal for determining long time-step system responses for ground source heat pump systems since the geometry of the borehole field is assumed to be densely packed, with a minimum surface area to volume ratio, as is typical for heat stores.

In North America, ground loop heat exchangers are commonly designed to dissipate heat rather than store it. In this case, vertical boreholes are often spaced as far apart as feasible.

2.2.3. THORNTON ET AL. IMPLEMENTATION OF HELLSTROM'S MODEL

Thornton et al. (1997) used Hellstrom's approach as part of a detailed component-based simulation model of a ground source heat pump system. The model was implemented in TRNSYS (Klein, et al. 1996). It was calibrated to monitored data from a family housing unit by adjusting input parameters such as the far-field temperature and the ground formation thermal properties. When calibrated, the model was able to accurately match measured entering water temperatures.

2.2.4. MEI AND EMERSON MODEL

Mei and Emerson (1985) developed a numerical model suitable for horizontal coils that included a model of the effects of frozen ground formation around the pipe. Their numerical model used an explicit finite difference scheme to solve three one-dimensional partial differential equations describing conduction radially through the pipe, frozen formation region, and far field region. These equations were coupled to a fourth one-dimensional partial differential equation representing the flow of heat along the pipe, resulting in a quasi two-dimensional model. The model used different time steps for the pipe wall and the frozen ground formation region, and another significantly larger time step for the fluid and unfrozen ground formation region. The size of the frozen region at each position along the pipe was extended or contracted accordingly throughout the simulation. Mei and Emerson reported comparisons with experimental data over a 48 day simulation period.

2.2.5. MURAYA'S MODEL

Muraya (1995) and Muraya, et al. (1996) used a transient two-dimensional finite element model to investigate the thermal interference between the U-tube legs. The model attempts to quantify this interference by defining a heat exchanger effectiveness based on ground formation and grout properties, shank spacing, far-field and loop temperatures, and heat dissipation rates. The model validation is conducted against two different applications of the analytical cylinder source solution using constant temperature and constant flux approaches. Based on the parametric studies performed, they were able to define an overall thermal effectiveness and a backfill effectiveness, both of which depended on the borehole geometry.

2.2.6. ROTTMAYER, BECKMAN AND MITCHELL MODEL

Rottmayer, Beckman and Mitchell (1997) developed a numerical U-tube heat exchanger model based on an explicit finite-difference technique. A two-dimensional finite difference formulation on a polar grid was used to calculate the lateral heat transfer over each 10ft (3 m) vertical section of the borehole. Conduction in the vertical direction was neglected but each section of the model was coupled via the boundary conditions to a model of flow along the U-tube. In this way a quasi three-dimensional model was produced which could account for the variations in fluid temperature with depth. The geometry of the circular U-tube pipes were approximated by a 'pie-sector' shape by matching the perimeter of the modeled non-circular tube to the actual circular pipe

perimeter. They found that the model under-predicted the heat transfer from the U-tube by approximately 5% when compared to an analytical model and attributed this to the simplified pipe geometry. To account for this, a 'geometry factor' of the order of 0.3 – 0.5 was used to modify the thermal resistances of ground formation and grout components of the fluid to grout in the finite difference equations. This size of this factor was determined so that the model gave the same steady state heat transfer rates as the analytical model.

2.2.7. SHONDER AND BECK MODEL

Shonder and Beck (1999) developed a one-dimensional thermal model where the borehole U-tube pipes are represented with a single pipe of equivalent diameter. The borehole model assumes a thin film of finite thickness around the equivalent diameter of the effective single pipe to account for the heat capacity of the U-tube pipes and the heat transfer fluid. The borehole model thus assumes one-dimensional transient heat conduction through the film, the grout, which fills the area between the 'outer surface' of the film and the borehole wall, and the surrounding soil formation. These equations are coupled through interface conditions while a time-varying heat flux is imposed at the inner surface of the film and a constant undisturbed far-field temperature is assumed at the far radial boundary. The initial temperature of the domain is assumed to be at the far-field temperature. The problem is solved using a finite difference grid and the Crank-Nicolson solution scheme. Using the numerical model, a parameter estimation procedure

is suggested based on Gauss' method as described by Beck and Arnold (1977) to predict effective thermal conductivity of soil formations.

2.3. CURRENTLY AVAILABLE METHODS FOR THE DETERMINATION OF THERMAL CONDUCTIVITY OF GROUND FORMATION

Farouki (1986) defines the thermal conductivity of a soil/ground formation as the amount of heat passing per unit time through a unit cross-sectional area of soil/ground formation under a unit temperature gradient applied in the direction of this heat flow. Although heat is transferred through this unit element also through convection, radiation, evaporation-condensation and other mechanisms the bulk of heat transfer is due to heat conduction. The soils and ground formations are made up of different compositions and layers; thus, the definition of the thermal conductivity is understood to suggest an effective thermal conductivity. Additional complications arise by considering other factors that effect the conductivity such as the moisture content of the formation since the effective conductivity of the same unit element will vary for different moisture contents. Similarly, anisotropic soils or formation layers will yield varying conductivity values depending on the direction of the heat applied. Moreover, some soils/ground formations may display hysteresis effects –memory of past states-after drying-wetting and freezing-thawing cycles where markedly different thermal properties are shown for the same moisture content (Wintercorn 1961, De Vries 1974).

The traditional approach to estimating the ground formation thermal properties in designing ground loop heat exchangers has been to first ascertain the type of ground formation that surrounds the borehole by physical analysis based on core samples taken from the boreholes. The core sample is subjected to a sieve test to determine the percentage of each type of sand, clay, silt and other rocks that make up the granular soils in the sample. Once the types of soils in the core sample are determined, the effective thermal conductivity of the formation may be estimated using tabulated data (EPRI 1989) for each type of soil based on its content in the sample. However, since thermal conductivity even for a seemingly homogeneous type of soil/ground formation in various publications and manuals is provided within a rather large band of values, the physical analysis, although necessary, may not give sufficient accuracy. In such cases, more detailed analyses are required to measure the effective thermal conductivity of the soil/ground formation.

The methods to measure the effective thermal conductivity of the soils/ground formations may be divided into steady state and transient methods (Farouki 1986). These methods may be used in laboratory conditions as well as in situ. In order to measure the effective thermal conductivity it is basically necessary to set up a temperature gradient across the soil sample that is being tested. In steady state methods, the sample should be in steady state when the measurement is made. This sometimes may take considerable time after the initial temperature differences have been applied. With transient methods the temperature of the sample varies with time making such methods more versatile, fast and easier to perform.

2.3.1. STEADY STATE METHODS

The most important steady state method for measuring the effective thermal conductivity of soils/ground formations is the guarded hot plate test, which has been standardized by the American Society for Testing and Materials (1963). In this test, two identical test specimens are placed above and below a flat-plate main heater unit that is surrounded by an outer guard heater. The guard eliminates the horizontal heat losses and causes heat from the main heater to flow vertically up or down the test specimen. Liquid-cooled heat sinks are placed adjacent to the outer surfaces of the specimen. A certain temperature drop is obtained across each specimen of known thickness. Since the amount of heat transferred per unit time and the test area of the specimen is known, the thermal conductivity can be calculated using Fourier's law of heat conduction. The method is quite time-consuming and suitable only for laboratory use.

Other steady state methods include Kersten's (1949) method that is similar to the guarded hot plate method but with a cylindrical configuration where the specimen is the annulus between the inside 'plate' and the outside 'plate', the in situ sphere method of Mochlinski (1964) and the heater meter method of Scott (1964).

2.3.2. TRANSIENT METHODS

The most important transient method is the thermal probe or thermal "needle" method (De Vries and Peck 1958), which is a rapid and convenient way of measuring the

effective thermal conductivity of soils and/or ground formations in the laboratory or in situ. The thermal “needle” consists of a heater producing thermal energy at a constant rate and a temperature-sensing element (a thermocouple or a thermistor). The “needle” is inserted into the ground/test specimen and the rate of rise in the temperature of the “needle” depends on the thermal conductivity of the surrounding formation. The theory of the thermal probe is based on the theory of the line heat source placed in a semi-infinite, homogeneous and isotropic medium. As discussed in earlier, Carslaw and Jaeger (1947), Ingersoll et al. (1954) and Hart and Couvillion (1986) provide variations of the general Fourier equation of one-dimensional heat conduction in cylindrical coordinates that can be used to explicitly solve for the thermal conductivity of the surrounding medium.

For the sake of completeness, other, although less used, transient methods are the periodic temperature wave method where the thermal diffusivity of the medium is estimated in situ by analyzing the attenuation and the lag of the annual temperature wave of the ground (Farouki 1986). Shannon and Wells (1947) measure the thermal diffusivity of a cylindrical soil specimen by applying a sudden temperature change to its boundaries and observing the temperature change in its center (temperature shock method).

3. DEFINITION OF THE PROBLEM AND OBJECTIVES

As the discussion of various ground loop heat exchanger system design and simulation methods in the Literature Review section shows there are advantages and disadvantages to each of the currently available methods; and each method should be evaluated for its individual merit depending on the given, specific application or on the desired range of applications. However, one major disadvantage common to all is that, without significant modifications, none of the currently available methods can accurately and reliably account for temperature variations in boreholes during relatively short time steps (weekly, daily, and hourly). A significant majority of the currently available methods assume an average temperature for the ground-loop heat exchanger on a monthly basis. This assumption severely limits the possibility of accounting for variations in the ground loop over shorter time periods that are very important when studying time-of-day variations, demand-side management and the benefits of geothermal heat pump systems to utilities.

In fact, the accuracy that is associated with the currently available methods decreases dramatically for small values of time. Ingersoll et al. (1948, 1954) state that noticeable error occurs using Kelvin's line source theory when the "time-to-pipe" ratio, the product of time and ground formation diffusivity divided by the pipe radius squared, is less than the value 20. Similar limitations are encountered with other currently available methods in regards to analyzing the short time-step behavior of ground-coupled

heat pump systems. Although some of the methods currently available may allow for approximations of the short-time step behavior, satisfactory analyses and reliable forecasts of heat pump entering fluid temperatures are not always possible.

Because of the shortcomings of the current methods, it is highly desirable to develop alternative system simulation methodologies for the analysis of heat flow between the ground formation and the vertical ground-loop heat exchanger for short time-steps. Such methodologies may allow the calculation of heat transfer fluid temperatures on an hourly or minutely basis based on variable rates of heat extraction and rejection, thermal characteristics of the formation, and ground-loop heat exchanger geometry.

Consequently, the study reported here has evolved with three purposes in mind. The first objective of this study is to analyze, evaluate and compare currently available analytical and numerical methods for vertical ground-loop heat exchangers with primary focus on system design and simulation. This will lay the necessary foundations for the ensuing work of developing an alternative design and simulation model and provide insights into various aspects of model practicality with respect to analyzing short time building dynamics.

The long-term response of borehole fields are commonly described by non-dimensional response curves known as ‘g-functions’ as developed by Eskilson (1987). (A detailed discussion of Eskilson’s model is provided in later sections) These are best suited to describe the performance of a particular borehole field configuration over the

time scale of a single month to several years. Thus, the second purpose of the research study is to calculate, by extending the long time-step response factors, the short time temperature response to pulses of heat and to derive similar non-dimensional response curves for periods less than one month to enable the analysis of short time ground loop heat exchanger dynamics. Such response curves can provide a computationally efficient method of determining the borehole thermal response for building energy simulation.

The third objective is to find the thermal properties of ground formation surrounding ground loop heat exchanger boreholes from short time scale test data by an inverse method. In this technique, the numerical model of the borehole is used in a parameter estimation algorithm where the ground formation and grout thermal properties such as the conductivity and the volumetric specific heat values are the parameters to be estimated. The objective function is defined as the sum of the mean square errors between the experimental temperatures and those predicted by the numerical model for a given set of parameter values. By minimizing the objective function, the “best” values of the ground formation and grout thermal conductivities are found.

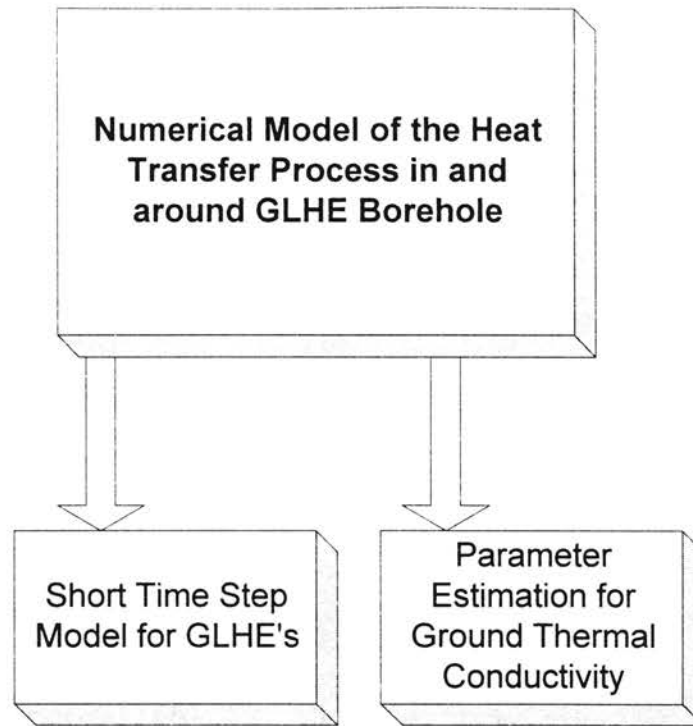


Figure 3.1. *Objectives.*

In summary, a numerical model of the vertical ground loop heat exchanger is developed that is used for the computation of short time-step temperature response factors. The model is also used inside a parameter estimation procedure to predict the thermal conductivity of ground formation surrounding the borehole. The response factors borehole model is cast as a TRNSYS component model and validated against experimental field data using an actual building. A detailed example using an actual small office building that uses a hybrid ground source heat pump system is described to illustrate the use of the short time step model.

4. TRANSIENT, TWO-DIMENSIONAL NUMERICAL MODEL OF THE VERTICAL GROUND HEAT EXCHANGER

A simplified representation of the numerical domain implemented to simulate the heat transfer in and around a ground heat exchanger borehole is provided in Figure 4.1. Since there is a symmetry axis through the borehole, only one half of the borehole is modeled. The exact grid resolution is a function of the borehole and U-tube pipe geometry and is determined by an automated parametric grid generation algorithm. The radius of the numerical domain needs to be selected large enough to allow for reasonably long simulation times.

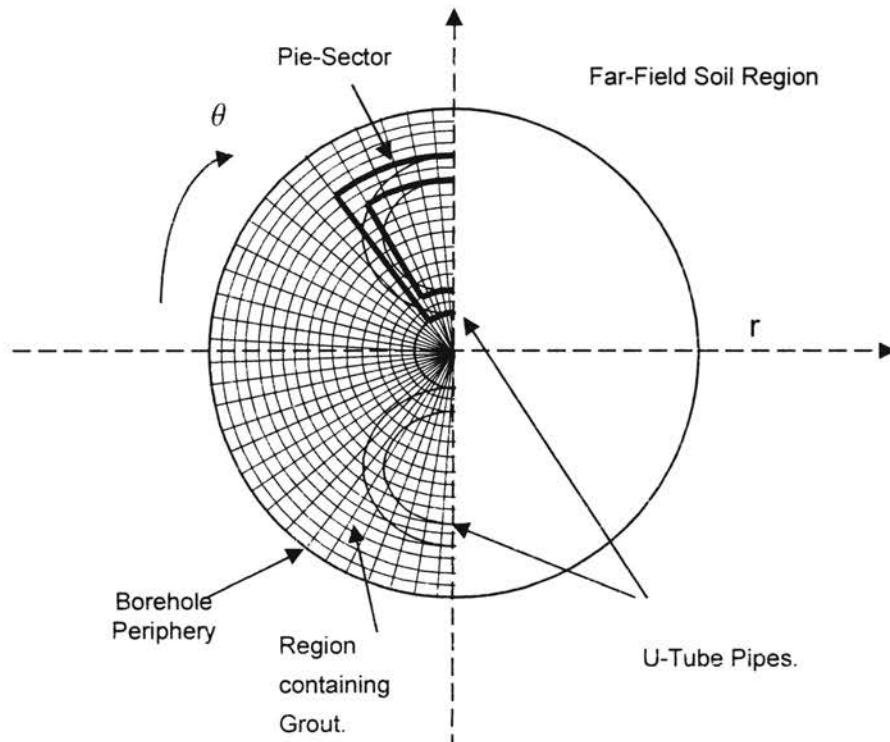


Figure 4.1. *Simplified representation of the borehole region on the numerical model domain using the pie-sector approximation for the U-tube pipes.*

The geometry of the circular U-tube pipes is approximated by “pie-sectors” over which a constant flux is assumed to be entering the numerical domain for each time step. The idea of the pie-sector approximation is based on simulating the heat transfer conditions through a circular pipe by matching the inside perimeter of the circular pipe to the inside perimeter of the pie-sector and by establishing identical heat flux and resistance conditions near the pipe walls. The convection resistance due to the flow of the heat transfer fluid inside the U-tubes is accounted for through an adjustment on the conductivity of the pipe wall material.

4.1. FINITE VOLUME APPROACH

Transient heat conduction in the ground loop heat exchanger is represented here in two dimensions. A two dimensional (horizontal) representation is reasonable if a number of assumptions are made.

- Three-dimensional effects at the ground surface and end of the U-tube are neglected.
- In-homogeneities in the ground formation properties are neglected.
- The effects of changing pipe temperature with depth are approximated.

The transient conduction equation in polar co-ordinates is expressed as:

$$\frac{1}{\alpha} \frac{\partial T}{\partial t} = \frac{\partial^2 T}{\partial r^2} + \frac{1}{r} \frac{\partial T}{\partial r} + \frac{1}{r^2} \frac{\partial^2 T}{\partial \theta^2} \quad (4.1)$$

This equation is discretized using a fully implicit finite volume approach (Patankar 1980, 1991). The typical arrangement of the finite volume cells on the polar grid is shown in Figure 4.2.

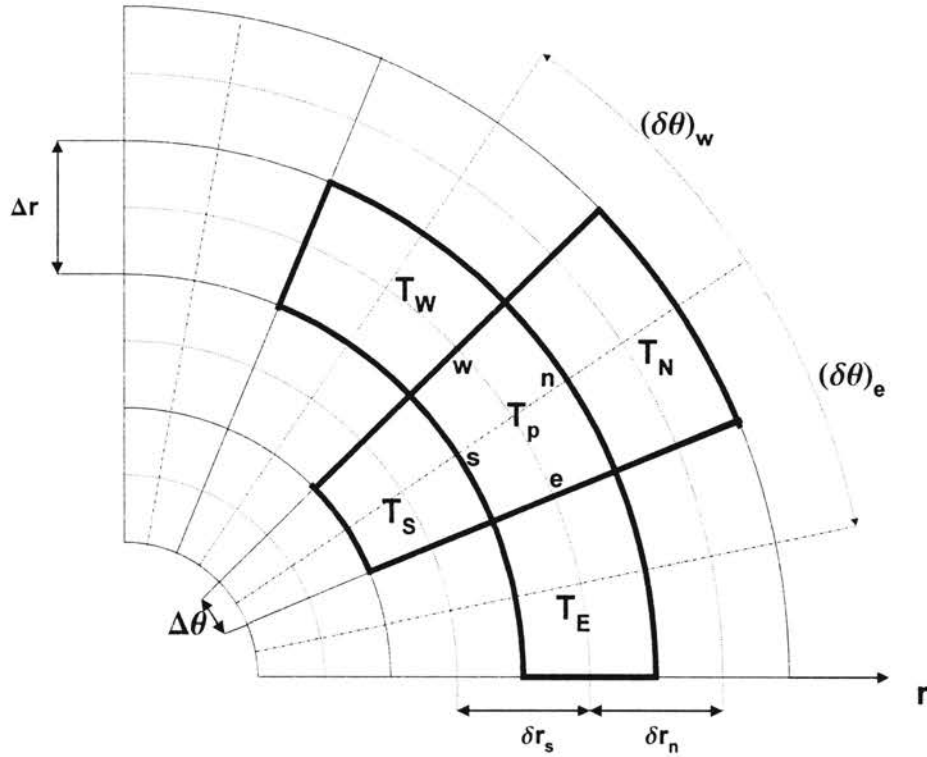


Figure 4.2. Notation of the Finite Control Volumes.

Using first order backwards differencing in time and second order central differencing in space the discrete equation is expressed as

$$a_p T_p = a_e T_e + a_w T_w + a_n T_n + a_s T_s + b \quad (4.2)$$

where

$$a_p = a_E + a_W + a_N + a_S + a_p^0 \quad (4.3)$$

and the coefficients a_n and b are defined as follows:

$$a_p^0 = \frac{(\rho c)_p \Delta V}{\Delta t} \quad (4.4)$$

$$a_E = \frac{k_e \Delta r_e}{r_e (\delta\theta)_e} \quad (4.5)$$

$$a_W = \frac{k_w \Delta r_w}{r_w (\delta\theta)_w} \quad (4.6)$$

$$a_N = \frac{k_n r_n \Delta\theta_n}{(\delta r)_n} \quad (4.7)$$

$$a_S = \frac{k_s r_s \Delta\theta_s}{(\delta r)_s} \quad (4.8)$$

$$b = S_C \Delta V + a_p^0 T_p^0 \quad (4.9)$$

The resulting algebraic equations are linear (the material properties being kept constant) and are solved with reasonable efficiency using a line-by-line Tri-diagonal matrix algorithm with block correction (Patankar 1991).

4.2. PARAMETRIC GRID GENERATION

An algebraic algorithm is developed to automatically generate numerical grids in polar coordinates for the ground loop heat exchanger geometry. This allows grids to be generated on the fly for a variety of borehole diameters, pipe diameters and pipe shank spacing combinations by varying a few control parameters. Advantage is taken of the symmetry of the borehole and U-tube assembly so that only half of each pipe of the U-tube is modeled (see Figure 4.3). The outer extent of the domain is selected so that it is large enough to approximate that of an infinite medium within the time scale of the calculations i.e. the boundary temperature does not rise above the initial condition or the boundary heat flux change from zero. Initial test simulations using the line source approach with calculations up to 200 hours indicated that an outer radius of 12 ft. (3.6 m.) was sufficiently large.

Temperature gradients nearest the U-tube pipes are generally the steepest—particularly when the short time scale thermal response is considered. The grid is designed accordingly denser in this region, with the actual grid spacing being largely determined by the need to accurately represent the pipe geometry as discussed below. Beyond the borehole, the grid spacing is gradually expanded in the radial direction to the domain boundary.

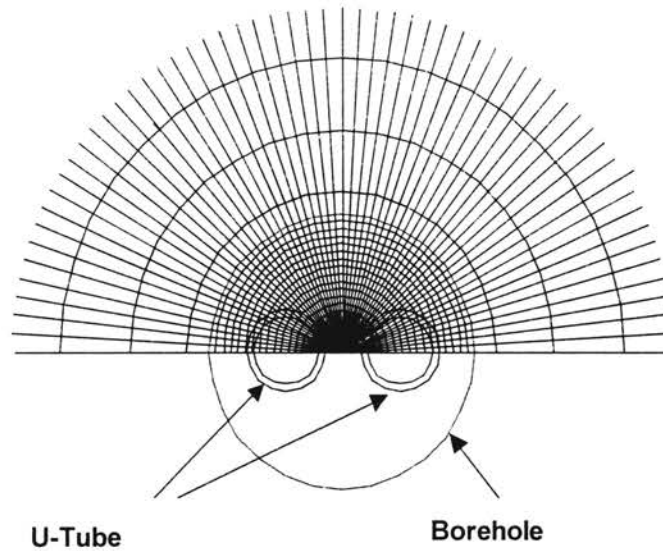


Figure 4.3. *Example numerical grid near the borehole center.*

4.3. PIE-SECTOR APPROXIMATION

Although it is straightforward to represent other borehole elements on the cylindrical coordinate system, care needs to be taken in the representation of the circular U-tube legs in the numerical domain. The polar coordinate system does not allow for a direct representation of a circular element that is offset from the center of the domain. A ‘pie-sector’ approximation of the circular pipe geometry is implemented, as shown in Figures 4.1 and 4.4.

The parametric grid generation algorithm determines the exact size and position of the pie-sector along with the thickness and the number of the cells representing the pipe wall. This allows the numerical grid to be quickly configured for a wide range of U-tube and borehole geometries. It will not have to be reconfigured manually for each

specific U-tube and borehole geometry. Referring to Figure 4.4, the geometry of the pie sector is determined as follows. The position of the pie sector within the grid (point A') is firstly computed by the shank spacing, which is made one of the input parameters. Since the pipe wall thickness is made an input parameter, the inside and the outside wall radii for the pie-sector on the domain can be determined (points A' and B'). Between points D and C, the cells representing the pipe vary in thickness and so the thickness at the mid-point of D-C needs to be fixed at the pipe thickness. The inside radial distance of the pie-sector (distance A-B) is fixed to correspond to the inside diameter of the pipe.

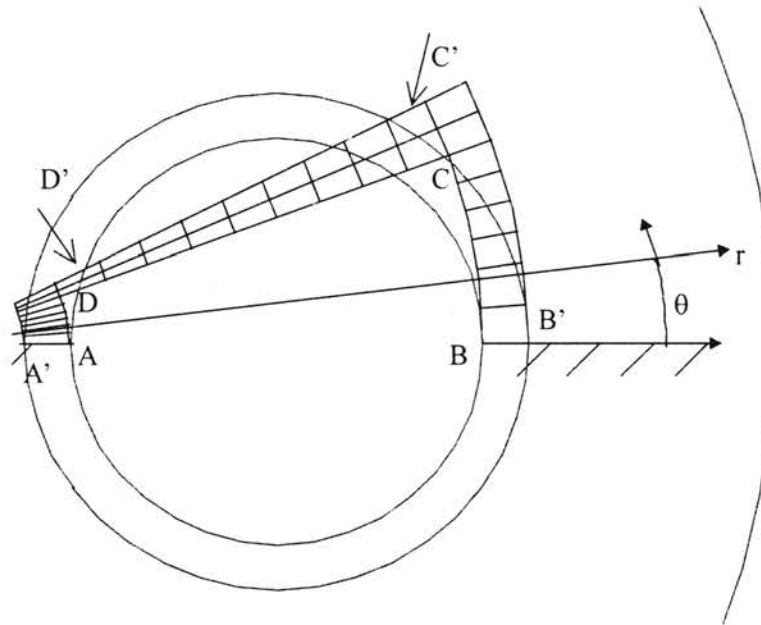


Figure 4.4. *The pie sector representation of the U-tube pipe.*

In order to approximate the heat flux boundary conditions at the pipe wall in the pie sector geometry, the inside perimeters have to be made equal. This is achieved by adjusting the distance between points B-C-D-A. It is convenient to use a fixed angular grid spacing $\Delta\theta$ throughout the whole domain, so that the distances A-D and B-C are

functions of the number of cells between these points and the total number of cells in the θ direction. This requires an iterative process until the perimeter of the pie sector closely matches, but is slightly greater than the pipe perimeter. Initial simulations showed that with approximately 200 cells in the radial and 100 in the θ direction the perimeter is matched to within 0.05%.

A further consideration, given the implementation of the boundary conditions via source terms, is the number of cells that are used to represent the pipe wall. A range of values is used and the corresponding sensitivity is investigated to arrive at the 'optimum' grid configuration.

4.4. BOUNDARY CONDITIONS

The fluid in the pipes of the U-tube is not explicitly modeled and so the heat transfer from the fluid is treated by a heat flux boundary condition at the pipe walls. This heat flux is fixed for the unit depth of borehole modeled but some attempt has been made to account for the variation of temperature between the flow and return legs of the U-tube. This has been done by assigning 60% of the total heat flux to one leg, and 40% to the adjacent leg. Although this heat transfer distribution is somewhat arbitrary and a fixed ratio may not be ideal, a sensitivity analysis showed only insignificant differences in average borehole temperature predictions when the distribution was varied between the 0%-100%-case and the 50%-50%-case. It is safe to assume that the fluid first entering the loop at a temperature T_m will typically display a higher temperature gradient relative

to the constant ground far field temperature $T_{farfield}$ than the fluid exiting the loop at a temperature of T_{out} , so that $|T_m - T_{farfield}| > |T_{out} - T_{farfield}|$.

At the start of the simulation, a constant far-field temperature (normally equal to the undisturbed ground temperature) is assumed to be effective over the entire domain. The physical domain is represented as a semi-circular grid by making use of the symmetry of the borehole geometry. The conditions at the symmetry plane are equivalent to a zero heat flux condition. At the outer edge of the domain (in the radial axis) a constant far-field temperature condition is applied. The amount of heat flux at the outer edge of the domain is continuously checked and verified to be zero or insignificantly small.

On the boundary surface of each of the finite control volumes along the perimeter of the pie-sector, a constant heat flux term is applied entering/exiting the numerical domain. The amount of this flux is matched with a constant flux that would be transferred through a unit depth of pipe. As the code used here (Patankar 1991) has no convenient way of applying wall heat flux boundary conditions at cells interior to the domain, the boundary conditions at the pipe inside surface have been implemented via source terms in the cells comprising the inside of the pipe wall. Since the volume of each control volume changes along the perimeter of the pie-sector, the source terms applied in these cells vary for a given boundary heat flux so that,

$$S_C = \frac{q_B A_{i,j}}{\Delta V_{i,j}}, \quad (4.10)$$

where S_C is the source term, $q_{B,i,j}$ is the boundary flux, $A_{i,j}$ is the boundary surface area, and $\Delta V_{i,j}$ is the volume of the corresponding cell.

4.5. CONVECTIVE RESISTANCE ADJUSTMENT

In order to be able to simulate the effects of the convective resistance due to fluid flow inside the U-tube pipe, an effective pipe conductivity is calculated using a combined convective and conductive resistance. The pipe resistance in Equation (4.11) and the convective resistance in Equation (4.12) are added to determine an effective resistance as given in Equation (4.13).

$$R_{pipe} = \frac{r_{out} \ln\left(\frac{r_{out}}{r_{in}}\right)}{k_{pipe}}, \quad (4.11)$$

$$R_{Convection} = \frac{1}{h_{in} \frac{r_m}{r_{out}}}, \quad (4.12)$$

$$R_{Eff} = \frac{r_{out} \ln\left(\frac{r_{out}}{r_{in}}\right)}{k_{Eff}}. \quad (4.13)$$

Considering that the total effective resistance is the sum of resistances due to convection and conduction and solving for k_{Eff} yields:

$$\frac{1}{k_{Eff}} = \frac{1}{k_{Pipe}} + \frac{1}{h_m \left(\frac{r_m}{r_{out}}\right) r_{out} \ln\left(\frac{r_{out}}{r_m}\right)}. \quad (4.14)$$

Using the Dittus-Boelter relation to approximate the Nusselt number for the pipe inside convection coefficient h_m , the equation (4.14) can be re-written as:

$$k_{Eff} = \left[\frac{1}{k_{Pipe}} + \frac{2}{\left[0.023 \text{Re}^{0.8} \text{Pr}^{0.35}\right] k_{Fluid} \ln\left(\frac{r_{out}}{r_m}\right)} \right]^{-1} \quad (4.15)$$

In equation (4.15), the exponent of the Prandtl number is averaged to account for both the heat extraction and rejection cases where the convective resistance is expressed as:

$$h_m = \frac{(0.023 \text{Re}^{0.8} \text{Pr}^{0.35}) k_{Fluid}}{D_m}, \quad (4.16)$$

It has been noted that the cells of the numerical grid representing the pipe wall vary in thickness due to the nature of the polar coordinate grid. In order to ensure a constant effective pipe wall thermal resistance some adjustment of the thermal

conductivity of these cells is necessary dependent on their thickness. The following linear approximation is used to adjust the conductivity for the thickness:

$$k_{Eff-Modified}(\theta) = k_{Eff} \frac{TotalCellWidth(\theta)}{PipeWallThickness} \quad (4.17)$$

4.6. MODEL VALIDATION AND ERROR ANALYSIS

Exact analytical solutions of the two-dimensional conduction heat transfer problem in a U-tube/borehole geometry, or a pie sector representation of it, do not exist. In view of this, some validation of the numerical method is attempted using a related problem with known analytical solutions in one dimension. In seeking to validate the numerical method, the first aim is to examine the significance of representing the pipes of the U-tube by a pie sector arrangement of cells. The second is to investigate the sensitivity of the solution to grid density and time step size.

The most comparable analytical case to that modeled numerically is that of transient conduction through an infinitely long hollow cylinder (with the inside and outside cylindrical surfaces co-axial). The numerical method was initially tested for this simpler co-axial geometry in order to verify that proper aspect ratios and the appropriate number of divisions have been selected. The numerical model results using a pie sector representation of a single pipe is compared with the analytical solution of a hollow cylinder, so that the effect of the simplified pipe geometry can be quantified. In these tests the numerical domain outside of the pipe is assigned a single value of thermal

conductivity (i.e. grout material was given the same thermal properties as the ground formation). The boundary conditions are a constant heat flux at the inside surface of the hollow cylinder at $r = r_{in}$ and a constant far-field temperature (equal to the initial temperature of the entire domain) at the outside surface at $r = r_{out}$. The implementation of these boundary conditions yields the following analytical solution for the temperature as a function of time and the radial coordinate (Carslaw and Jaeger 1947).

$$T(r,t) = \frac{r_{in} q_c}{k} \log\left(\frac{r_{out}}{r}\right) + \frac{\pi q_c}{k} \sum_{n=1}^{\infty} e^{-\alpha \beta_n^2 t} \frac{J_0^2(r_{out} \beta_n) [J_0(r \beta_n) Y_1(r_{in} \beta_n) - Y_0(r \beta_n) J_1(r_{in} \beta_n)]}{\beta_n [J_1^2(r_{in} \beta_n) - J_0^2(r_{out} \beta_n)]}$$

(4.18)

where β_n 's are the positive roots of

$$J_1(r_{in} \beta) Y_0(r_{out} \beta) - Y_1(r_{in} \beta) J_0(r_{out} \beta) = 0 \quad (4.19)$$

Comparisons have been made between the time varying temperatures at the inside surface of the cylinder with the numerical result being given by an area weighted average of the inside surface temperature of the pie-sector cells. In order to make a meaningful comparison between the analytical solution and the numerical results, a modification is to the temperature given by the above analytical solution to account for the additional resistance at the inside pipe wall, which is accounted for in the numerical model. This has been done by calculating an increase in resistance that would normally apply in

steady state conditions. This is given in terms of an adjustment to the inside pipe surface temperature given by the analytical solution as follows:

$$\Delta T_{adj.} = \frac{Q_c}{2\pi r_m L} \left\{ \frac{r_m \ln\left(\frac{r_{out}}{r_m}\right)}{k_{pipe}} + \frac{1}{h_m} \right\} \quad (4.20)$$

Although some error is introduced by assuming this resistance, which is the same as in steady state conditions, this error diminishes rapidly with time.

4.6.1. VALIDATION TEST CASES

Six different test cases were established for making the comparisons between the numerical results and the analytical solutions. These used a range of different pipe diameters, far field temperatures, heat fluxes and thermal conductivities. The borehole geometry and material thermal properties have been selected to include common values used in vertical ground loop heat exchangers. In the test cases the applied heat fluxes varied between 212 Btu/hr-ft² (668.6 W/m²) and 135 Btu/hr-ft² (425.7 W/m²). The parameters varied between each of the test cases are given in Table 4.1. The remaining parameters common to all test cases are given in Table 4.2. All of the test case calculations were run for a simulated time of 192 hours.

TABLE 4.1

Input Data varied for model validation test cases

Property	Test Case					
	1	2	3	4	5	6
Q Btu/hr-ft ² (W/m ²)	211.9 (668.5)	211.9 (668.5)	169.7 (535.4)	169.7 (535.4)	134.4 (423.9)	134.4 (423.9)
$T_{farfield}$ F (C)	63.0 (17.2)	48.0 (8.9)	63.0 (17.2)	48.0 (8.9)	63.0 (17.2)	48.0 (8.9)
k_{soil} Btu/hr-F-ft (W/m-K)	1.5 (2.6)	1.0 (1.73)	1.5 (2.6)	1.0 (1.73)	1.5 (2.6)	1.0 (1.73)
k_{grout} Btu/hr-F-ft (W/m-K)	1.5 (2.6)	1.0 (1.73)	1.5 (2.6)	1.0 (1.73)	1.5 (2.6)	1.0 (1.73)
$D'_{PipeOutc}$ ft. (mm)	0.0875 (26.5)	0.0875 (26.5)	0.1096 (33.4)	0.1096 (33.4)	0.1383 (42.2)	0.1383 (42.2)
$d_{PipeWall}$ ft. (mm)	0.0079 (2.4)	0.0079 (2.4)	0.01 (3.0)	0.01 (3.0)	0.013 (3.9)	0.013 (3.9)

TABLE 4.2

Input Data common to all validation test cases

k_{pipe} Btu/hr-F-ft (W/m-K)	0.226 (0.391)
$(\rho c)_{pipe}$ Btu/ft ³ -F (kJ/m ³ -K)	30.0 (2,012.1)
$(\rho c)_{soil}$ Btu/ft ³ -F (kJ/m ³ -K)	35.0 (2,347.5)
$(\rho c)_{grout}$ Btu/ft ³ -F (kJ/m ³ -K)	35.0 (2,347.5)
$r_{borehole}$ ft. (mm)	0.1458 (44.4)

4.6.2. SENSITIVITY TO GRID RESOLUTION AND TIME STEP

Given the way in which the heat flux boundary condition are applied at the cells representing the inside surface of the pipe—and the importance of the temperature gradient prediction in this region to the short time scale response— effort is made to investigate the grid independence of the numerical solution. This is done by making calculations with varying number of cells, say 1, 2, 4 or 8 cells, representing the thickness of the pipe wall. (As the number of cells in the pipe wall is increased in the radial direction, some increase in the number of cells in the angular direction is also required to ensure the cell aspect ratio is not excessive.) The temperature predictions have been compared in terms of relative error where the error is scaled according to the difference between the analytically determined surface temperature and the far field (initial) temperature at each time step so that,

$$RelativeError = \frac{[T_{Analytical} - T_{Predicted}]}{[T_{Analytical} - T_{FarField}]} \times 100(\%) \quad (4.21)$$

The resulting relative errors found after one hour and 192 hours of simulation time are given in Table 4.3. The distribution of the relative error with time for different grid resolutions at the pipe wall is given in Figure 4.5. It can be seen that there is a noticeable difference between the results with one and two cells representing the pipe wall. There is further improvement in agreement with the analytical temperatures as the grid density is increased to four and eight cells. However, there is a smaller difference between the cases

TABLE 4.3

**Relative error (%) between the analytical and numerical results
for each test case at 1 and 192 hours simulated time (3-min. time steps)**

		Case #1		Case #2		Case #3		Case #4		Case #5		Case #6	
Time		1 hr	192hr	1 hr	192hr	1 hr	192hr	1 hr	192hr	1 hr	192hr	1 hr	192hr
Number of Cells	1	-4.48	-2.51	-3.24	-1.58	-5.39	-3.14	-3.80	-2.11	-1.95	-0.32	-1.43	-0.11
	2	-0.62	-0.48	-0.08	-0.93	-1.70	-1.63	-0.48	-0.83	-2.07	-1.75	-0.80	-0.88
	4	2.91	-0.49	3.44	-0.02	2.62	-0.57	3.17	-0.06	1.85	-0.62	2.65	-0.13
	8	11.15	1.29	8.88	0.32	8.59	0.03	8.49	0.75	8.28	0.69	8.06	0.43

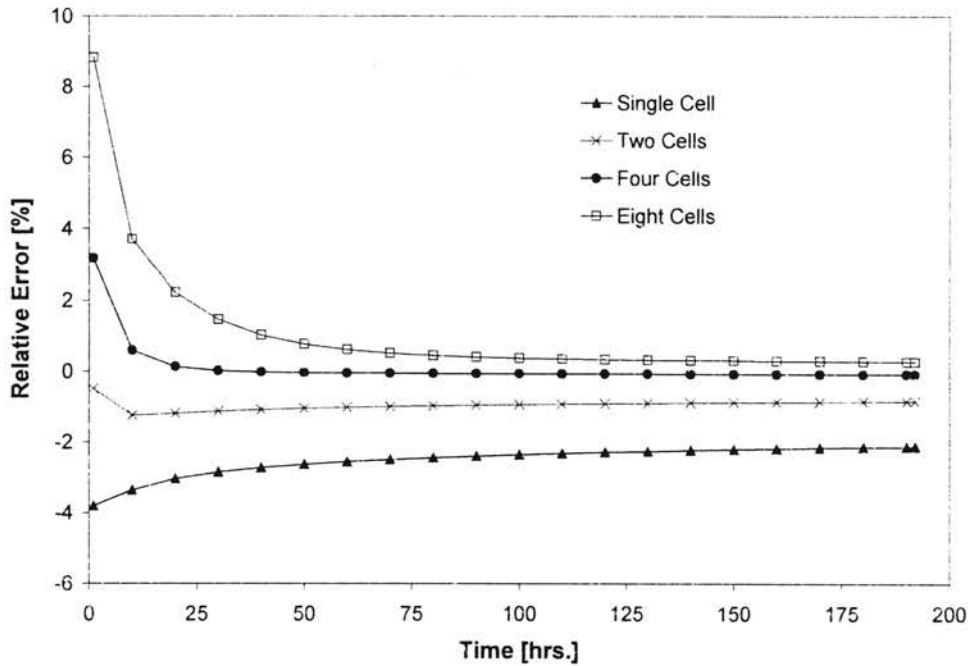


Figure 4.5 Variation of the relative error of the calculated temperature with different grid resolution for the pipe wall thickness (for Test Case #4 with 3-minute time steps).

with four and eight cells. From these results, four cells representing the thickness of the pipe wall was selected as the most appropriate number to simulate the pipe geometry with

the pie-sector approximation. The relative error for this case is consistently less than 1% after 192 hours of simulation time (Table 4.3) and further increase in the grid resolution does not appear to justify the increased computational cost.

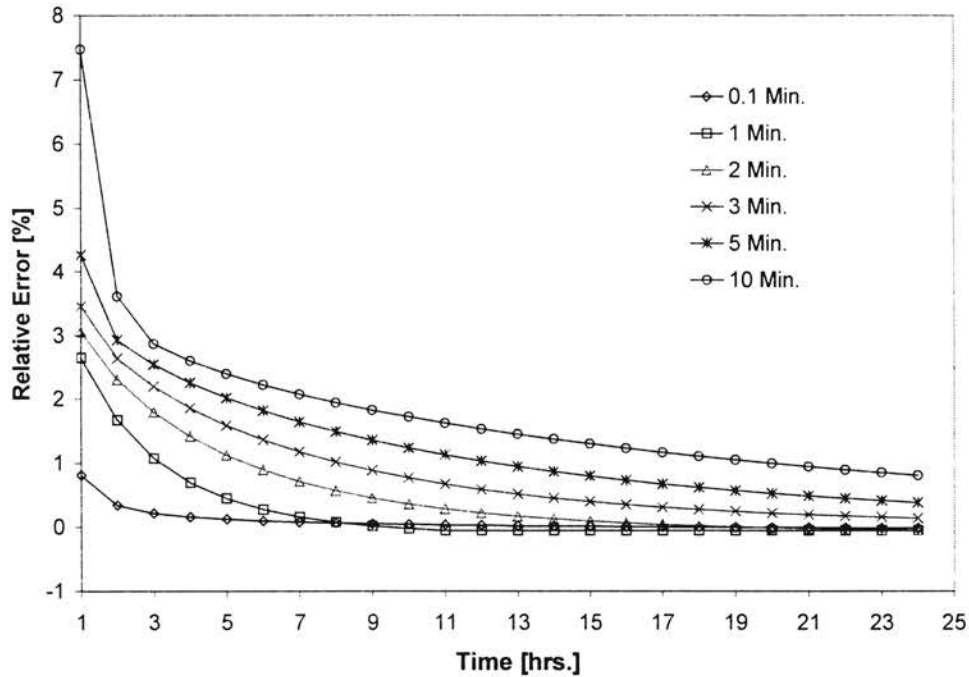


Figure 4.6 Variation in the relative error of the calculated temperature with time step size (Test Case #4).

The first order fully implicit backward differencing in time approach taken here has the advantage that the numerical solution is stable with a wide range of time step size. This differencing scheme however, gives only first order accuracy in time and some variation in accuracy with time step size could be expected. In view of this, calculations were made using the parameters of test case number 4 and with time steps in the range 0.1-10 minutes. The resulting variation in the relative error of the temperature prediction using this range of time steps is shown for the first 24 hours of the calculation in Figure 4.6. The relative errors can be seen to decrease with smaller time steps and are generally

greatest near the beginning of the calculation. This later feature can be expected as under these boundary conditions the rate of temperature change decreases with time. As the pipe surface temperature approaches the steady-state value, the relative influence of the time step on the temperature predictions therefore becomes smaller. Again there is a point of diminishing returns in selecting a shorter time step size in light of the increased computing times. Three-minute time steps were chosen for use in further analysis on the basis of it being a reasonable compromise between prediction accuracy and computational speed.

The parametric grid generation scheme is intended to deal with U-tubes with a range of shank spacing. (Shank spacing is defined here as the size of the gap between the pipes of the U-tube.) One feature resulting from the representation of the pipe by a pie sector is that its exact shape in the grid varies depending on the shank spacing (i.e. distance from the origin). This arises because in order to match the perimeter of the pipe with that of the pie-sector the included angle of the pie-sector has to increase if it is positioned nearer the origin. When comparing the calculated temperature for a single pipe with those of the analytical model, as here, one would ideally want the predictions to be insensitive to the position of the pipe in the numerical domain. (Where there are two pipes with heat fluxes applied however, there may be some real sensitivity to shank spacing.)

To examine the sensitivity of the results to the position of the pie sector a number of calculations were made with the position from the grid origin varying from 0.012 ft.

(3.6mm) to 0.037 ft (11.3mm) and other parameters as test case number 4. The resulting error distribution for these calculations is shown in Figure 4.7. Again, the errors appear largest near the beginning of the calculation. The smallest errors are given by the cases with the pie-sector having the smaller offset from the origin. However, the relative error for each of these calculations is contained within a band of less than 1 % after about 12 hours indicating that the sensitivity of the comparison with the analytical solution to pie-sector position is only very slight.

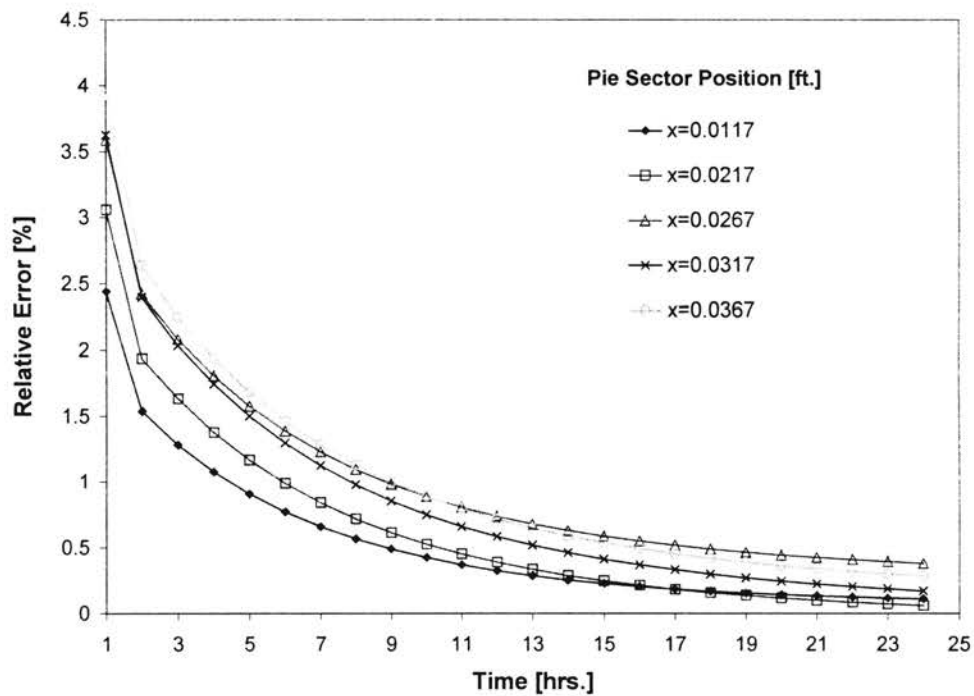


Figure 4.7 Variation in the relative error of the calculated temperature with pie-sector position (Test Case #4).

The grid generation and time stepping practice finally adopted was to use four grid cells to represent the pipe wall thickness and to use time steps of 3 minutes. Figure

4.8 shows the results for test case number four where the predicted inner surface temperature is shown against that given by the analytical model. In this case the relative error is about 3% after the first hour of simulation and decreases to a value of approximately 0.15% of the total temperature rise after the 24th hour, reducing to a final value of 0.06% after 192 hours. Figure 4.9 illustrates the same results plotted for the first hour. Even though some lag is observed in the predicted temperature over the first hour, the relative error remains small and diminishes thereafter. The absolute temperature error after the first three minutes is approximately 2.7°F (1.5°C) decreasing to 0.5°F (0.28°C) after thirty minutes. Similar behavior was observed in other five test cases, where the average relative error was found to be smaller than 1% of the temperature rise.

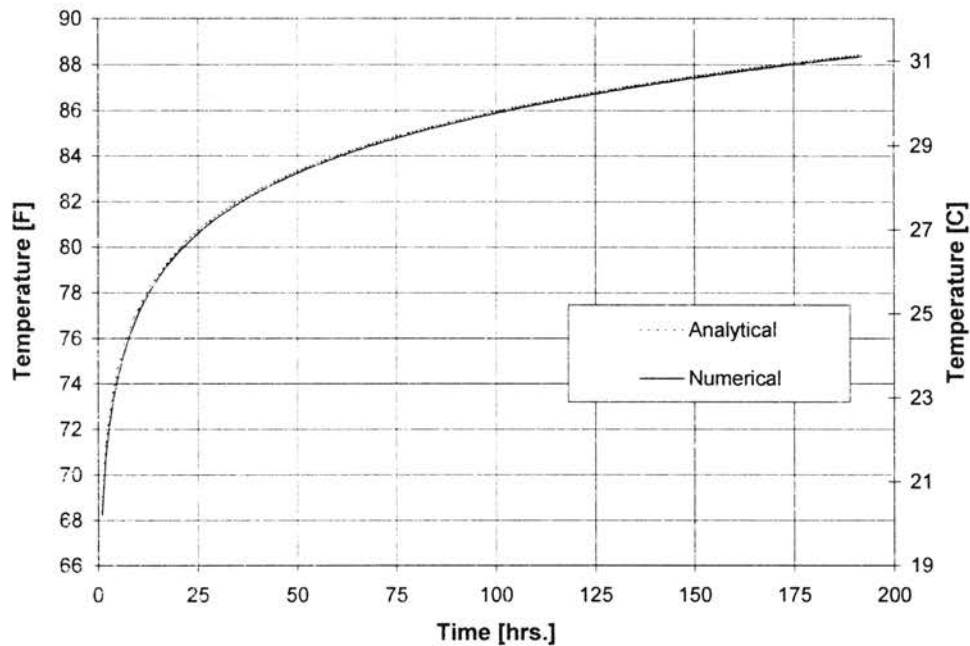


Figure 4.8 Comparison of the numerical and analytical model temperature predictions. Test Case #4. Pipe Wall Thickness approximated with four Cells. Time Step = 3 minutes.

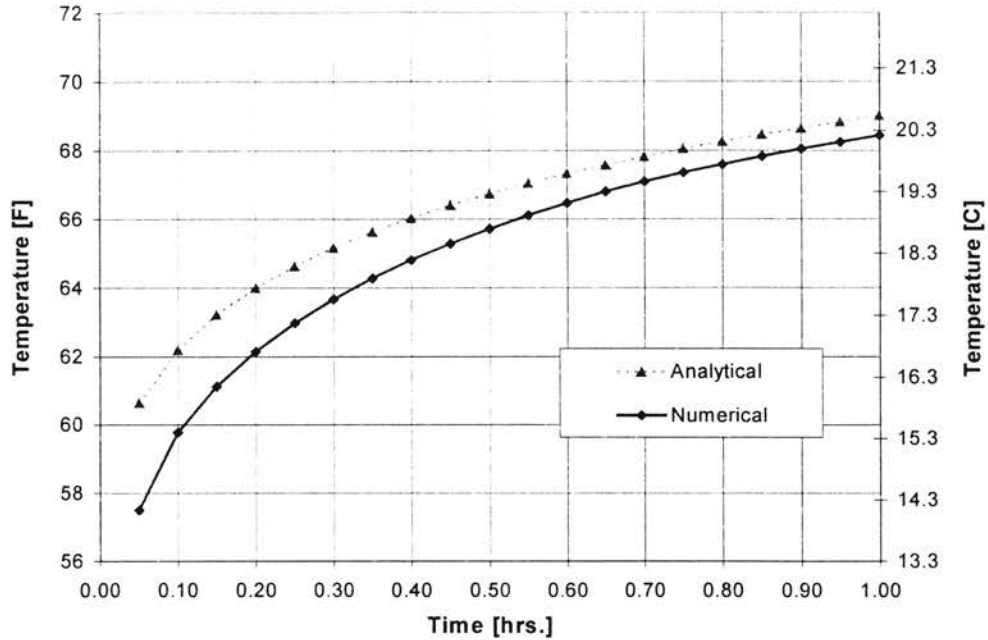


Figure 4.9 Comparison of the numerical and analytical model temperature predictions over the first hour of simulation (Test Case #4).

4.7. DISCUSSION OF THE RESULTS

A transient, two-dimensional finite volume numerical model has been developed for calculation of conduction heat transfer in and around the borehole of a vertical U-tube ground loop heat exchanger. A method has been devised that allows the numerical grid for a range of borehole and U-tube configurations to be generated automatically from a small set of geometric parameters.

A range of calculations was made to validate the results of the numerical model against the time varying temperatures given by a comparable analytical model. The grid generation practices and time step size have been refined so that the numerical model is capable of predicting the pipe surface temperature with an average relative error of

$\pm 1\%$ compared to the analytically calculated temperature. The errors were found to be more significant in the first hours of simulation where the temperature differences were smallest and the rate of change of temperature greatest. The errors always diminished rapidly and became insignificant before the end of 192-hour period considered here. These errors are considered acceptably small for the prediction of short time scale response of the heat exchanger for design and simulation purposes.

Although the discretization errors have been adequately minimized, and the pie-sector representation of the pipe geometry in the polar coordinate system shown to be sufficient, this has required a notably dense computational grid (approximately 100 by 200 cells). Further benefit may be gained by using a boundary-fitted grid system that would allow more accurate representation of the borehole geometry. Such an approach may also require a less dense grid for a given level of accuracy and therefore offer some decrease in computational load.

The numerical model is developed for use in two applications that require the prediction of the short time scale response of the borehole. The first is to provide the thermal response of the heat exchanger on shorter time scales (up to one month) for heat exchanger design purposes and component-based simulation (See Chapter 5). This has been done by using the numerical model to derive non-dimensional thermal response curves (Yavuzturk and Spitler 1999). The second application is modeling the short-term response under in-situ conductivity test conditions (See Chapter 8). In this case, the model has been used to solve the inverse heat transfer problem associated with estimating

5. SHORT TIME-STEP RESPONSE FACTOR MODEL

5.1. ESKILSON'S LONG TIME-STEP TEMPERATURE RESPONSE FACTOR MODEL

Eskilson's (1987) approach to the problem of determining the temperature distribution around a borehole is a hybrid model combining analytical and numerical solution techniques. A two-dimensional numerical calculation is made using the transient finite-difference equations on the radial-axial coordinate system for a single borehole in homogeneous ground with constant initial and boundary conditions. The capacitance of the individual borehole elements such as the pipe wall and the grout are neglected. The solution obtained using a basic step pulse allows the calculation of response to any heat input by considering piece-wise constant heat extractions/rejections and superpositioning them in time as a series of step pulses.

The temperature response of the borehole from the discretized equations is converted to a series of non-dimensional temperature response factors. (Eskilson calls these response factors g-functions. They should not be confused with g-functions used in the cylinder source solution.) The g-function allows the calculation of the temperature change at the borehole wall in response to a step heat input for a time step. Once the response of the borehole field to a single step heat pulse is represented with a g-function, the response to any arbitrary heat rejection/extraction function can be determined by

devolving the heat rejection/extraction into a series of step functions, and superimposing the response to each step function.

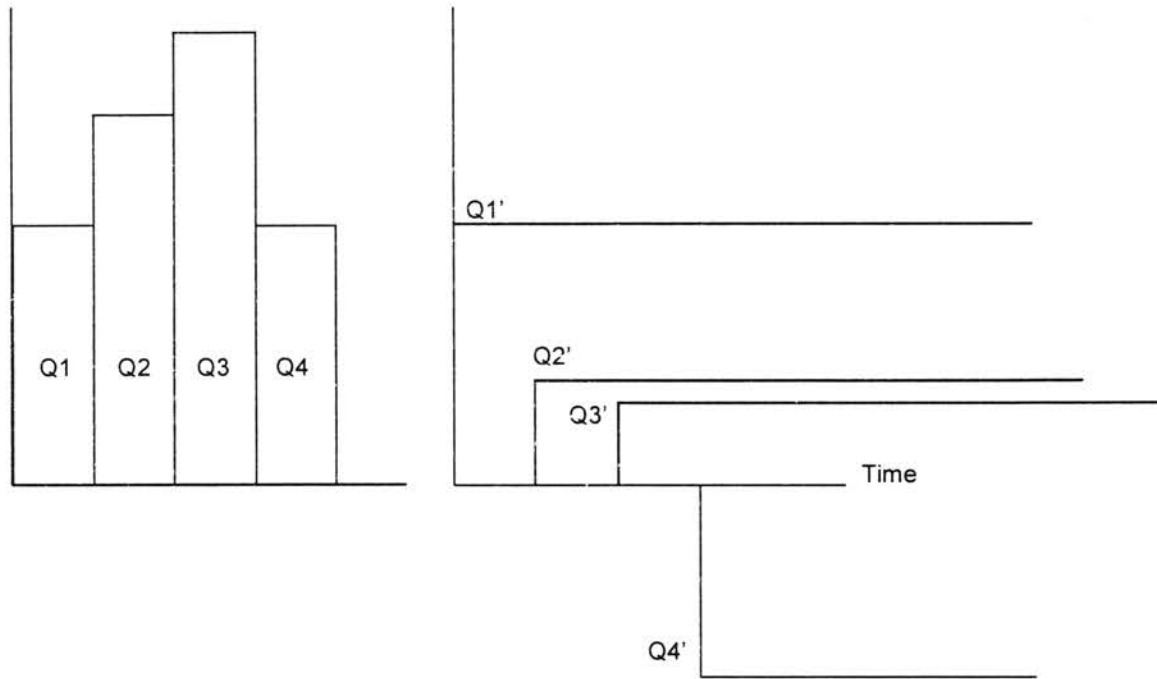


Figure 5.1. *Superposition of piece-wise linear step heat inputs in time. The step heat inputs Q_2 , Q_3 and Q_4 are superimposed in time on to the basic heat pulse Q_1 .*

This process is graphically demonstrated in Figure 5.1 for four months of heat rejection. The basic heat pulse from zero to Q_1 is applied for the entire duration of the four months and is effective as $Q_1' = Q_1$. The subsequent pulses are superimposed as $Q_2' = Q_2 - Q_1$ effective for 3 months, $Q_3' = Q_3 - Q_2$ effective for 2 months and finally $Q_4' = Q_4 - Q_3$ effective for 1 month. Thus, the borehole wall temperature at any time can be determined by adding the responses of the four step functions. Mathematically, the superposition gives the borehole temperature at the end of the n^{th} time as:

$$T_{borehole} = T_{ground} + \sum_{i=1}^n \frac{(Q_i - Q_{i-1})}{2\pi k} g\left(\frac{t_n - t_{i-1}}{t_s}, \frac{r_b}{H}\right) \quad (5.1)$$

where:

t = time (s)

t_s = time scale = $H^2/9\alpha$

H = borehole depth ft (m)

k = ground thermal conductivity Btu/hr-ft-°F (W/m-°C)

$T_{borehole}$ = average borehole temperature in °F (°C)

T_{ground} = undisturbed ground temperature in °F (°C)

Q = step heat rejection pulse Btu/hr-ft (W/m)

r_b = borehole radius ft (m)

i = index to denote the end of a time step. (the end of the 1st hour or 2nd month etc.)

Figure 5.2 shows the temperature response factor curves (g-functions) plotted versus non-dimensional time for various multiple borehole configurations and compares them to the temperature response factor curve for a single borehole. The g-functions in Figure 5.2 correspond to borehole configurations with a fixed ratio of 0.1 between the borehole spacing and the borehole depth. The thermal interaction between the boreholes is stronger as the number of boreholes in the field is increased. The interaction increases as time of operation increases.

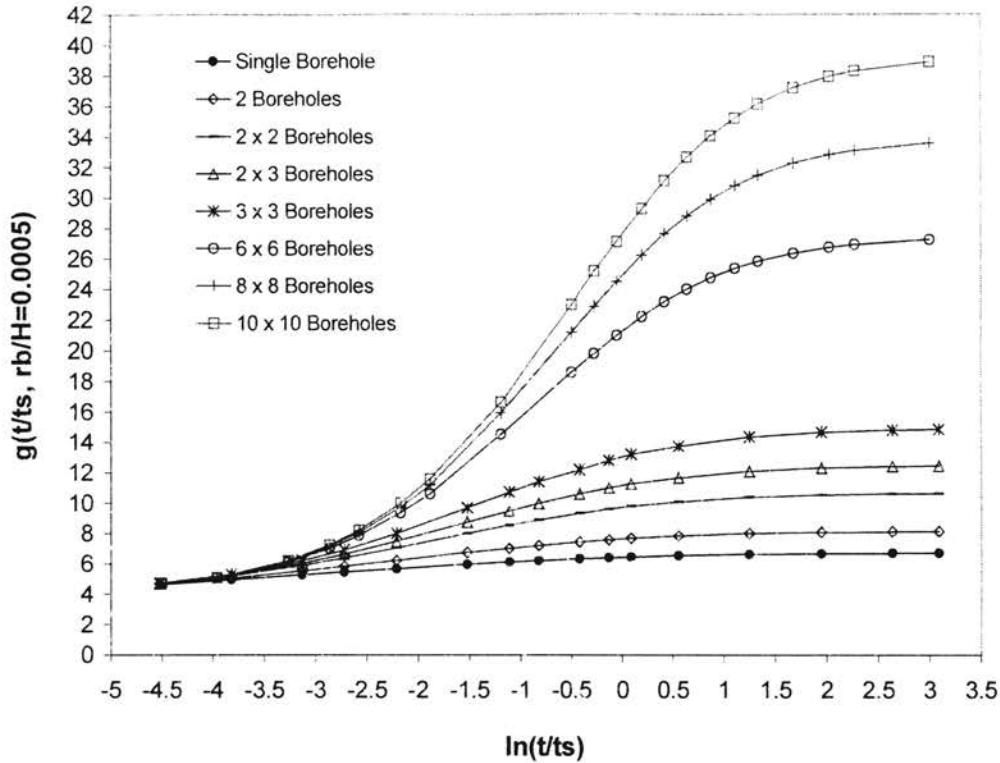


Figure 5.2. Temperature response factors (*g*-functions) for various multiple borehole configurations compared to the temperature response curve for a single borehole.

The detailed numerical model used in developing the long time-step *g*-functions approximates the borehole as a line source of finite length, so that the borehole end effects can be considered. The approximation has the resultant problem that it is only valid for times estimated by Eskilson, to be greater than $\frac{5r_{\text{Borehole}}^2}{\alpha}$. For a typical borehole, that might imply times from 3 to 6 hours. However, for the short time step model, it is highly desirable that the solution be accurate down to an hour and below. Furthermore, much of the data developed by Eskilson does not cover time periods of less than a month. (For a heavy, saturated soil and a 250 ft (76.2 m) deep borehole, the *g*-function for the single borehole presented in Figure 5.2 is only applicable to about 60 days.)

5.2. SHORT TIME-STEP TEMPERATURE RESPONSE FACTORS

The approach to extending the current long time-step model to short time steps involves the use of the numerical model, described in Chapter 4, to develop g-functions that are suitable for shorter time periods (hourly or less) than currently available. The numerical model is used to determine the time-dependent average borehole temperatures for a step pulse of a given borehole geometry and known ground thermal conductivity. The temperature response is non-dimensionalized to form g-function values.

5.2.1. DEVELOPMENT OF SHORT TIME-STEP g-FUNCTIONS

The numerical model that is used to compute short time-step average borehole temperatures uses a transient two-dimensional implicit finite volume discretization on a polar grid. It was developed to simulate the heat transfer over a vertical U-tube ground heat exchanger of a ground-source heat pump system and has been validated by comparison to applicable analytical solutions. The details of the numerical model is discussed in Chapter 4.

The numerical approach that is used to develop the short time-step g-functions also models the thermal effects of the individual borehole elements such as the resistance of the pipe and grout material due to heat conduction and the convection resistance due to the flow of the heat transfer fluid inside the U-tube pipes. Since the g-function values as

developed by Eskilson (Figure 5.2) do not include these thermal resistance effects, the short time-step g-function values need to be adjusted accordingly. The following relationships are used for the grout, U-tube pipes and the convection resistance per unit borehole length:

$$R_{\text{Grout}} = \frac{1}{k_{\text{Grout}} \beta_0 \left(\frac{D_{\text{Borehole}}}{D_{\text{Pipe}}} \right)^{\beta_1}} \quad (5.2)$$

$$R_{\text{Convection}} = \frac{1}{2\pi D_{\text{in}} h_{\text{in}}} \quad (5.3)$$

$$R_{\text{Pipe Conduction}} = \frac{\ln\left(\frac{D_{\text{out}}}{D_{\text{in}}}\right)}{4\pi k_{\text{Pipe}}} \quad (5.4)$$

$$R_{\text{Total}} = R_{\text{Grout}} + R_{\text{Convection}} + R_{\text{PipeConduction}} \quad (5.5)$$

where,

β_0, β_1 = Resistance shape factor coefficients (Paul 1996) based on U-tube shank spacing.

Paul's (1996) shape factor coefficients are based on experimental and finite element analysis of typical borehole and pipe geometry. Shape factor coefficients of

$\beta_0 = 20.100377$ and $\beta_1 = -0.94467$ are suggested for a typical 0.125" (3.2 mm) U-tube shank spacing.

R = thermal resistance in F per Btu/hr-ft (in C per W/m).

D = diameter in ft (m).

k = thermal conductivity in Btu/hr-ft-F (W/m-C).

h_{in} = convection coefficient based on the inside diameter in hr-ft²-F/Btu (m²-C/W).

The convection coefficient is determined with the Dittus-Boelter correlation:

$$h_{in} \cong \frac{0.023 Re^{0.8} Pr^n k_{Fluid}}{2r_{in}}, \quad (5.6)$$

where n=0.4 for heating and n=0.3 for cooling; a mean value of 0.35 is used.

The total borehole resistance in $\frac{F}{BTU/hr - ft}$ ($\frac{C}{W/m}$) for each time step is multiplied by the heat transfer rate per unit length of borehole for that time step to calculate the temperature rise adjustment. This temperature rise due to the total borehole resistance needs to be subtracted from the temperature value obtained through the numerical model to determine the actual temperature rise for that time step. Consequently, equation (5.1) is recast to solve for the g-function with a single step pulse and modified to account for the borehole thermal resistance:

$$g\left(\frac{t_1}{t_s}, \frac{r_b}{H}\right) = \frac{2\pi k \{T_{borehole} - (R_{Total} Q) - T_{ground}\}}{Q} \quad (5.7)$$

The resulting short time-step g-function values are plotted in Figure 5.3 side by side with the long time-step g-function values for a single borehole and an 8 X 8-borehole field as given by Hellstrom (1998)*.

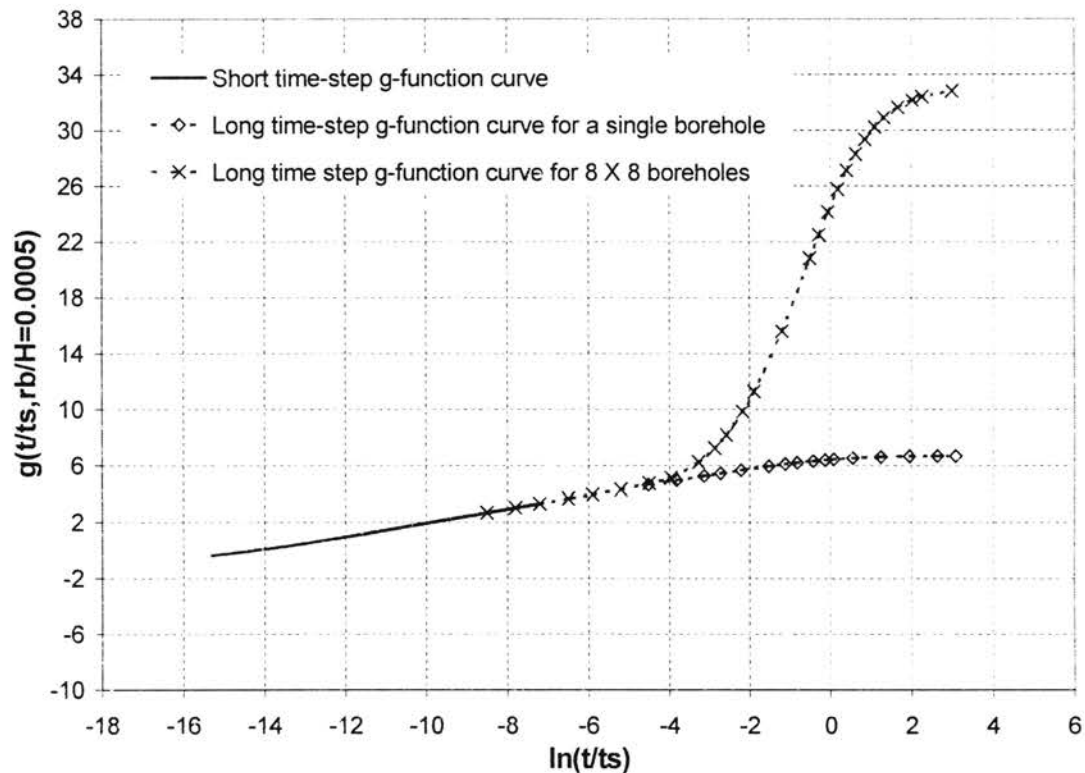


Figure 5.3. Short time-step g-function curve as an extension of the long time-step g-functions plotted for a single borehole and a 8 X 8 borehole field.

The independently generated short time-step g-functions line up very well with Eskilson's long time-step g-functions. They are stored as a series of points

* Figure 5.3 provides the g-functions for an 8X8-borehole field as extended by Hellstrom. Hellstrom appended the original g-functions of Eskilson using the line source approach for shorter time steps, thus allowing for time steps down to about 100 hours.

$[g(\frac{t}{t_s}, \frac{r_b}{H}), \ln(\frac{t}{t_s})]$ and are appended to the set of long time-step g-functions. For typical ratios of borehole radius to borehole depth, the short time-step g-function data correspond to time steps between 2 ½ minutes and 200 hours. Although some overlapping between the long and short time-step g-functions can be seen in Figure 5.3, the long time-step g-functions are applicable for times longer than 200 hours. In use, g-function values are determined by linear interpolation between the nearest points.

5.2.2. AGGREGATION OF GROUND LOADS

The short time-step g-functions developed thus far can be implemented in an algorithm to predict short time-step loop temperature variations. However, this would require that short time-step ground loads be devolved into individual step pulses and be superimposed in time for each time-step using the corresponding short time-step g-function. Since the number of superposition calculations is proportional to the square of the number of time steps, an 8760-hour annual simulation creates a significant computational burden. Such an algorithm has been developed within the framework of this study, but it is a computationally inefficient way of determining short-term temperature variations on the ground loop heat exchanger.

In order to be able to reduce the computational time, an aggregation algorithm is developed for the ground loads considering that the importance of a load at a given time step diminishes for subsequent time steps as time progresses. That is, loads that occur more than a certain time ago can be ‘lumped’ together into larger blocks. Thus, the

history of a multitude of short time-step loads can be represented in single load 'blocks' to be superimposed onto loads that are more recent.

For the computation of temperatures inside the very first user-defined time block no load aggregation is performed. The load aggregation begins once the first time block has passed. (Using the earlier example, this means that the load aggregation would only start after the 730th hour of the simulation. Average borehole temperatures for earlier hours would be computed without any load aggregation with the short time-step g-functions). For any given time-step after the first load-aggregated time block, the average borehole temperature is computed by first superimposing the aggregated loads from the 730-hour blocks and then by superimposing the short time-step loads upon the aggregated longer time-step block loads.

Figure 5.4 shows a comparison of temperature responses based on hourly loads with temperature responses obtained through load aggregation for the first week and the first month for a typical case. As expected, the longer time blocks are averaged, the greater is the deviation from the actual hourly temperatures when the aggregation routine switches back to the hourly simulations.

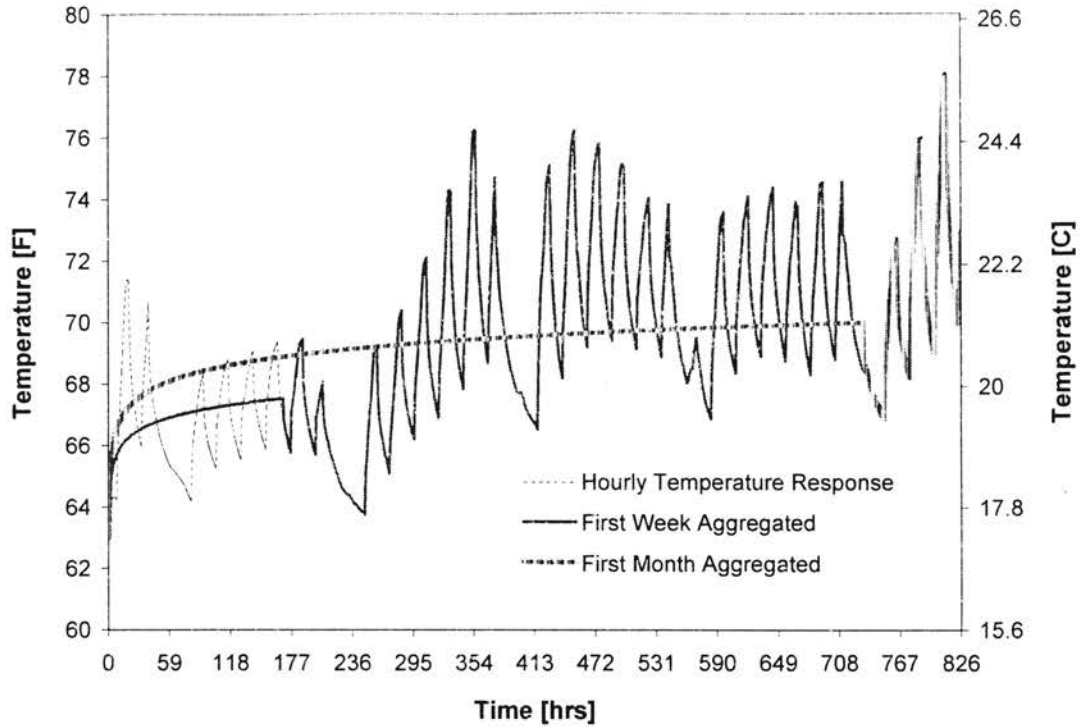


Figure 5.4 Comparison of temperature responses based on hourly loads with temperature responses obtained through load aggregation for first week average and first month average loads for a typical case.

To provide an example for the load aggregation, consider a set of hourly load data where the computation of the average borehole temperature for the 2281st hour is sought. Defining the load aggregation time block to be 730 hours, the hourly short time-step loads can be aggregated for 3 larger time blocks. The average load values for each of these larger time blocks are determined by summing the hourly loads and then dividing the sum by 730 hours. The superpositioning of these 3 sets of aggregated loads with the corresponding longer time-step g-functions (in this example g-function values for 730, 1460 and 2190 hour duration) yields the temperature response at the end of the 2190th hour of simulation. Since the average borehole temperature at the end of the 2281st hour

is sought, the hourly loads for the remaining 91 hours are then superimposed in hourly steps with the corresponding hourly g-function values to obtain the temperature at the 2281st hour.

$$T_{2281} = T_{\text{ground}} + \sum_{m=1}^3 \left[\frac{(\bar{q}_m - \bar{q}_{m-1})}{2\pi k_{\text{ground}}} g \left(\frac{t_{2281} - t_{(730m-730)}}{t_s}, \frac{r_b}{H} \right) \right] + \sum_{n=2191}^{2281} \left[\frac{(q_n - q_{n-1})}{2\pi k_{\text{ground}}} g \left(\frac{t_{2281} - t_{n-1}}{t_s}, \frac{r_b}{H} \right) \right] \quad (5.8)$$

where,

m = index for the load aggregated time blocks.

n = index for the hourly time steps.

\bar{q} = average aggregated load in Btu/hr-ft [W/m].

q = hourly load in Btu/hr-ft [W/m]

T_{2281} = temperature at the end of the 2281st hour.

t = time.

Note that $q_{2190} = \bar{q}_3$

The direct superposition of temperature responses based on aggregated loads with temperature responses based on short time-steps introduces an error in the final temperature as illustrated in Figure 5.5. The load aggregation block for this example is assumed to be 730 hours to represent a month. A deviation of about 2.0 °F (1.1 °C) is

predicted after one month of load aggregation. This error diminishes quickly after a few hours and goes practically to zero after about 48 hours of hourly history.

The aggregation algorithm keeps track of all hourly ground loads up to the current time-step. An average ground load is then computed for user-definable 'blocks' of time (for example, if the ground loads are given in hourly time steps then 730 hours worth of hourly loads may be averaged over this time period to represent one aggregate load for the 730-hour time block).

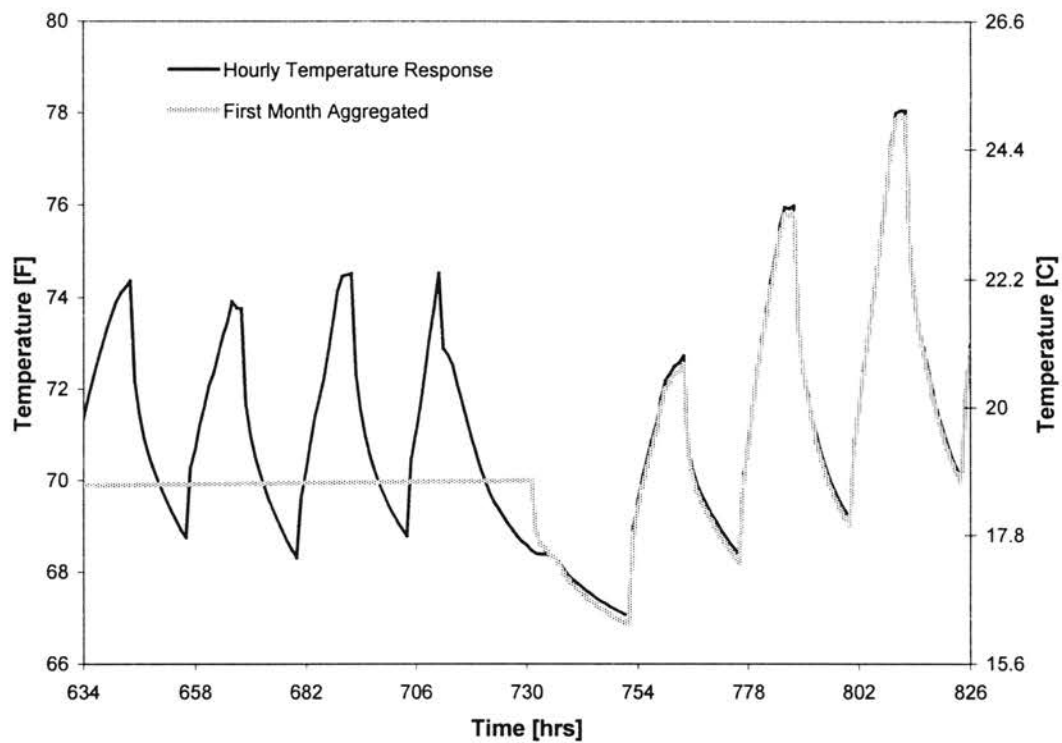


Figure 5.5. Hourly history versus aggregated history for a typical case.

To reduce/eliminate the error at the start of the hourly load period, the aggregation algorithm is modified so that a user-defined minimum hourly history period during which only short time-step load superposition occurs always precedes the computation of the current average borehole temperature. To expand on the above example of determining the temperature at the 2281st hour, the incorporation of a minimum hourly history period of say 96 hours would result in that the 3rd load aggregation would not be performed since the remaining number of hours (91 hours) are less than the required minimum hourly history period specified. In this case, note that $q_{1460} = \bar{q}_2$.

$$T_{2281} = T_{\text{ground}} + \sum_{m=1}^2 \left[\frac{(\bar{q}_m - \bar{q}_{m-1})}{2\pi k_{\text{ground}}} \mathcal{G} \left(\frac{t_{2281} - t_{(736m-730)}}{t_s}, \frac{r_b}{H} \right) \right] + \sum_{n=1461}^{2281} \left[\frac{(q_n - q_{n-1})}{2\pi k_{\text{ground}}} \mathcal{G} \left(\frac{t_{2281} - t_{n-1}}{t_s}, \frac{r_b}{H} \right) \right] \quad (5.9)$$

Figure 5.6 shows a comparison of minimum hourly history periods of 24, 192 and 730 hours. In the short time-step model, the minimum hourly history period is an adjustable variable that can easily be changed by the user. Currently, the algorithm uses a minimum hourly history period of 192 hours.

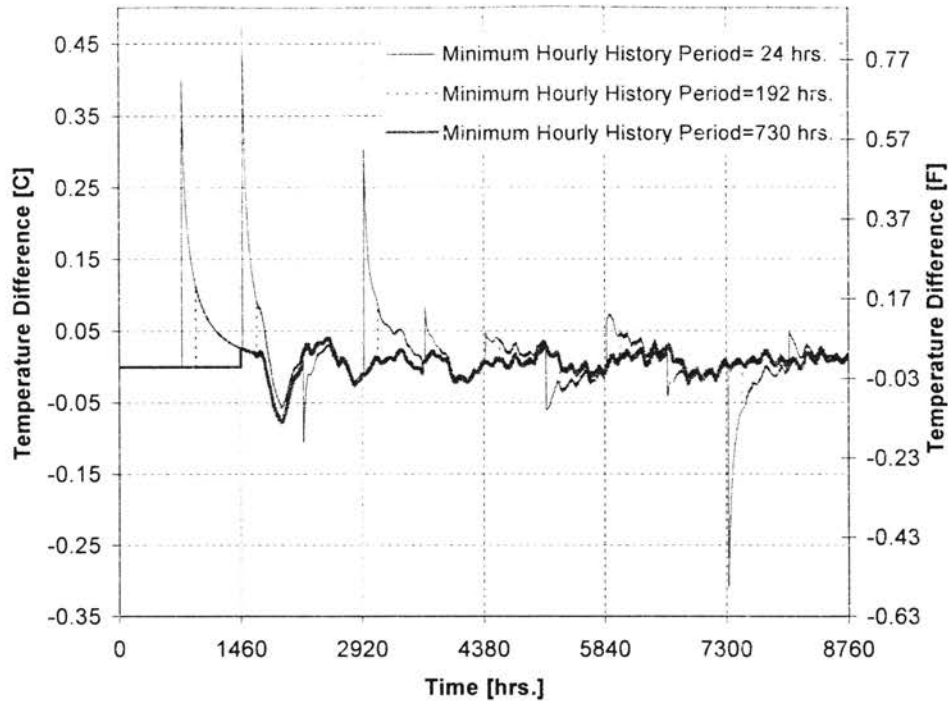


Figure 5.6. Comparison of the error in predicted exiting temperatures for various minimum hourly history periods.

As greater hourly history periods are selected the differences in average borehole temperature predictions between the load-aggregated and non-load-aggregated schemes decrease. If a minimum hourly history period of 8760 hours were to be selected for an annual simulation the block load-aggregated scheme collapses into the hourly scheme without any change in the total simulation time. However, with a minimum hourly history period of 192 hours, the computation time is reduced to approximately 10% of the time required for the non-aggregated scheme for an annual simulation. For a 20-year simulation, the computation time of the aggregated scheme is reduced to significantly less than 1% of the non-aggregated scheme due to the factorial relationship between the number of superposition calculations and the number of time steps.

The load aggregation algorithm has been developed above by example. The algorithm may be summarized for an hourly simulation in pseudo-code as follows.

Define An Aggregated Load Block (p) in Hours and Minimum Hourly History Period.

Read Borehole Geometry Parameters (Number of Boreholes, Borehole Depth, Radius.)

Read Ground and Fluid Thermal Properties (Ground Conductivity, Volumetric Specific Heat of Ground and Heat Transfer Fluid).

Read Short and Long Time-Step g-functions (Interpolate and store all g-functions for the simulation).

Do Loop n=1 to Number of Hours (nf)

Compute the Ground Load for the Current Time Step using Entering Fluid Temperature (For the first time step T_{FarField} may be used).

Compute the Number of the Current Aggregated Load Block (calb) using the Minimum Hourly History Period and Aggregate Ground Loads in Blocks up to the Current Load Block.

If (The Current Time is Less Than the Sum of a Single Aggregated Load Block and Minimum Hourly History Period) \rightarrow No Load Aggregation.

Compute Average Borehole Temperature by Superposition of the decomposed Short time Step Load Profile using the corresponding g-functions with equation (5.10).

$$T_{nf} = T_{\text{ground}} + \sum_{n=1}^{nf} \left[\frac{(q_n - q_{n-1})}{2\pi k_{\text{ground}}} g \left(\frac{t_{nf} - t_{n-1}}{t_s}, \frac{r_b}{H} \right) \right] \quad (5.10)$$

Else \rightarrow Load Aggregation.

If (The Difference between the Current Time and the product of the Number of the Current Aggregated Load Block and a Single Aggregated Load Block is Greater Than Minimum Hourly History Period) \rightarrow

Compute Long Time-Step Temperature Differences by Superposition of Aggregated Loads using the corresponding g-functions.

Compute Short Time-Step Temperature Differences by Superposition of Hourly Loads using the Short Time-Step g-functions.

Compute Average Borehole Temperature by Superposition of the Short and Long Time Step Temperature Differences with equation (5.11).

$$T_{nf} = T_{\text{ground}} + \sum_{m=1}^{calb} \left[\frac{(\bar{q}_m - \bar{q}_{m-1})}{2\pi k_{\text{ground}}} g\left(\frac{t_{nf} - t_{(pm-p)}}{t_s}, \frac{r_b}{H}\right) \right] + \sum_{n=nf-((calb)p)}^{nf} \left[\frac{(q_n - q_{n-1})}{2\pi k_{\text{ground}}} g\left(\frac{t_{nf} - t_{n-1}}{t_s}, \frac{r_b}{H}\right) \right] \quad (5.11)$$

Else →

Use equation (5.12) to compute the Average Borehole Temperature by Superposition of the Short and Long Time Step Temperature.

$$T_{nf} = T_{\text{ground}} + \sum_{m=1}^{calb-1} \left[\frac{(\bar{q}_m - \bar{q}_{m-1})}{2\pi k_{\text{ground}}} g\left(\frac{t_{nf} - t_{(pm-p)}}{t_s}, \frac{r_b}{H}\right) \right] + \sum_{n=nf-((calb-1)p)}^{nf} \left[\frac{(q_n - q_{n-1})}{2\pi k_{\text{ground}}} g\left(\frac{t_{nf} - t_{n-1}}{t_s}, \frac{r_b}{H}\right) \right] \quad (5.12)$$

Endif

Endif

Continue Loop

5.3. COMPONENT MODEL FOR TRNSYS

TRNSYS (Klein, et al. 1996) is a transient system simulation program with a modular structure that allows the use of externally developed mathematical simulation models for system components. Utilizing the short time-step g-functions, a TRNSYS component model of the ground loop heat exchanger was developed. The component

model allows for an annual or longer hourly building simulation incorporating a ground-coupled heat pump system. Shorter time steps than an hour may be used.

Although TRNSYS solves all equations in the component models simultaneously, TRNSYS models are cast in input/output form. The ground loop heat exchanger component model was formulated with the entering fluid temperature and the fluid mass flow rate as input variables. However, the short time step model described above assumed the heat rejection/extraction per unit length of borehole was the fundamental input variable and yields the average fluid temperature. Therefore, it is necessary for the component model to internally solve for the average fluid temperature, exit fluid temperature and heat rejection/extraction per unit length of borehole simultaneously.

The model parameters include the borehole depth and radius, the ground and fluid thermal properties, far-field ground temperature, the borehole thermal resistance, and the complete set of response factors. The short time-step model output variables for the current time step are the fluid temperature exiting the ground loop, the mass flow rate of the fluid and the average fluid temperature of the borehole field. A schematic of model inputs and outputs are given in Figure 5.7 along with model internal parameters.

Because the model uses historical data, all hourly ground loads are stored. Some computational speed improvement is achieved by pre-computing all hourly g-functions up to 8760 hours and passing them to the load aggregation and superposition routine as required for all time steps up to the current time step.

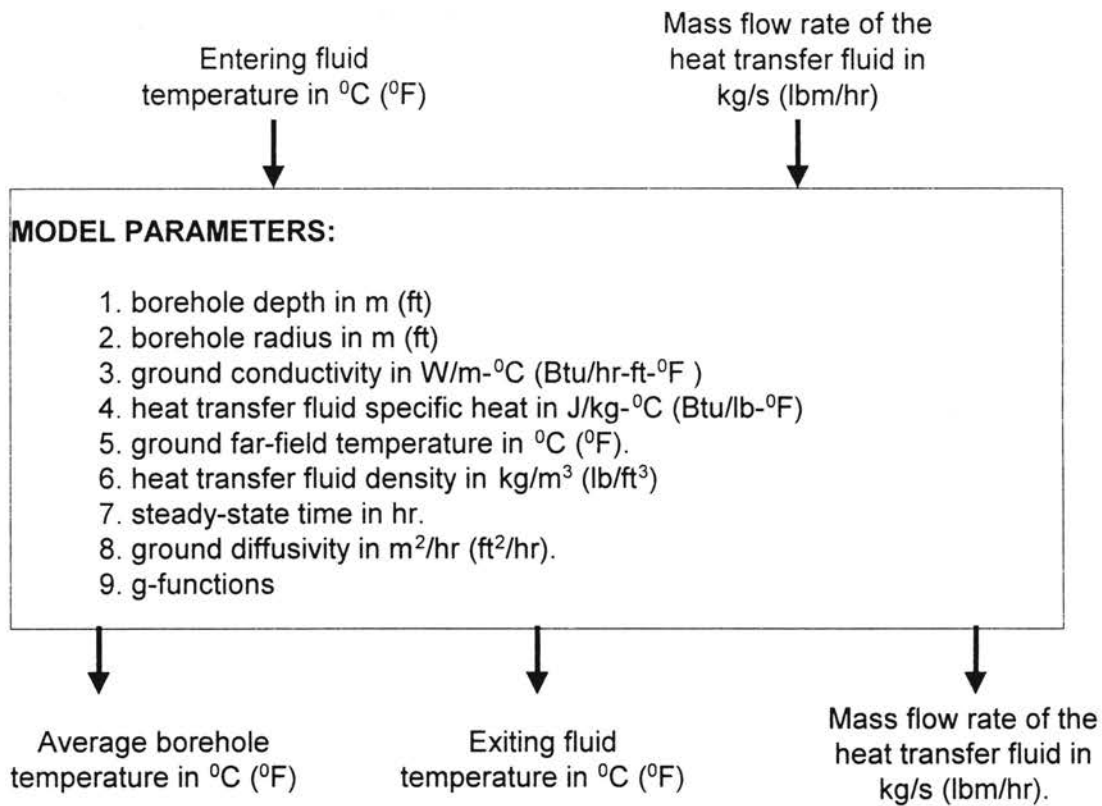


Figure 5.7. *TRNSYS short time-step component model configuration.*

A simple water-to-air heat pump component model, which also reads hourly building loads from a file, was developed for testing purposes. Although TRNSYS has detailed heat pump and building models, a simplified model was desired. The simplified model is intended to be used with the total hourly building loads and the heat pump model merely translates an hourly building load into an exiting fluid temperature based on the entering fluid temperature and mass flow rate.

The model uses a quadratic curve fit of manufacturer's catalog data to compute the heat of rejection in cooling mode, the heat of extraction in heating mode, and the heat pump power consumption as functions of entering water temperature. Outputs provided

by the model include the exiting fluid temperature, the power consumption, and the fluid mass flow rate.

5.4. EXAMPLE APPLICATION FOR THE USING THE COMPONENT MODEL

An example application is provided using an actual building located in downtown Tulsa, Oklahoma that represents a cooling dominated commercial building. It is a four-story, 45,000-ft² (4182 m²) office building, with a peak load of approximately 100 tons (352 kW). The building is to be gutted and completely renovated. The renovation will include an atrium with double pane, low-emissivity glass. However, the building loads are dominated by internal heat gains and the solar heat gains from the atrium skylights. Consequently, the building requires cooling year round. The building load profile is shown in Figure 5.8. (Heat rejection is shown as positive, heat extraction as negative.)

The modeled borehole loop field consists of 100 boreholes, each 250 ft. (76.2 m) deep, arranged in a 10 X 10 rectangular configuration and spaced 25 ft. (7.6 m). A very simple schematic of the system configuration is given in Figure 5.9.

The average borehole temperature increases, as expected from the building loads, during the summer months as a result of higher cooling needs for those months. The average temperature response to the loads in Figure 5.8 is shown in Figure 5.10. Entering and exiting water temperatures for the months of January and July are provided in Figures 5.10 and 5.11.

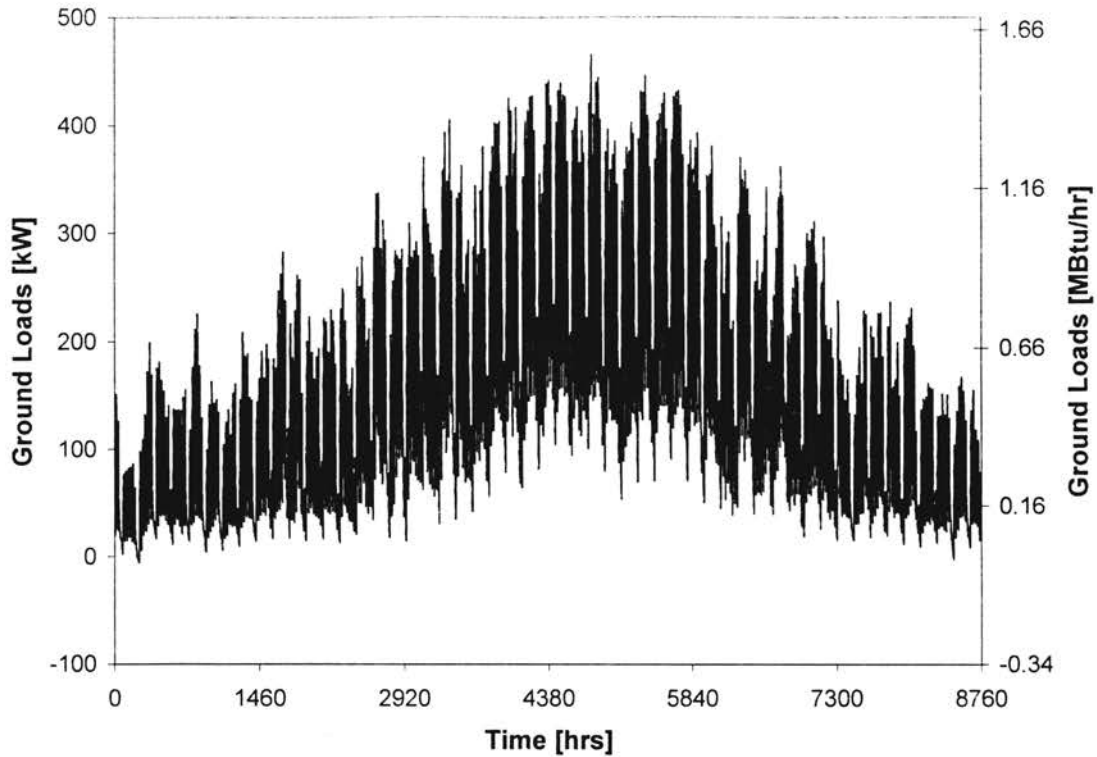


Figure 5.8. Annual hourly building load profile for the example building in Tulsa.

A comparison of the average borehole temperatures between the first and the 8760th hour of simulation show that the average borehole temperature after the first year is about 10 °F (5.6 °C) higher than at the start of the simulation. In later years, the fluid temperatures would rise to the point that the heat pumps would fail. This is indicative of ground loop heat exchanger being undersized. Either the ground loop heat exchanger needs to be larger, or supplemental heat rejection units such as cooling towers could be used to avoid long-term thermal build-up in the ground. While existing design tools can be used to estimate the correct size of the ground loop heat exchanger, a short time-step model of the ground loop heat exchanger, coupled with component models of the

building, heat pumps, and cooling tower can predict the impact of cooling tower sizing and operating strategy on the ground loop heat exchanger size and system operating cost.

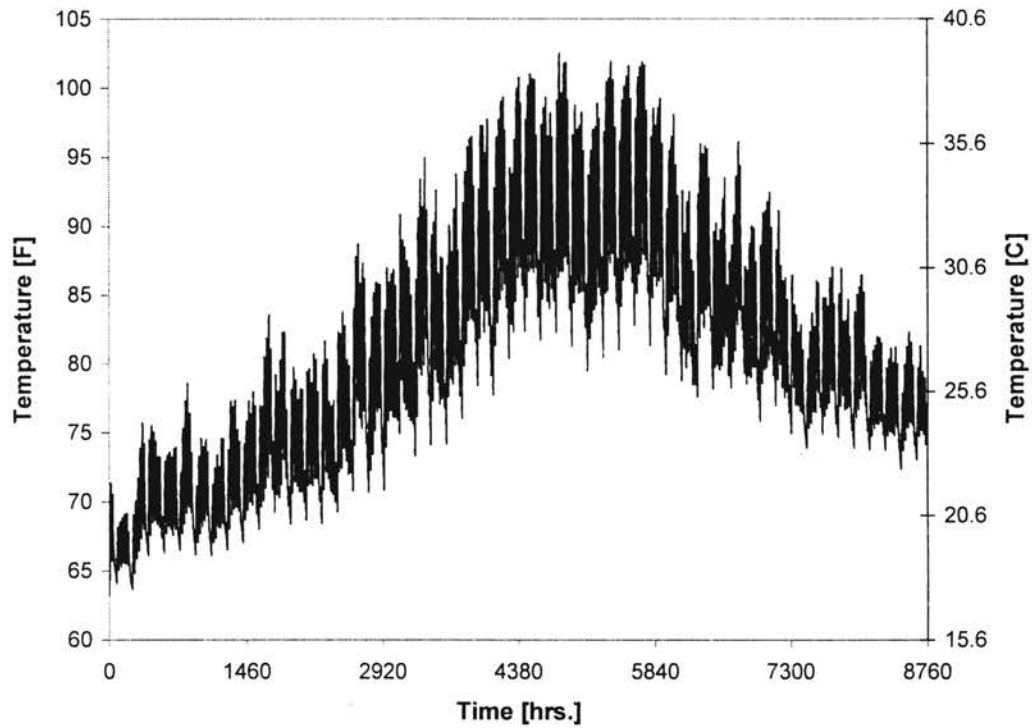


Figure 5.9. Hourly average borehole temperature profile for the example building in Tulsa, Oklahoma as a result of an annual simulation with TRNSYS.

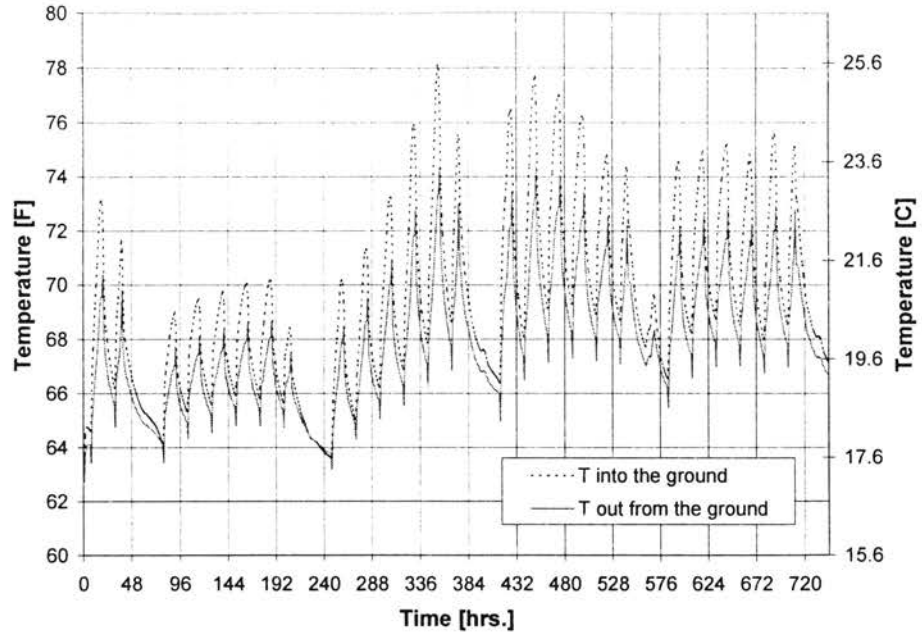


Figure 5.10. Hourly input and output temperatures to the ground during the month of January for the example building in Tulsa, Oklahoma.

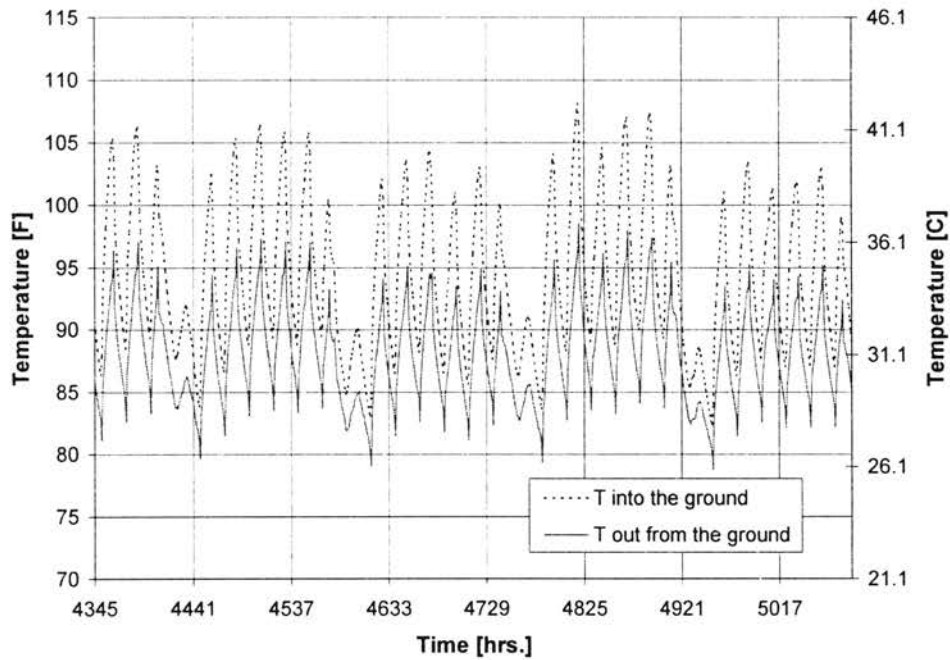


Figure 5.11. Hourly input and output temperatures to the ground during the month of July for the example building in Tulsa, Oklahoma.

5.5. DISCUSSION OF THE RESULTS

The short time-step response factors are a very useful extension of the long time-step response factors developed by Eskilson allowing for an hour-by-hour or shorter time-step evaluation of system energy consumption and electrical demand. A more accurate and detailed assessment of the short-term behavior of ground-coupled heat pump systems can thus be made for design of ground loop heat exchangers, energy analysis of ground source heat pump systems, and design of hybrid ground source systems.

The short time-step response factors were used in conjunction with a load aggregation algorithm to develop a short time-step ground loop heat exchanger model, which was cast as a component model for TRNSYS. A simple, but useful, model of a water-to-air heat pump was developed. An annual hourly simulation is performed for an example building to demonstrate the models.

It would be highly desirable to have an experimental validation for the model. Unfortunately, to date, only little, if any, suitable* data exists and the collection of such data is not trivial. Parts of the short time-step temperature response factors model have been verified analytically (Yavuzturk, et al. 1999) and experimentally (Hellstrom, 1991). Additional experimental validation is provided in Chapter 6, using operating data collected at the Maxey elementary school in Lincoln, NE.

* A suitable data set would include a high-quality independent measurement of the ground thermal properties at the site. Monitoring of the system, which would include accurate measurements of the loop flow rate and inlet and outlet temperatures, would have to commence at the beginning of the system operation.

6. SHORT TIME-STEP RESPONSE FACTOR MODEL VALIDATION

In order to assess the validity of the short time step temperature response factor model, a comparison of model predictions to actual field data is desirable. Although the availability of high-quality field data is unfortunately scarce, measured data are available for the operation of a ground source heat pump system collected at the Maxey Elementary School in the Lincoln, NE school district. The data set is fairly recent (Shonder 1999) and consists of 10-minutely measurements of entering and exiting fluid temperatures and fluid flow rate on the loop for a period of several years. The building was placed in service in August 1995. The collection of 10-minute operating data started in November 1995 (Carlson 1998). The data used to validate the short time step model come from the period starting from November 1995 and ending in December 1996.

6.1. DESCRIPTION OF THE MAXEY ELEMENTARY SCHOOL GROUND SOURCE HEAT PUMP SYSTEM

The Maxey Elementary School has about 70,000 ft² (6,500 m²) of floor area that is served by 54 heat pumps distributed in the classrooms and activity areas. The single-story building houses about 50 staff members serving about 500 students.

The borehole field of the ground source heat pump system consists of 120 vertical boreholes arranged in a 10x12 rectangular configuration. Each borehole is 240 ft (73.2 m) deep and has a diameter of 4.5 inches (114.3 mm). The ground loop heat exchangers

are 1 inch (25.4 mm) nominal high-density polyethylene U tube pipes. The boreholes are spaced 20 ft (6.1 m) apart from each other, center-to-center. The heat transfer fluid circulated in the U-tubes of the ground heat exchanger is a 22% aqueous propylene glycol solution. The heat transfer fluid re-circulation pumps are variable speed pumps and have a maximum rated capacity of 575 gpm (36.2 L/s). The boreholes are grouted with a mixture of sand and fine gravel up to 10 ft (3 m) below the ground surface. A bentonite plug is used in the top 10 ft (3m) to plug the boreholes. Fluid flow to and from the borehole field is through buried horizontal piping that is connected to the re-circulation pumps and the HVAC system in the mechanical room of the building. The measurement of temperature and flow rate data is made in the mechanical room.

6.2. MONITORED FIELD DATA

The Maxey system is designed to maintain a minimum flow through the ground loop during the winter months even when there may be only minimal or no heating demand. During the summer months, the circulation pumps are turned off when there is no demand on the borehole field. At these times, the entering fluid temperature is observed to drift above 70 °F (21.1 °C) during weekday nights and above 80 °F (26.7 °C) during weekends as the temperature sensors come into equilibrium with the mechanical room. Figures 6.1 and 6.2 provide the time variation for the heat pump entering fluid temperature and the heat transfer fluid flow rate observed at the Maxey Elementary School from 12:00am on 1/1/1996 to 11:55pm on 12/31/1996. The temperature ‘spikes’ in Figure 6.1 are representative of no or low fluid flow conditions.

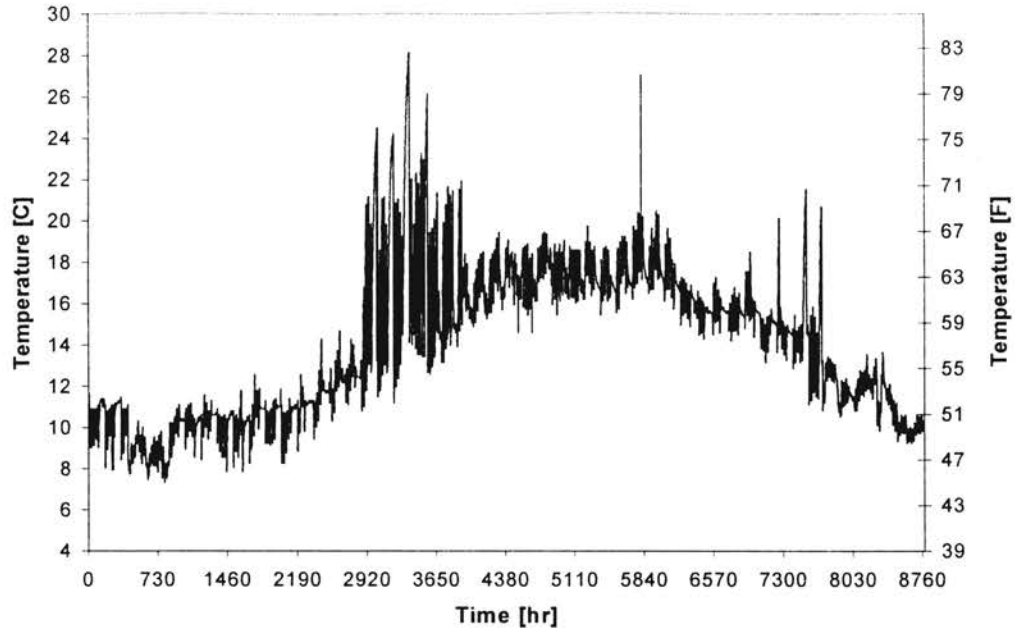


Figure 6.1 *Heat pump entering fluid temperatures from 12:00am 1/1/1996 to 11:55pm 12/31/1996 plotted hourly.*

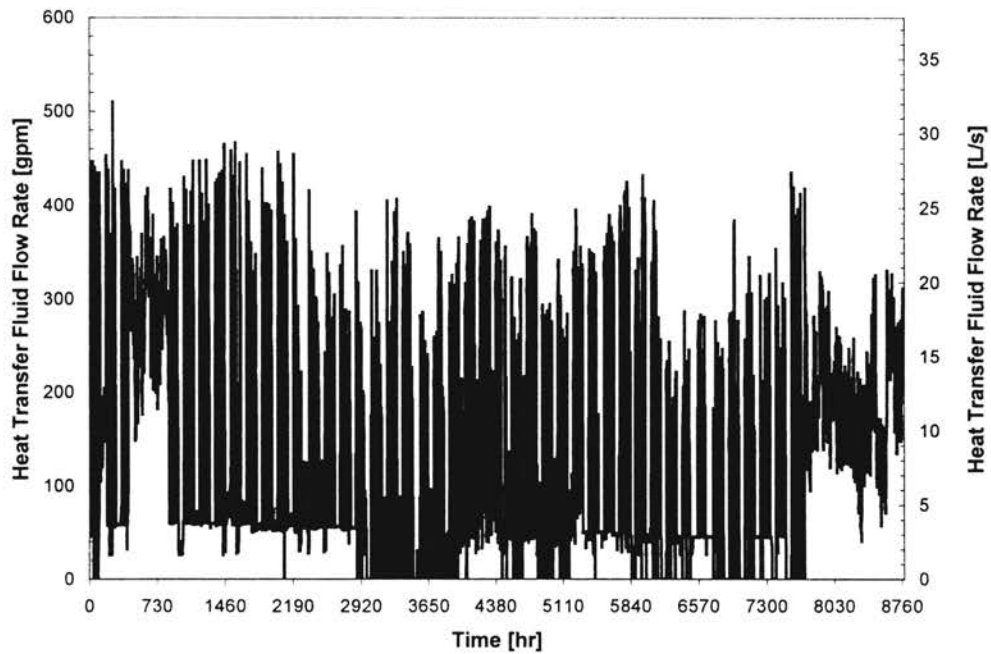


Figure 6.2 *Heat transfer fluid flow rate 12:00am 1/1/1996 to 11:55pm 12/31/1996 plotted hourly (processed to remove flow rates below 50gpm).*

The data collection at the Maxey system started in November 1995 although the system was placed in service about three months earlier. This time gap is significant, since there is no way of accurately adjusting for the unrecorded thermal disturbances in the ground during this time. However, in order to approximately account for this thermal disturbance 'history', data from the same time period (from August 1996 to November 1996) is assumed to have repeated for the same period in 1995 for which data are missing. Although this approach is clearly not ideal, it, nevertheless, seems to be the best approximation available under the circumstances.

In addition, the no or low-flow conditions on the system are somewhat problematic in the monitored field data. During some time intervals, the data set contains flow rates and flow rate changes without corresponding temperatures and temperature changes. One explanation for such behavior may be that these are due to spurious scans by the instruments of the data acquisition system. For this reason, in the analyses presented here, when the fluid flow rate is below 50 gpm (3.15 L/s), experimental temperature results are not shown. Also, the flow rate into the ground loop heat exchanger is set to zero. Since no continuous set of measured data was, thus, available, discontinuities in temperature predictions of the model were unavoidable.

Furthermore, the location of instrumentation for data acquisition at the site is not ideal. The mechanical room of the Maxey building is about 100 - 150 yards (91 - 137 m) away from the borehole field. Also, the borefield and the building are not at the same elevation, but the borefield is about 6-8 ft (1.8-2.4 m) lower than the building. The model

predictions for the heat pump entering fluid temperature are temperature responses of the borehole field (exiting fluid temperatures from the borefield), and stipulate adiabatic conditions between the borefield and the mechanical room of the building. However, it is safe to assume that there would be heat gains/losses through horizontal piping buried at varying depths from the building to the field.

Finally, data for a number of time intervals were not obtained by the data acquisition system. It is possible that local power outages during data recording may have caused the instrumentation to shut down. The missing data were filled after the fact (Carlson 1998) using best engineering estimates for the time intervals in question. Nevertheless, reliability of the filled data points must be questioned.

6.3. COMPARISON OF MODEL PREDICTIONS AND FIELD DATA

For a meaningful comparison between the predicted and experimental heat pump entering water temperatures, a series of adjustments are required to the experimental data as well as to the short time step component model. The adjustments attempt to account for variations of the heat transfer fluid flow in the ground loop as well as address the no or low flow conditions of the system.

6.3.1. ADJUSTMENTS TO FIELD DATA

An adjustment in the field data is required to reflect the no-flow behavior of the system. This may be accomplished by ‘removing’ the corresponding temperature data

for low or no flow cases in the final comparison. This is justified, since, during no or low flow time intervals, an erroneous heat pump entering fluid temperature is measured that has ‘drifted’ towards the air temperature of the mechanical room. In the analyses presented here, system simulations are performed by assuming that no load demand was placed on the ground loop at time intervals of no or low fluid flow. This was implemented by setting the fluid flow rate to zero.

6.3.2. ADJUSTMENTS TO THE SHORT TIME STEP COMPONENT MODEL

The short time step component model as discussed in Chapter 5 requires a constant fluid flow rate in the ground loop and a constant borehole thermal resistance. Since, in reality, the fluid flow rate is not constant during the operation of the ground source heat pump system at Maxey, the short time step component model needed to be modified to account for the resulting variable borehole resistance.

The total thermal resistance of a borehole is estimated as the sum of thermal resistances due to the borehole grout, the pipe material and the fluid flow (See Equation [5.5]). The grout thermal resistance is estimated using the approach of Paul (1996), which uses so-called resistance shape factor coefficients. The grout thermal resistance is dependent on the position of the U-tube and its shank spacing in the borehole. Although it is very unlikely that all 120 boreholes at the Maxey school site have identical borehole/U-tube geometry, a constant grout resistance is nevertheless assumed for all boreholes for practical reasons. Similarly, a well-mixed grout with a constant thermal conductivity is stipulated. The thermal resistance due to the grout can then be calculated using Equation

(5.2). The thermal resistance due to high-density polyethylene pipe is determined using Equation (5.4).

In order to account for the variations in the total borehole thermal resistance, the convective thermal resistance due to the fluid flow is adjusted for each time step considering the change in the flow rate of the heat transfer fluid. Since the variable fluid flow rate only impacts the inside convective heat transfer coefficient h_i , this adjustment is implemented by recomputing h_i for each time step in determining the borehole thermal resistance due to convection,

$$R_{\text{Convection}}(t) = \frac{1}{2\pi D_{\text{in}} h_{\text{in}}(t)} \quad (6.1)$$

where

$$h_i(t) = \frac{Nu(t) \cdot k_{\text{Fluid}}}{D_i} \quad (6.2)$$

The time-dependent Nusselt number in Equation (6.2) is determined based on the flow characteristics of the heat transfer fluid through the calculation of the Reynolds number

$$Re(t) = \frac{v(t)D_i}{\nu} \quad (6.3)$$

This equation for the Reynolds number may be recast in the following form to include the volumetric flow rate of the heat transfer fluid:

$$\text{Re}(t) = \frac{\dot{V}(t)D_i}{A_i\nu} = \frac{4\dot{V}(t)}{\pi D_i \nu} \quad (6.4)$$

For laminar flow conditions ($\text{Re} < 2300$), it is sufficient to use a constant Nusselt number of 4.36, when a uniform surface heat flux and fully developed flow is assumed in the ground loop (see also Incropera and Dewitt 1980). For fully turbulent flow ($\text{Re} > 10000$), Dittus-Boelter correlation is used as given by Incropera and Dewitt (1980):

$$\text{Nu}(t) = 0.023\text{Re}(t)^{0.8} \text{Pr}^{0.35} \quad (6.5)$$

The exponent of the Prandtl number ($\text{Pr} = \frac{\nu}{\alpha}$) is approximated with 0.35 for both heating and cooling modes.

For the transition region between fully turbulent and laminar flow ($2300 < \text{Re} < 10000$), a correlation proposed by Gnielinski (Incropera and Dewitt [1980]) is used

$$\text{Nu}(t) = \frac{(f/8)\text{Re}\text{Pr}}{1.07 + 12.7(f/8)^{0.5}(\text{Pr}^{0.67} - 1)} \quad (6.6)$$

where f is the friction coefficient and is determined using Petukhov's relationship as given by Incropera and Dewitt (1980):

$$f = [0.790 \ln(Re) - 1.64]^{-2} \quad (6.7)$$

6.3.3. SHORT TIME STEP MODEL PREDICTIONS

A comparison between the predicted and experimental hourly heat pump entering fluid temperatures is provided in Figures 6.3 through 6.8 for the months of January, March, August, October, November and December 1996 to show a range of agreements between the predicted and measured temperatures. The hourly system simulations are performed on TRNSYS (Klein et al. 1996) using the short time step response factor component model described in Chapter 5 as modified in Chapter 6.3.2.

The analysis of the model predictions and measured entering fluid temperatures in Figures 6.3 through 6.8 show reasonable agreement. The maximum deviation of the temperature predictions is observed when the heat transfer fluid flow rate shows significant discontinuities in the data set. This is especially noticeable for the month of August (Figure 6.5) when the elementary school building is essentially shut down for the summer break. The best agreement between the predicted and measured temperatures is observed when the fluid flow rate in the loop is relatively continuous as in the second month of November and the month of December. Presumably, this is due to the

problematic data at low flow rates and the approximations made to deal with low flow fluid rates.

The ‘spikes’ in the temperature predictions are due to peculiarities in the data set, where fluid flow changes are scanned for some time intervals without corresponding temperature responses and/or changes. Figures 6.6 and 6.7 provide best examples to illustrate such occurrences. These spurious fluid flow data are kept in the simulations when their magnitude was greater than 50 gpm (3.2 L/s).

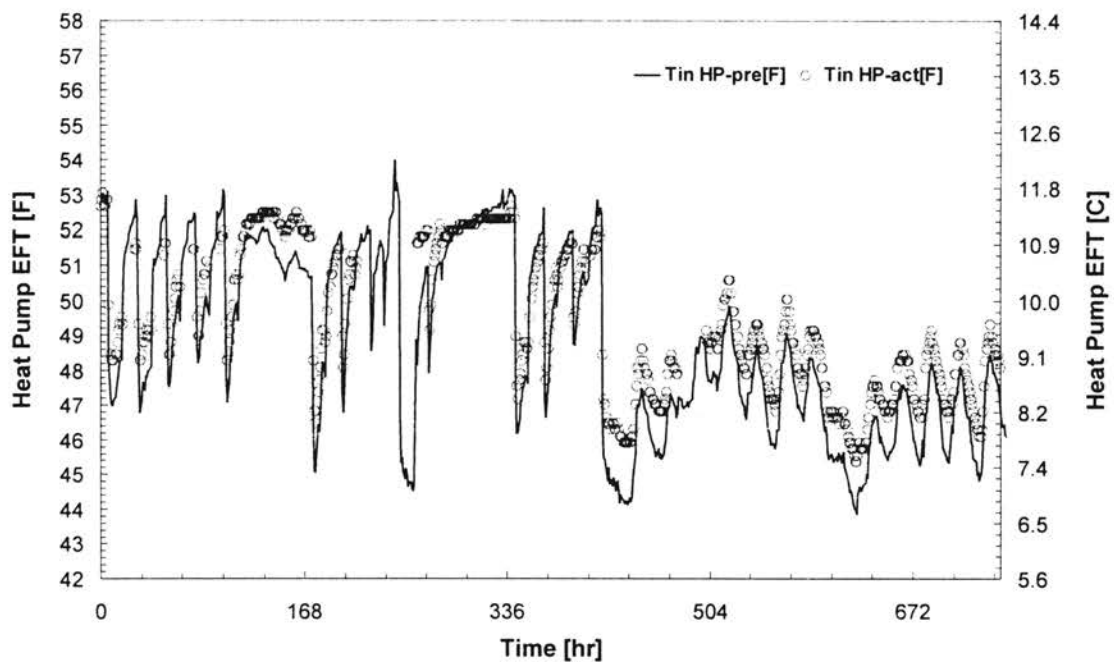


Figure 6.3 Comparison of hourly heat pump entering fluid temperatures. Predicted versus experimental for the month of January 1996.

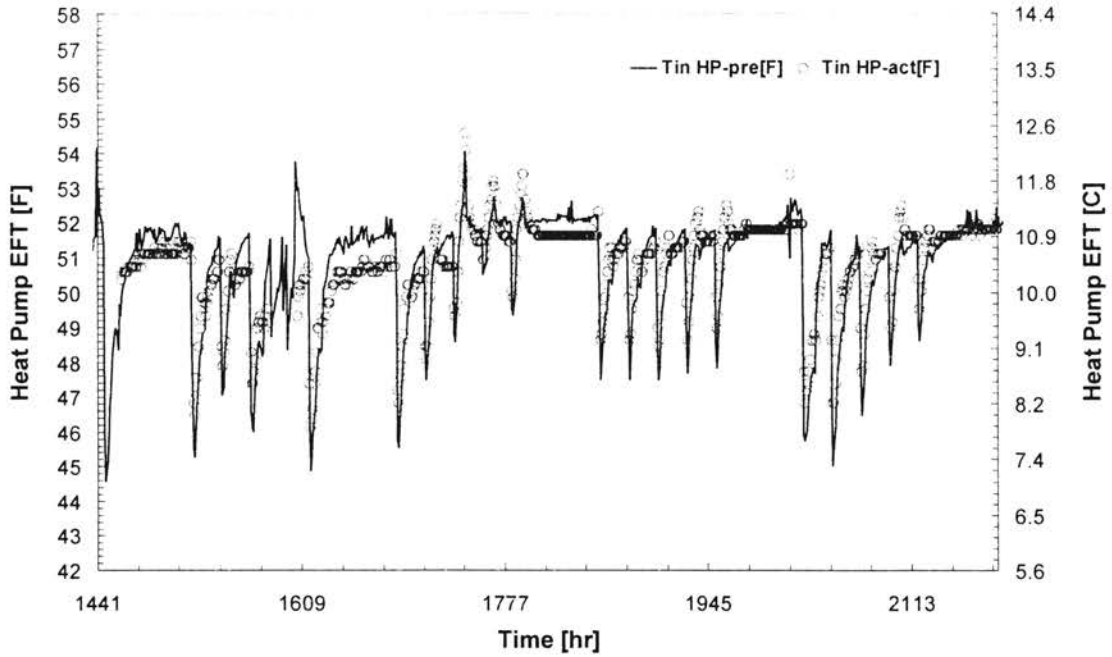


Figure 6.4 Comparison of hourly heat pump entering fluid temperatures. Predicted versus experimental for the month of March 1996.

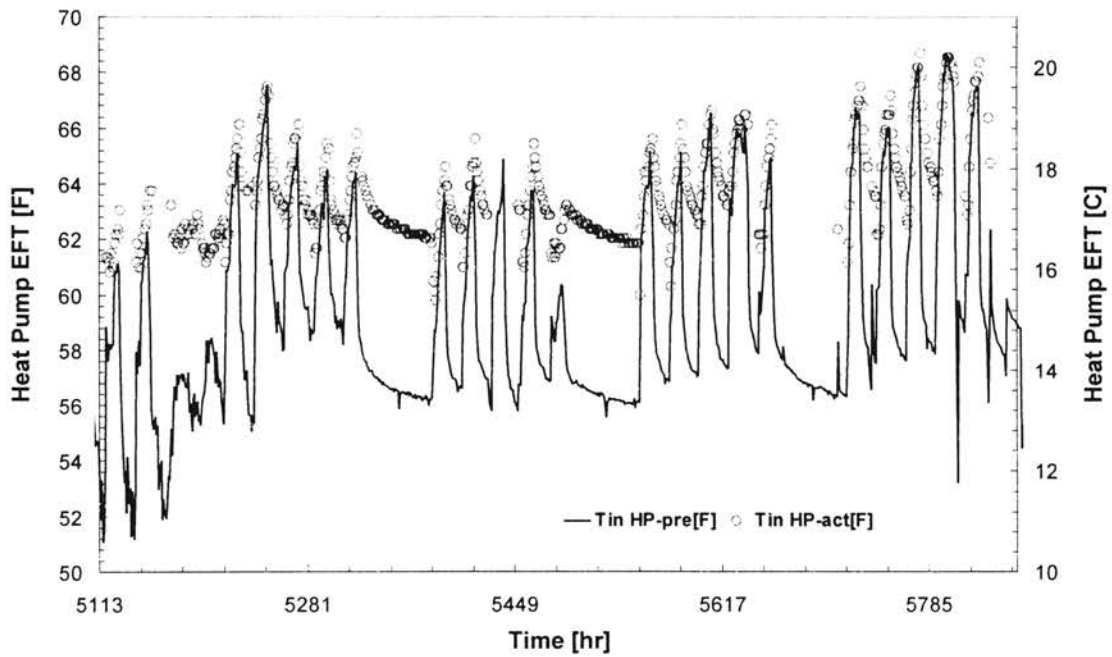


Figure 6.5 Comparison of hourly heat pump entering fluid temperatures. Predicted versus experimental for the month of August 1996.

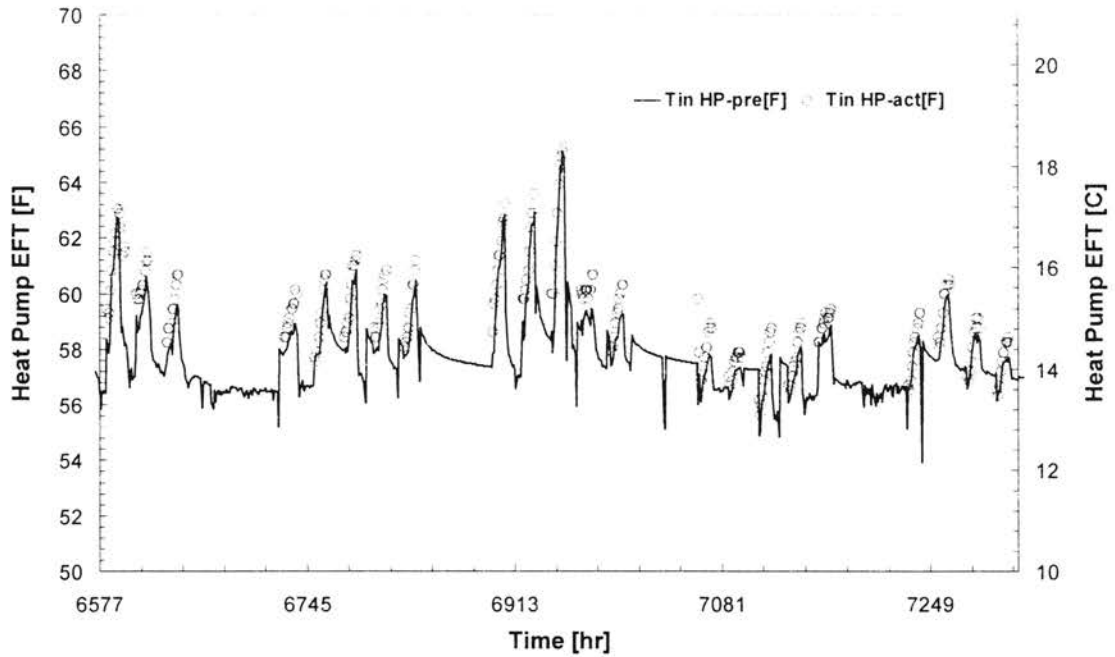


Figure 6.6 Comparison of hourly heat pump entering fluid temperatures. Predicted versus experimental for the month of October 1996.

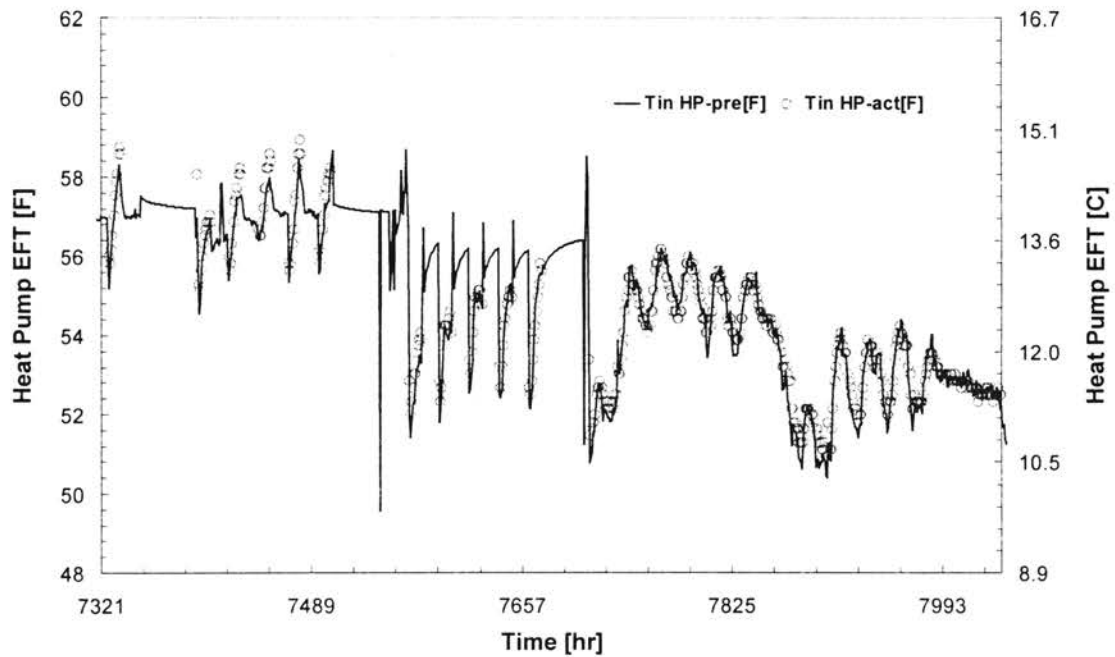


Figure 6.7 Comparison of hourly heat pump entering fluid temperatures. Predicted versus experimental for the month of November 1996.

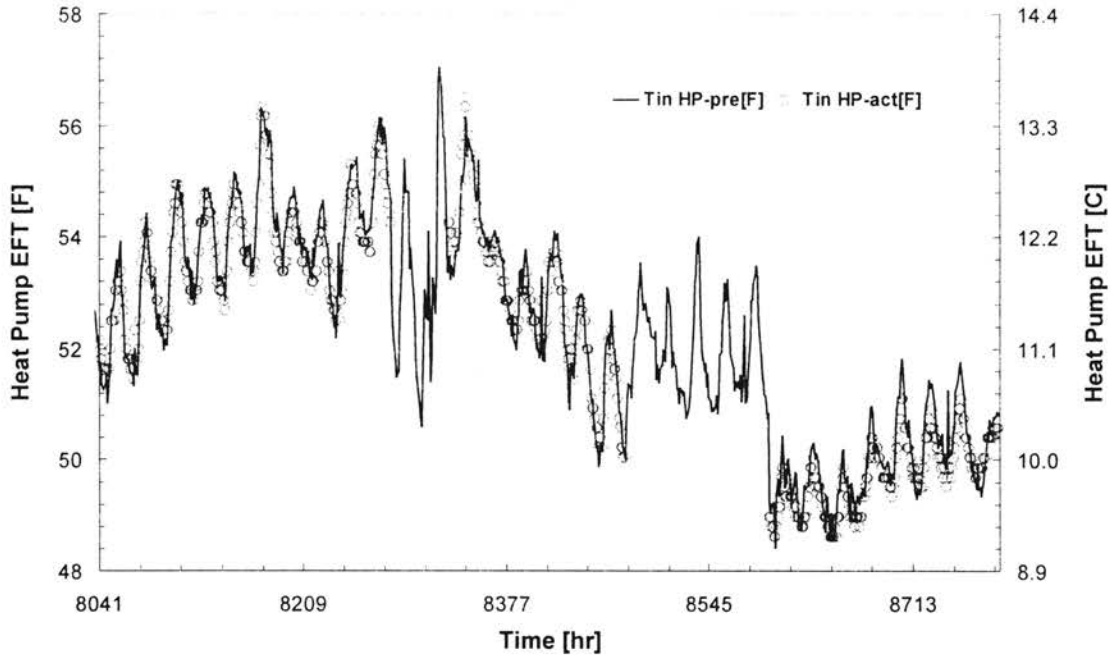


Figure 6.8 Comparison of hourly heat pump entering fluid temperatures. Predicted versus experimental for the month of December 1996.

6.4. SENSITIVITY ANALYSIS

A series of sensitivity analyses are performed to assess the influence of errors associated with the predicted heat pump entering fluid temperature. The sensitivity analyses focus on the impact of the entering fluid temperatures on the system power consumption, since the uncertainty in the predicted temperature has a corresponding uncertainty in the system power consumption. Two different effects are considered:

- i) The system power consumption is computed using the predicted and the actual heat pump entering fluid temperatures on an hour-by-hour basis. For the months of August and December 1996, the relative error at the

hour when the maximum system power consumption occurs can then be calculated. This is interesting to see the effect of the model on the peak electricity.

- ii) The total actual and predicted power consumptions are compared for the months of August and December 1996. The accumulative power consumption for a month is of interest for determining the electrical cost. The comparison for the months of August and December will show the impact of the model for the months with the best and worst predictions.

6.4.1. POWER CONSUMPTION SENSITIVITY ANALYSIS BASED ON MAXIMUM POWER CONSUMPTION.

A direct comparison between actual and predicted power consumption can be made when the system power consumption is computed using the predicted and the measured heat pump entering fluid temperatures. Figures 6.9 and 6.10 show the results of this analysis for the worst and best case months, August and December 1996 respectively. As can be observed from Figures 6.9 and 6.10, the power consumption is minimally affected by the errors in the entering fluid temperature prediction.

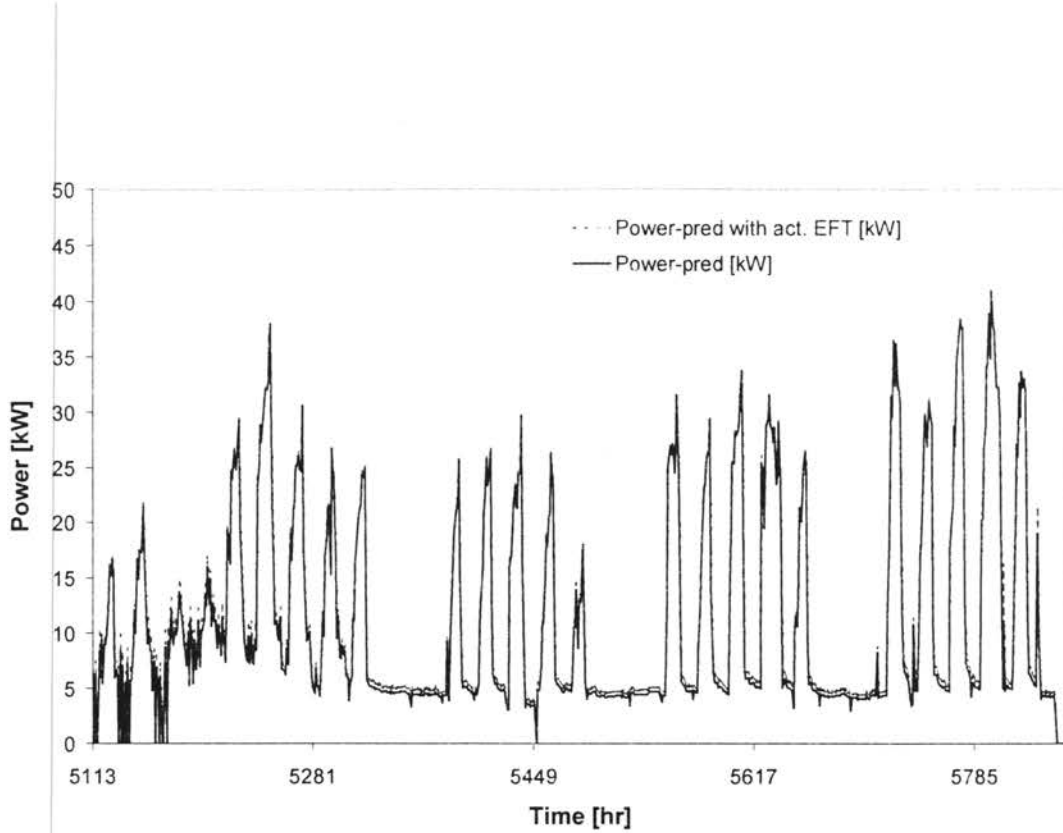


Figure 6.9 Comparison of hourly heat pump power consumption for the month of August 1996, considering predicted and actual heat pump EFT.

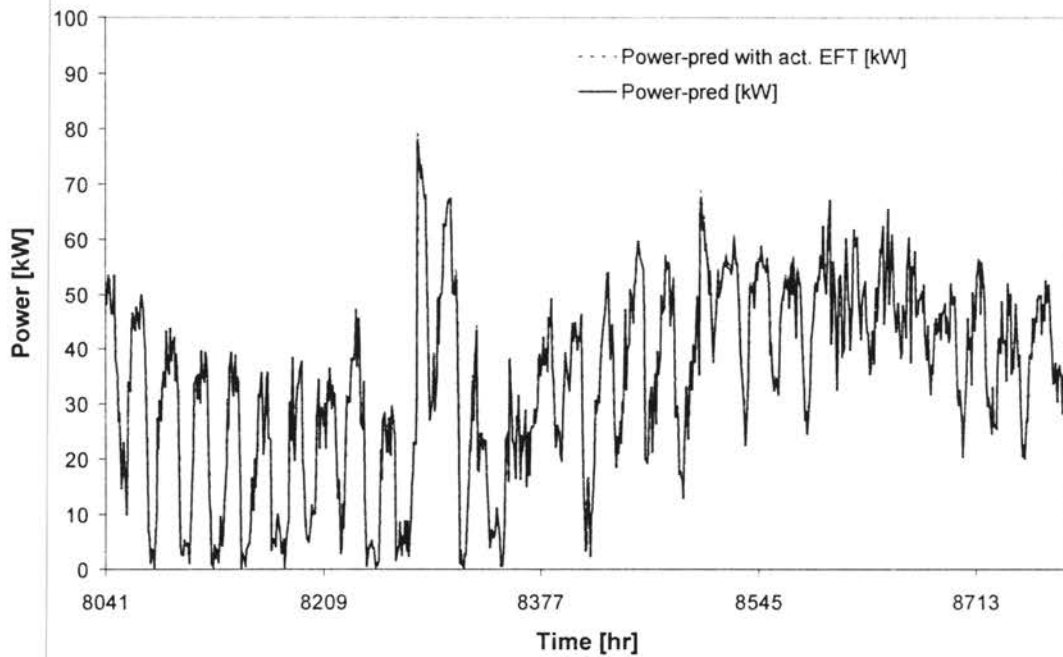


Figure 6.10 Comparison of hourly heat pump power consumption for the month of December 1996, considering predicted and actual heat pump EFT.

For the month of August, the maximum power consumption is recorded for the 5799th hour of the year (Figure 6.9). At this time step, the predicted power consumption of the heat pump is only about 0.5% higher than the power consumption determined using the measured heat pump entering fluid temperature.

For the month of December, the maximum power consumption is recorded for the 8282nd hour of the year (Figure 6.10). For this time step, the predicted power consumption of the heat pump is about 1.4% higher than the power consumption determined using the measured heat pump entering fluid temperature. However, it should be noted that data for the 8282nd hour of year are 'filled' data. Therefore, a second maximum is also investigated, which occurs at the 8501st hour of the year. The predicted power consumption at this hour is about 0.9% lower than the actual power consumption.

The analyses thus indicate that the errors, for both the best and worst case months, are within acceptable limits. This error envelope of 0.5% to 1.0% was consistently observed also for other months of the year for all time steps containing actual measured data (not 'filled' data).

6.4.2. POWER CONSUMPTION SENSITIVITY ANALYSIS BASED ON TOTAL ERROR IN POWER CONSUMPTION FOR THE BEST AND WORST PREDICTION MONTHS.

In order to estimate the effect of uncertainties in the ground loop heat exchanger model on the heat pump power consumption estimates, the total actual and predicted power consumptions are compared for the months of August and December 1996. The

comparison for the months of August and December will demonstrate the effects of the model for the best and worst months. The results of the analyses are provided in Table 6.1 below.

TABLE 6.1
Comparison of Total Error on Maxey Elementary School Power
Consumption for the Months August and December 1996

	Months	
	August 1996	December 1996
Total Power Consumption (predicted) [kWh]	8,338	25,457
Total Power Consumption (actual) [kWh]	8,665	25,555
Deviation [%]	3.8	0.4

The results show an excellent agreement in the predicted and actual power consumption for the heat pump for the month of December. Because of the relatively continuous operating data for this period, the error is only about 0.4% and can safely be considered very small. As expected, the error for the month of August (about 3.8%) is significantly higher than for the month of December. This relatively high percentage of deviation is due to discontinuities in system operating data set for this month.

6.5. DISCUSSION OF MODEL VALIDATION

The analyses presented here show that the goodness of the agreement between the predicted and the actual heat pump entering fluid temperature predictions depend on the

continuity of the experimental data. The maximum deviations in the entering fluid temperatures are observed during periods where the heat transfer fluid flow was either frequently interrupted (See Figures 6.5, 6.6 and 6.7 corresponding to the months of August, October and early November 1996) or a series of apparently spurious data were reported, coinciding with low flow rates. Best agreements can be found during the winter months (second half of November and December 1996), where there is a relatively continuous set of data, all at a moderate-to-high flow rates.

It is safe to assume that some heat will be lost through the horizontal piping runs between the building and the borefield. The errors that may be associated with horizontal piping are, however, difficult to estimate, since the depth of the horizontally buried piping from/to the borefield is not constant and the surrounding temperature changes throughout the year. Accordingly, the magnitude of the impact of ambient environmental conditions will be different for different portions of the horizontal piping at different times of the year. The heat losses through the horizontal piping are most significant when the system is switched on and off as it is done during the summer months of the system operation. This may also help to explain the relatively high deviation between the total power consumption in August 1996 as compared to the consumption in December 1996.

Nevertheless, comparison of temperature predictions overall shows reasonable agreement to the measured data. The sensitivity analyses indicate that the system power

consumption is only sensitive to errors in the predicted heat pump entering fluid temperature within acceptable limits.

7. EXAMPLE APPLICATION USING A HYBRID GROUND SOURCE SYSTEM

7.1. BACKGROUND ON HYBRID GROUND SOURCE HEAT PUMP SYSTEMS

A significant number of commercial buildings are cooling-dominated, especially in southern climates. When used in cooling-dominated buildings, ground-source heat pumps that utilize vertical, closed-loop ground heat exchangers can experience performance degradation as the entering fluid temperature to the heat pump increases over time. This temperature increase is due to the imbalance between the amount of heat extracted from the ground and the amount of heat rejected into the ground. For systems with severely undersized ground heat exchangers, the entering fluid temperature to the heat pump may be so high that the heat pump fails.

Nevertheless, it is possible to avoid this problem by either increasing the total length of the installed ground loop heat exchanger and/or increasing the spacing between the ground loop heat exchanger boreholes. However, first costs may be significantly higher so that a ground source heat pump system may not be competitive with conventional alternatives. For many commercial buildings, there may not be enough land area for a properly sized ground loop heat exchanger.

In order to decrease the system first cost and to improve the system performance, one of the options available to the prudent designer is a hybrid ground source heat pump

application. Hybrid systems utilize supplemental heat rejecters such as open cooling towers, closed-circuit fluid coolers or surface heat rejecters interconnected on the building return side between the heat pump and the ground loop heat exchangers. The supplemental heat rejecter is typically sized so that the annual heat rejection to the ground approximately balances the annual heat extraction from it. Excess heat is then rejected through one or more supplemental heat rejecters. With the supplemental heat rejecter(s), the ground loop heat exchanger may be significantly smaller.

It should be noted, however, that supplemental heat rejecters, especially open cooling towers and fluid coolers, require periodic maintenance. Additional operating costs also result from cooling tower and pump electricity consumption. If the fluid circulation system is not carefully designed the cost of fan and pump energy may become significant, negating the potential savings attained through a hybrid system. However, the first cost of supplemental heat rejecters and increased operating costs due to additional fan and pump circulation energy are expected to be small compared to the savings in drilling costs and heat pump operating costs for cooling dominated buildings.

The actual amount of heat transferred to and from the ground loop heat exchanger varies continuously due to changing building energy requirements. These changes result in short time-step fluctuations in the supply and return temperatures of the ground heat exchanger that can typically vary up to 10–18 °F (5.6–10.0 °C) over a given day. The coefficient of performance (COP) of the heat pump is affected by these short time temperature variations. In cases where time-of-day electricity rates are applicable, the

impact of fluctuating performance on the system operating cost may be even more significant. For a detailed building energy analysis, a ground loop heat exchanger simulation model is called for that can reliably and efficiently predict the short-term fluctuations in the heat pump entering fluid temperatures. This enables the determination of energy consumption and demand on an hour-by-hour basis.

Although the size and the number of total annual operating hours of the supplemental heat rejecters may be estimated based on the annual building loads and the maximum available size of the borefield for a given area, the decision under what conditions to activate the heat rejection and its short time impact on the ground loop heat exchangers is somewhat complex. Recently published works (Kavanaugh 1998, Kavanaugh and Rafferty 1997, Phetteplace and Sullivan 1998) only use a set point control, usually an upper temperature limit for entering fluid temperature to the heat pump returning from the ground heat exchanger and do not consider more sophisticated system control strategies. In order to quantify the impact of various operating strategies on ground loop heat exchanger size and operating cost, a simulation model that can account for changes in the hourly load profile and interaction between the ground loop heat exchanger and heat rejecter is highly desirable.

Therefore, in this study, the short time-step simulation model described in Chapter 5 is used that allows for an hour-by-hour building energy analysis. Using hourly weather data from a typical meteorological year for a specific location, the simulation model is capable of predicting the entering and exiting heat transfer fluid temperatures on

the borefield on hourly or less time intervals. An hour-by-hour system analysis allows for more sophisticated and flexible control strategies. An example strategy may be the ‘recharge’ of the borefield at certain time intervals during a day to lower the heat pump entering fluid temperatures.

The objective of this analysis is to present a comparative study to investigate the advantages and the disadvantages of several system operating and control strategies using an hour-by-hour system simulation model for two different climate conditions. The short time-step simulation approach taken will allow for a more detailed assessment of the ground loop heat exchanger behavior as well as for the analysis of the impact of various control strategies on system operating costs.

A small office building (actually located in Stillwater, Oklahoma) is used as the example building. The building loads analysis for each climate region was performed using BLAST (1986). The simulations for the short time-step building energy analysis and ground loop heat exchanger temperatures were performed using TRNSYS by Klein et al. (1996).

7.2. REVIEW OF LITERATURE

A review of recent literature on hybrid ground source heat pump systems yielded only a modest number of references to research articles and a few references to reports dealing with actual applications.

ASHRAE (1995) discusses the advantages of hybrid ground source heat pump applications considering capital costs and available surface area limitations for a 100% ground coupled system. A design procedure is suggested for cooling-dominated buildings that sizes the capacity of the supplemental heat rejecters based on the difference between the monthly average cooling and heating loads of a given building rather than the peak loads. The ground loop is sized to meet the building heating loads while the cooling load in excess of the heating load is met through supplemental heat rejection. For closely spaced vertical boreholes, it is suggested that it may be advantageous to operate the supplemental heat rejection unit during night hours for cold storage in the ground. A series of general guidelines is given discussing the integration of the supplemental heat rejecters into internal piping, the need for an isolation plate heat exchanger when an open cooling tower is used, the set point control of heat rejection based on an upper limit of heat pump entering fluid temperatures, cold storage in the ground through night operation, and the possible year around operation of the rejecters in southern climates.

Kavanaugh and Rafferty (1997) discuss hybrid ground source heat pump systems within the framework of ground loop heat exchanger design alternatives. Primary factors that may mandate the consideration of a hybrid system are the high cost of long loops when the design relies on the ground to meet 100% of the building heating and cooling requirements, the unavailability or cost of space and the high cost of high-efficiency heat pumps. The sizing of the supplemental heat rejecters is based on peak block load at the design condition. The nominal capacity is calculated based on the difference between the

ground loop heat exchanger lengths required for cooling and heating. Recommendations are made for the integration of the supplemental heat rejecters into the ground source heat pump piping system. Fluid flow control options for the careful flow balancing in the system to optimize the system and the flow stations are discussed.

Kavanaugh (1998) revises and extends the existing design procedures as recommended in ASHRAE (1995) and in Kavanaugh and Rafferty (1997). This revised design procedure addresses issues such as ground heat exchange and heat buildup, system control methods, piping arrangements, freeze protection, auxiliary energy consumption and maintainability. The revised method, in addition to sizing the ground loop heat exchanger of the hybrid system and the supplemental heat rejecter, proposes a method for balancing the heat transfer in the ground formation on an annual basis in order to limit heat pump performance degradation due to heat buildup in the borefield. The annual operating hours of the supplemental heat rejecter needed to balance the heat rejection and extraction in the ground are calculated based on a set point control of the ground loop temperature (a typical range of 80°F [27°C] to 90°F [32°C] is given). The revised procedure is then applied to a multi-story office building considering three different climates to investigate the appropriateness of the hybrid application. Installation cost savings and operating cost issues are discussed. The author concludes that the economic value of hybrid systems is most apparent in warm and hot climates where cooling loads are the highest. Although hybrid systems with heat recovery options are deemed somewhat attractive for moderate climate regions, no economic value could be justified for cold climate even with heat recovery.

Phetteplace and Sullivan (1998) describe a 24,000 ft² (2,230 m²) military base administration building in Fort Polk, LA that uses a hybrid ground source heat pump system. The system uses 70 vertical closed-loop boreholes, each 200 ft (61 m) deep with 10 ft (3.3 m) spacing. The paper presents performance data for a period of 22 months including performance data from portions of two heating and cooling seasons. The observed data show that, over the period of monitoring, the amount of heat rejected to the ground is about 43 times higher than the amount of heat extracted from it. This is indicative of a very heavily cooling dominated building. The supplemental heat rejecter is a 275 kW (938 kBTU/hr) cooling tower and is controlled with a differential controller that activates the cooling tower fans when the heat pump exiting fluid temperature reaches 97°F (36°C) and deactivates it when this temperature falls below 95°F (35°C). The authors report some heat buildup in the ground due to an imbalance of heat extraction and rejection in the ground. This is attributed to differential controller set point temperatures that are too high. Lowering of these control points is expected to dissipate the heat buildup at the cost of increasing the operating hours of the cooling tower. The relative energy consumption of the major system components over the study period is provided where the heat pumps account for 77% of the total energy consumption, the circulating pumps for 19%, the cooling tower fan for 3% and the cooling tower pump for 1%.

Singh and Foster (1998) explore first cost savings that resulted from using a hybrid ground source heat pump design on the Paragon Center building located in

Allentown, PA and an elementary school building in West Atlantic City, NJ. The Paragon center illustrates the need for a hybrid application as a direct result of geological conditions at the site where boreholes drilled deeper than 110 ft (33.5 m) collapsed due to high ground water flow in limestone strata. The building area is 80,000 ft² (7,436 m²). The hybrid system consists of 88 boreholes each approximately 125 ft (38 m) deep and a closed-circuit fluid cooler of 422 kW (1,440 kBTU/hr) maximum capacity. The elementary school expansion building in West Atlantic City is an example of a hybrid system where the available space for the borehole field was not sufficient to accommodate the number of boreholes required to fully meet the building cooling loads. The building area is approximately 63,000 ft² (5,856 m²). A closed-circuit fluid cooler of 411 kW (1,402 kBTU/hr) capacity is used, decreasing the required number of boreholes by more than 25% to 66 bores, each about 400 ft (122 m) deep. In both of the reported examples, a significant system first cost savings is achieved though with slightly higher operating and maintenance costs.

A more detailed study of the hybrid ground source heat pump system in the Paragon Center office building is provided by Gilbreath (1996). The study gives design suggestions for hybrid systems using the Paragon Center as an example and attempts to establish methods for monitoring system performance through the measurement of energy consumption, demand and loop temperatures. The impact of various control options based on the percentage assistance of the cooling tower in rejecting excess heat is investigated. Effects of heat recovery and fluid flow control are discussed. An installation and operating cost analysis is provided comparing the hybrid application to

the ground source heat pump system without supplemental heat rejection to assess and quantify potential cost savings.

7.3. SUPPLEMENTAL HEAT REJECTION

Open-circuit cooling towers and closed-circuit fluid coolers are commonly used for supplemental heat rejection in hybrid ground source heat pump systems. Water is typically used as a heat transfer medium to remove heat from the heat transfer fluid in the ground loops. Open-circuit cooling towers are typically used in conjunction with isolation plate heat exchangers, in order to avoid a mixing of the loop heat transfer fluid and the cooling water. Air-cooled closed-circuit fluid coolers are modular units that accomplish the cooling effect by directly rejecting heat to the atmosphere. However, the first cost and the fan energy consumption of these devices are generally high. Kavanaugh (1998) estimates lower first costs for open-circuit cooling towers with isolation plate heat exchanger than for fluid coolers.

Recent research on hybrid ground source heat pumps focuses on surface heat rejecters such as shallow heat rejecters under pavements or in ponds. Surface heat rejecters consist of a series of pipes inserted in the concrete layers of pavements for heating of parking lots during winter months or laid out close to the bottom surface of ponds.

In this study, the supplemental heat rejecter is a mechanical draft, open-circuit cooling tower used in combination with an isolation plate heat exchanger.

7.4. HYBRID SYSTEM OPERATION USING THE SHORT TIME-STEP SIMULATION MODEL

7.4.1. EXAMPLE HYBRID SYSTEM DESCRIPTION

The example small office building was completed in 1997 and is located in Stillwater, Oklahoma. The total area of the building is approximately 14,205 ft² (1,320 m²). The building was a candidate for a ground source heat pump system application though, in the event, a conventional system was installed.

In order to determine the annual building loads for the example building using BLAST (1986), the following approach was taken:

- i) Eight different thermal zones were identified in the building. For each zone, a single zone draw through fan system is specified as a surrogate for a ground source heat pump. The coil loads on this system are equivalent to those of a ground source heat pump system.
- ii) The office occupancy is set to 1 person per 100 ft² (9.3 m²) with a heat gain of 450 BTU/hr (131.9 W) 70% of which is radiant.
- iii) The office equipment heat gains are set to 1.1 W/ft² (12.2 W/ m²) as suggested by Komor (1997).

- iv) The lighting heat gains are set to 1 W/ft² (11.1W/m²).
- v) Day time (8am-6pm, Monday-Friday), night time and weekend thermostat settings are specified for each zone. During the day, the temperature set point is 68.0°F (20.0°C). For the night, only heating is provided, if necessary, and the set point is 58.0°F (14.4°C).

7.4.2. CLIMATIC CONSIDERATIONS-BUILDING LOADS

The example building is analyzed considering two different climatic regions each represented by the Typical Meteorological Year (TMY) weather data: A typical hot and humid climate is simulated using Houston, TX, a more moderate climate is simulated using Tulsa, OK. The results of the BLAST building loads analysis are shown in Figure 7.1 for both regions considered. The building loads are determined on an hour-by-hour basis for 8760 hours. The cooling loads are shown as negative loads on the building.

As expected, the cooling loads are greatest for Houston, TX typical weather conditions where the example building is heavily cooling-dominated. As the example building is considered in a relatively cooler climate (Tulsa, OK), the building becomes somewhat less cooling dominated, and an increase in heating loads is observed.

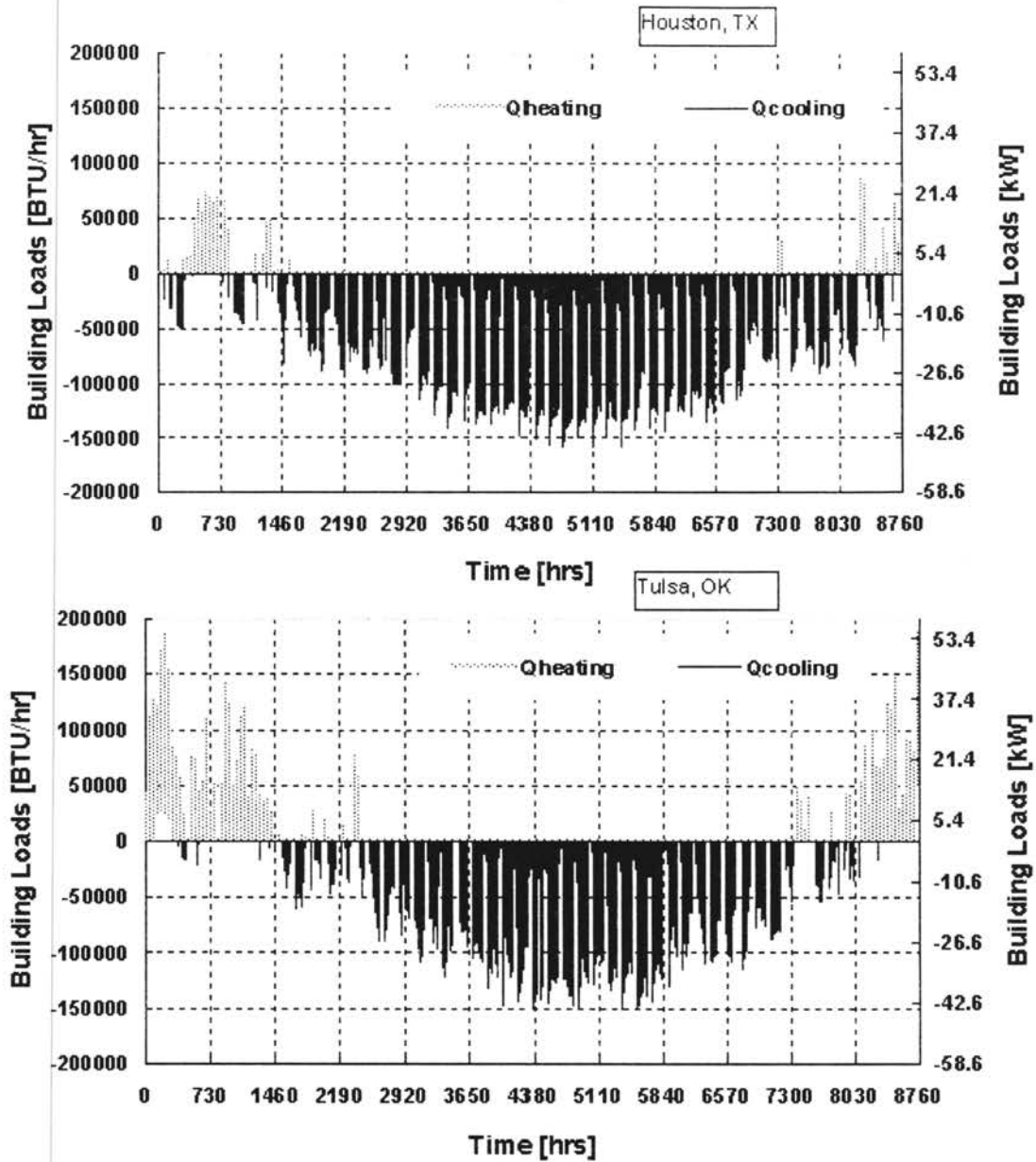


Figure 7.1 - Annual hourly building loads considering Houston, TX and Tulsa, OK typical climatic conditions.

Two other climate regions were initially considered: A climate where heating and cooling loads are expected to be balanced for the example building over a year as Indianapolis, IN, and a heating dominated climate region as International Falls, MN.

However, initial calculations of the total borehole loop length for both climate regions indicated that a hybrid ground source heat pump system would not be ideal for those regions because of relatively low building cooling loads.

7.4.3. HYBRID SYSTEM COMPONENT CONFIGURATION

A schematic of the hybrid ground source heat pump system application is shown in Figure 7.2. The hybrid system uses an open cooling tower with an isolation plate heat exchanger. Two independent fluid circulation loops are designed that are serviced with fluid circulation pumps #1 and #2.

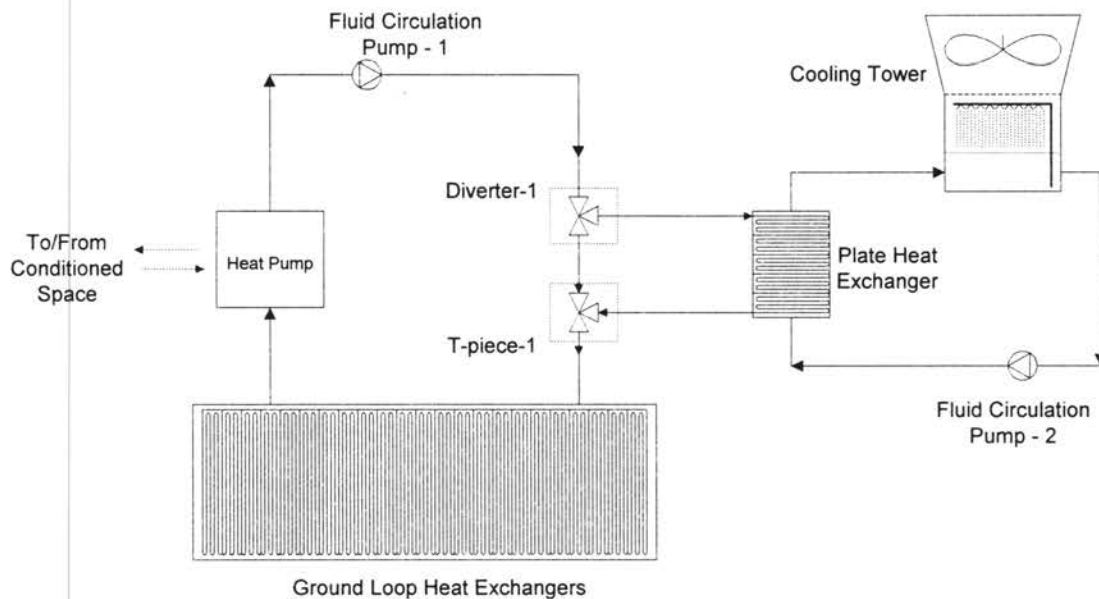


Figure 7.2 - Hybrid ground source heat pump system component configuration diagram.

The design contains a bypass (Diverter-1, T-piece-1) so that pumping energy may be conserved when the cooling tower is not being used.

The operation and performance of the hybrid system is simulated using TRNSYS (Klein et al. 1996). Standard TRNSYS library component models are used for components such as the diverters, T-pieces, fluid circulation pumps, plate heat exchanger and the cooling tower. A simple heat pump component model as described by in Chapter 5.3 is used. The ground loop heat exchanger model is described in Chapter 5.2.

7.4.4. GROUND LOOP HEAT EXCHANGER AND COOLING TOWER SIZING

One of the determining factors in sizing the length of the ground loop heat exchangers and in determining the capacity of the cooling tower in a hybrid ground source heat pump system design is the peak entering fluid temperature (EFT) to the heat pump from the borehole field. A significant number of 'off-the-shelf' heat pumps are designed by their manufacturers for peak EFT's ranging between 85.0°F (29.4°C) to 95.0°F (35.0°C). The EFT's can be as high as 110.0°F (43.3°C) with high-efficiency rated heat pumps. Heat pump peak entering fluid temperatures above the rated operating temperatures degrade the performance of the heat pump. Similarly, there are lower limits for the heat pump entering fluid temperature that depend on the heat pump and the type of heat transfer fluid used in the loops. For high heating demands during winter months, this temperature may be near the freezing point of the working fluid. Any ground loop and supplemental heat rejecter design must therefore be constrained by limits on the peak

EFT to the heat pump. Currently available methods for determining the required total length of ground loops use approaches that iterate between the total loop length and the maximum and the minimum heat pump EFT's for a specified duration (say 20-25 years) of system operation.

Currently available methods for the sizing of supplemental heat rejecters attempt to balance the annual ground energy rejection with the annual ground energy extraction. Theoretically, the average borehole field temperature will then not increase from year-to-year because no long-term temperature rise in the ground is thus allowed to occur. However, some control strategy must be implemented to achieve an annual balance. A very common approach is to activate the supplemental heat rejecters when the loop temperature is greater than a certain upper limit. It is, therefore, possible to decrease the size of the supplemental heat rejecter by increasing the required operating hours (settle for a smaller unit but operate it longer) or to increase the size of it by decreasing the required operating hours (settle for a bigger unit but operate it less). Accordingly, the supplemental heat rejecter sizing procedure may be somewhat flexible. The component model used allows for an hour-by-hour computation of the total amount of heat rejected through the cooling tower. For a control strategy, it is thus possible to determine the actual size of the supplemental heat rejecter based on the amount of hourly heat rejection. Nevertheless, it should be noted that the objective of this study is not to develop or recommend procedures for sizing supplemental heat rejecters, but rather to investigate the effects of various control strategies on the system operation. Nevertheless, an optimal

design procedure would be an excellent topic for future research. Additional details of the cooling tower sizing are provided in Appendix A.

Initially, a large cooling tower was selected. Then, the final required cooling tower capacity was determined by simulating with the large cooling tower, and determining the required cooling tower capacity when the peak entering fluid temperature to the heat pump occurs. The cooling towers are probably slightly oversized, as the peak capacity was specified at the design wet bulb temperature, even though that may not be coincident with the peak EFT. The simulated capacity of the cooling tower changes from one climatic region to another (Houston, TX vs. Tulsa, OK) due to the local wet bulb temperatures and the required fluid flow rates. An air flow rate of about 5300 cfm (9000 m³/hr) is drawn through the cooling tower, operating on a simple on/off switch.

7.4.5. OPERATING AND CONTROL STRATEGIES

The control strategies are selected to provide comparisons between system operations with and without the use of supplemental heat rejection. Admittedly, the selection of the system operating and control strategies for systems with supplemental heat rejection can be somewhat arbitrary, although an attempt has been made to include commonly employed control schemes. The objective here is to investigate the impact of each control strategy on the system operation rather than suggest a specific operating procedure. Including the case of optimum ground loop heat exchanger design for a climate region, ten system operating and control strategies were investigated:

Base case: The ground loop heat exchanger length is designed without the use of any supplemental heat rejecters. System fully relies on the ground loop heat exchanger to meet the building loads.

Case 2: The ground loop heat exchanger length is designed considering the use of supplemental heat rejecters, yielding a smaller ground loop heat exchanger size. However, no supplemental heat rejection is included in the simulations. This ‘undersized’ ground loop case is of interest to illustrate the heat buildup and its effects on the loop temperatures at the heat pump.

Case 3: In this control strategy, the cooling tower is activated when the heat pump entering or exiting fluid temperatures are greater than a set value. The following two strategies are considered:

Case 3a) $Ex_{FT} > 96.5^{\circ}\text{F}$ (35.8°C).

Case 3b) $E_{FT} > 96.5^{\circ}\text{F}$ (35.8°C)

Case 4: This case uses a differential temperature control approach for the operation of the cooling tower and the circulation pump on the secondary system loop. The difference between either the heat pump entering or the exiting fluid temperatures and the ambient wet bulb temperature is used as the control criterion. It is subdivided into three strategies. The operation of the cooling tower may be based on:

Case 4a) The cooling tower fan and the secondary fluid circulation loop pump are activated whenever the difference between the heat pump entering fluid temperature and the ambient air wet bulb temperature is greater than 3.6°F (2.0°C). The cooling tower fan and the secondary fluid circulation loop pump are turned off when this difference is less than 2.7°F (1.5°C).

Case 4b) The cooling tower fan and the secondary fluid circulation loop pump are activated whenever the difference between the heat pump entering fluid temperature and the ambient air wet bulb temperature is greater than 14.4°F (8.0°C). The cooling tower fan and the secondary fluid circulation loop pump are turned off when this difference is less than 2.7°F (1.5°C).

Case 4c) The cooling tower fan and the secondary fluid circulation loop pump are activated whenever the difference between the heat pump exiting fluid temperature and the ambient air wet bulb temperature is greater than 3.6°F (2.0°C). The cooling tower fan and the secondary fluid circulation loop pump are turned off when this difference is less than 2.7°F (1.5°C).

Case 5: The operating and control strategy is based on cool storage in the ground to avoid a long-term temperature rise. The cool storage effect is achieved by operating the supplemental heat rejecters for 6 hours during the night. As a precaution to avoid potentially high loop temperatures, a set point control is also built in. Any heating load

during the recharge period is neglected. Three different sub-strategies are considered to assess the impact of ground recharge in different seasons:

Case 5a) The cooling tower fan and the secondary loop circulation pump are activated between 12:00 a.m. and 06:00 a.m. throughout a year. In addition, the supplemental heat rejecter is operated when the entering fluid temperature to the heat pump exceeds 96.5°F (35.8°C).

Case 5b) This strategy is very similar to 5a. The only difference is that the cooling tower fan and the secondary loop circulation pump are activated between 12:00 a.m. and 06:00 a.m. only during the months of January through March (ground recharge during cold season).

Case 5c) Similar to 5a but the cooling tower fan and the secondary loop circulation pump are activated during ground recharge between 12:00 a.m. and 06:00 a.m. only during the months of June through August (ground recharge during hot season).

7.4.5.1. BASE CASE-OPTIMUM DESIGN OF THE BOREFIELD WITHOUT SUPPLEMENTAL HEAT REJECTION

This is the reference case, to which all other cases will need to be compared. For base case, the ground loop heat exchanger is sized for use without any supplemental heat rejection. In the analyses of this study, the optimal ground loop size for each climatic region is based on a peak EFT of approximately 96.5°F (35.8°C). The size was determined by adjusting the borehole depth so that the maximum temperature determined

with a 20 year simulation just reached the specified peak EFT. The borehole depth was then rounded to the nearest 10 ft (3.1 m).

The system simulation for this case included only the heat pump, the ground heat exchangers, and the circulation pump of the main loop. Using the building loads for the two climatic regions, the model is run on an hour-by-hour basis for the design simulation period of 20 years. Heat pump EFT's for the first two years are plotted in Figure 7.3. These results are based on a fluid flow rate of 3.0 gpm ($0.68 \text{ m}^3/\text{hr}$) of water per borehole and on undisturbed ground temperatures of $T_{\text{FarField Houston}} = 73.0^\circ\text{F}$ (22.8°C), $T_{\text{FarField Tulsa}} = 63.0^\circ\text{F}$ (17.2°C). For both climates, a constant thermal conductivity of 1.2 BTU/hr-ft- $^\circ\text{F}$ (2.08 W/m-K) is assumed for the ground formation. Identical single borehole geometries with constant borehole resistance (borehole radius of 3.5 inches [88.9 mm], U-tube pipe size of 1.25 inches [31.75mm] and thermally enhanced grout with $k_{\text{grout}}=0.85$ BTU/hr-ft-F [1.47 W/m-K] are assumed) are configured for the comparison.

The ground loop heat exchanger for Houston comprised 36 boreholes in a 6X6 configuration, each borehole drilled to 250.0 ft (76.2 m) deep, 12.5 ft (3.8 m) apart. The maximum predicted EFT to the heat pump after two years is about 86.0°F (30.0°C) rising to a maximum of 96.6°F (35.9°C) after 20 years of simulation. The minimum EFT of the 20 year simulation is 71.3°F (21.8°C) occurring in the first year. The design for Tulsa has 16 boreholes in a 4X4 configuration, each borehole drilled to 240 ft (73.2 m), 12 ft (3.7 m) apart. The maximum EFT after 2 years of simulation is about 89.4°F (31.9°C)

rising to 96.4°F (35.8°C) after 20 years. For Tulsa, the minimum EFT to the heat pump is 50.2°F (10.1°C).

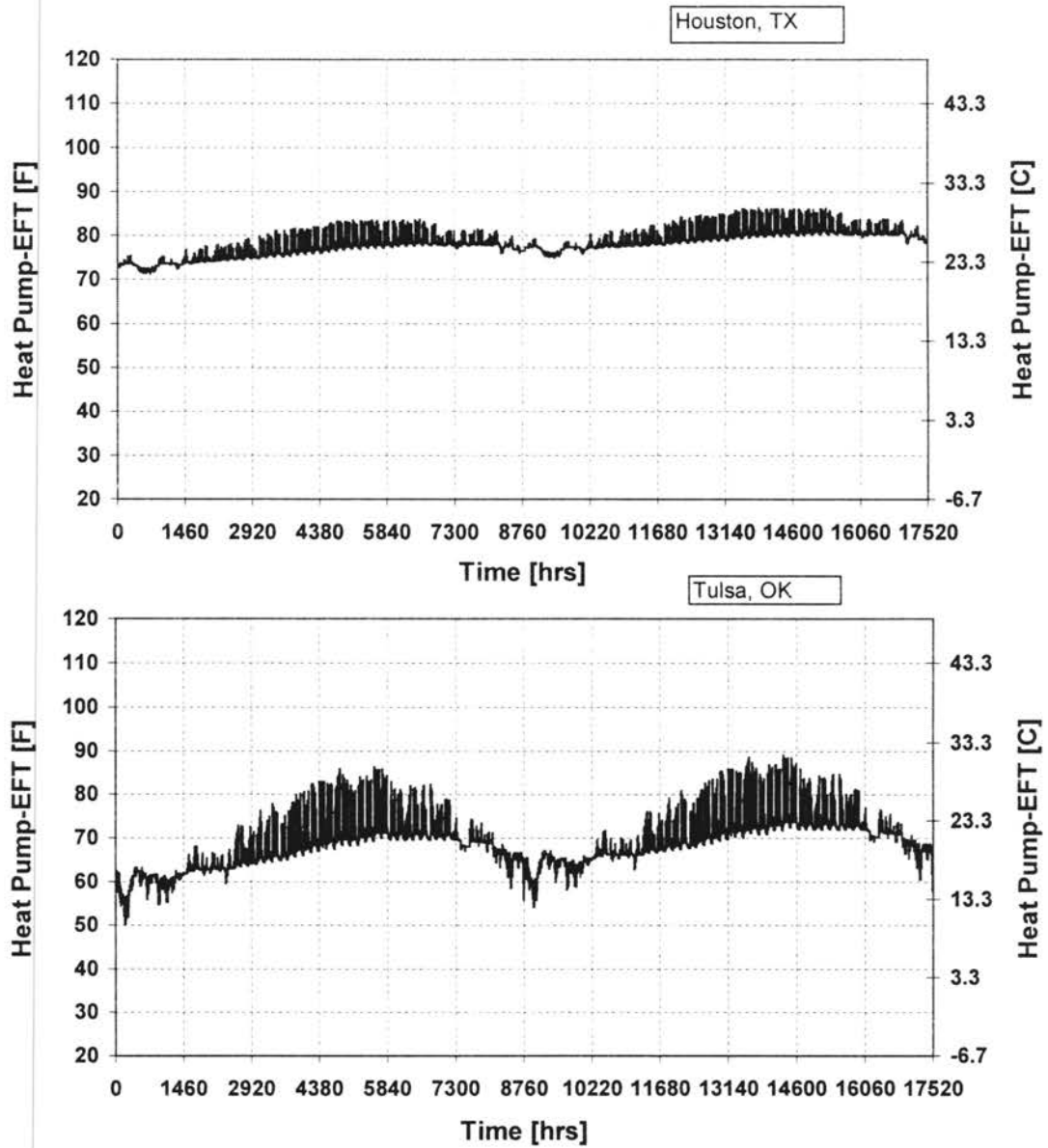


Figure 7.3 – Hourly entering fluid temperatures to the heat pump considering Houston, TX, and Tulsa, OK typical climatic conditions. Base Case.

The daily fluctuations in the heat pump EFT's increase significantly as the example building is considered in relatively colder climates. This is because, in colder climates, a smaller ground heat exchanger is required to meet the peak EFT for a given peak cooling load. Naturally, the smaller ground heat exchanger results in a larger daily fluctuation in EFT over a day.

TABLE 7.1
System Simulation Summary for Base Case

	HOUSTON, TX			TULSA, OK		
	1 st year	20 th year	20-year average	1 st year	20 th year	20-year average
Power Consumption-Heat Pump [kWh]	20,399	25,904	24,245	17,931	20,660	19,927
Power Consumption-Fluid Circulation Pump [kWh]	16,177	16,177	16,177	7,190	7,190	7,190
Total Power Consumption-[kWh]	36,577	42,082	40,423	25,122	27,850	27,117

The power consumption of the heat pump and the circulating pump for the base case are provided in Table 7.1 for both Tulsa and Houston TMY conditions. The percent power consumption distribution between the fluid circulation pump and the heat pump is 40% / 60% for Houston and 23.5% / 76.5% for Tulsa respectively. The power consumption of the fluid circulation pump is significantly smaller in Tulsa than in Houston due to the shorter loop length for Tulsa.

7.4.5.2. UNDERSIZED DESIGN OF THE BOREFIELD WITHOUT SUPPLEMENTAL HEAT

REJECTION

The operation of the undersized borehole field without any supplemental heat rejection is interesting for it illustrates the effects of the long-term temperature rise in the ground due to reduced ground loop heat exchanger length. The borefield for Houston TMY conditions is designed with 12 boreholes in a 3X4 configuration each 250 ft (76.2 m) deep. This represents a 2/3 reduction from the base case. For Tulsa TMY conditions, the borefield is reduced from 16 boreholes to nine boreholes arranged in a 3X3 configuration with each borehole drilled to 240 ft (73.2 m).

The hourly heat pump entering fluid temperatures for Houston and Tulsa are shown in Figure 7.4. Even for the first two years of simulation, the EFT's to the heat pump are already over 110.0°F (43.3°C). A 20-year simulation predicts heat pump EFT's in excess of 120.0 °F (48.9 °C). The temperature fluctuations are observed to occur in a significantly wider band than in the base case. This is because an unchanged amount of heat is required to be rejected through a shorter loop length. Accordingly, the heat transfer fluid entering the heat pump from the ground is at a higher temperature. If this excess heat were not to be dissipated through supplemental rejection, the COP of the heat pump would deteriorate significantly over time.

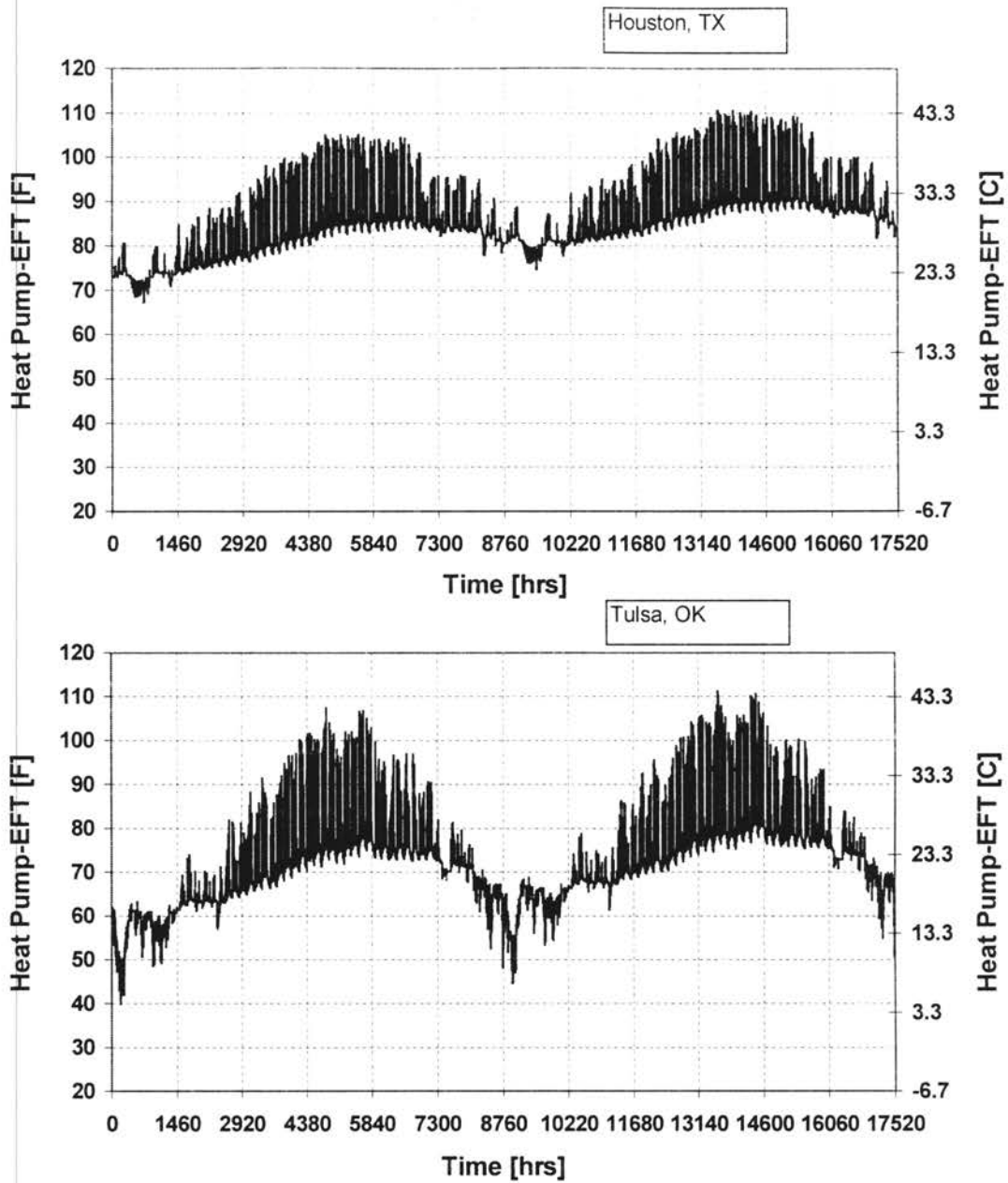


Figure 7.4 – Hourly entering fluid temperatures to the heat pump for typical Houston, TX and Tulsa, OK climatic conditions. Case 2.

Table 7.2 shows the power consumption of the heat pump and the fluid circulation pump for Tulsa and Houston. In this case without any supplemental heat rejection, the power consumption on the fluid circulation pumps is lowered significantly due to shorter loop lengths. However, since a long-term temperature rise is allowed to occur in the

borefield, the heat pump operates with lower efficiency. This results in a sizeable increase in the power consumption of the heat pump for both Tulsa and Houston TMY conditions. Although the total system power consumption remains almost unchanged as compared to the base case, the heat pump power consumption for Houston and Tulsa is significantly higher. It should be noted here that the heat pump power consumptions are based on curve fits of catalog data. Necessarily, they are extrapolated to higher temperatures than are supported by the catalog data. Therefore, the accuracy of the power consumption data may be reduced. Perhaps it should suffice to say that the heat pumps are running with EFT's outside the recommended operating range, most probably with additional deleterious effects.

TABLE 7.2
System Simulation Summary for Case 2

	HOUSTON, TX			TULSA, OK		
	1 st year	20 th year	20-year average	1 st year	20 th year	20-year average
Power Consumption-Heat Pump [kWh]	26,583	37,458	34,424	21,680	25,985	24,855
Power Consumption-Fluid Circulation Pump [kWh]	5,392	5,392	5,392	4,044	4,044	4,044
Total Power Consumption-[kWh]	31,976	42,851	39,817	25,724	30,030	28,900

7.4.5.3. SET POINT CONTROL FOR THE HEAT PUMP ENTERING AND EXITING FLUID TEMPERATURES

A set point control for the operation of the supplemental heat rejecters is straightforward. With this control strategy, the cooling tower is activated whenever the heat pump exiting (Case 3a) or entering (Case 3b) fluid temperature reaches 96.5°F (35.8°C). The upper limit of 96.5°F (35.8°C) is selected considering the design maximum entering fluid temperature in the base case design. The operating hours of the cooling tower, the energy consumption resulting from supplemental heat rejection including the cooling tower fan and the pumping energy for the secondary fluid circulation loop (circulation pump-2), the energy consumption due to the heat pump operation and the main fluid circulation loop (circulation pump-1) are given in Tables 7.3 and 7.4 for both climate regions.

In cooling dominated buildings, the temperature of the fluid exiting from the heat pump to the borefield will typically be higher than the temperature entering the heat pump. A set point control scheme that is based on the heat pump exiting temperature will therefore activate the cooling tower more often. Similarly, the duration of the cooling tower operation in general will depend on building cooling loads. The higher the building loads, the more heat will need to be rejected, the longer and/or the more often the supplemental heat rejecters will be activated.

A comparison between Tables 7.1 and 7.3, shows that the annual average power consumption of the heat pump is slightly decreased for both climate regions when

compared to the base case. The heat pump operates more efficiently due to slightly lower entering fluid temperatures to the heat pump. Overall, however, the savings in electricity consumption are somewhat larger due to reduced pumping costs associated with a smaller borefield.

TABLE 7.3
Hybrid System Simulation Summary for Control Strategy 3a

	HOUSTON, TX			TULSA, OK		
	1 st year	20 th year	20-year average	1 st year	20 th year	20-year average
Operation of the Cooling Tower [hr]	523	750	704	317	440	415
Power Consumption-Cooling Tower Pump [kWh]	31	45	42	19	26	25
Power Consumption-Cooling Tower [kWh]	193	277	260	117	162	153
Power Consumption-Heat Pump [kWh]	22,734	24,086	23,877	19,227	19,953	19,813
Power Consumption-Main Circulation Pump [kWh]	5,392	5,392	5,392	4,044	4,044	4,044
Total Power Consumption-[kWh]	28,351	29,802	29,573	23,408	24,187	24,036

The increase in operating hours for both control sub-strategies in later years of simulation is due to small temperature rise in the ground. Accordingly, the cooling tower must run somewhat longer. The set point temperature may be lowered to reduce the long-term temperature rise.

TABLE 7.4

Hybrid System Simulation Summary for Control Strategy 3b

	HOUSTON, TX			TULSA, OK		
	1 st year	20 th year	20-year average	1 st year	20 th year	20-year average
Operation of the Cooling Tower [hr]	236	604	541	84	272	233
Power Consumption-Cooling Tower Pump [kWh]	14	36	32	5	16	14
Power Consumption-Cooling Tower [kWh]	87	223	200	31	100	86
Power Consumption-Heat Pump [kWh]	24,459	25,653	25,413	20,742	21,384	21,264
Power Consumption-Main Circulation Pump [kWh]	5,392	5,392	5,392	4,044	4,044	4,044
Total Power Consumption-[kWh]	29,953	31,306	31,039	24,823	25,546	25,409

Hourly heat pump entering fluid temperatures and heat rejection in the cooling tower for Case 3a are provided in Figure 7.5 for Houston TMY conditions. The maximum entering fluid temperature to the heat pump is 96.8°F (36.0°C) occurring in the 20th year of the simulation. The results for Tulsa are qualitatively similar.

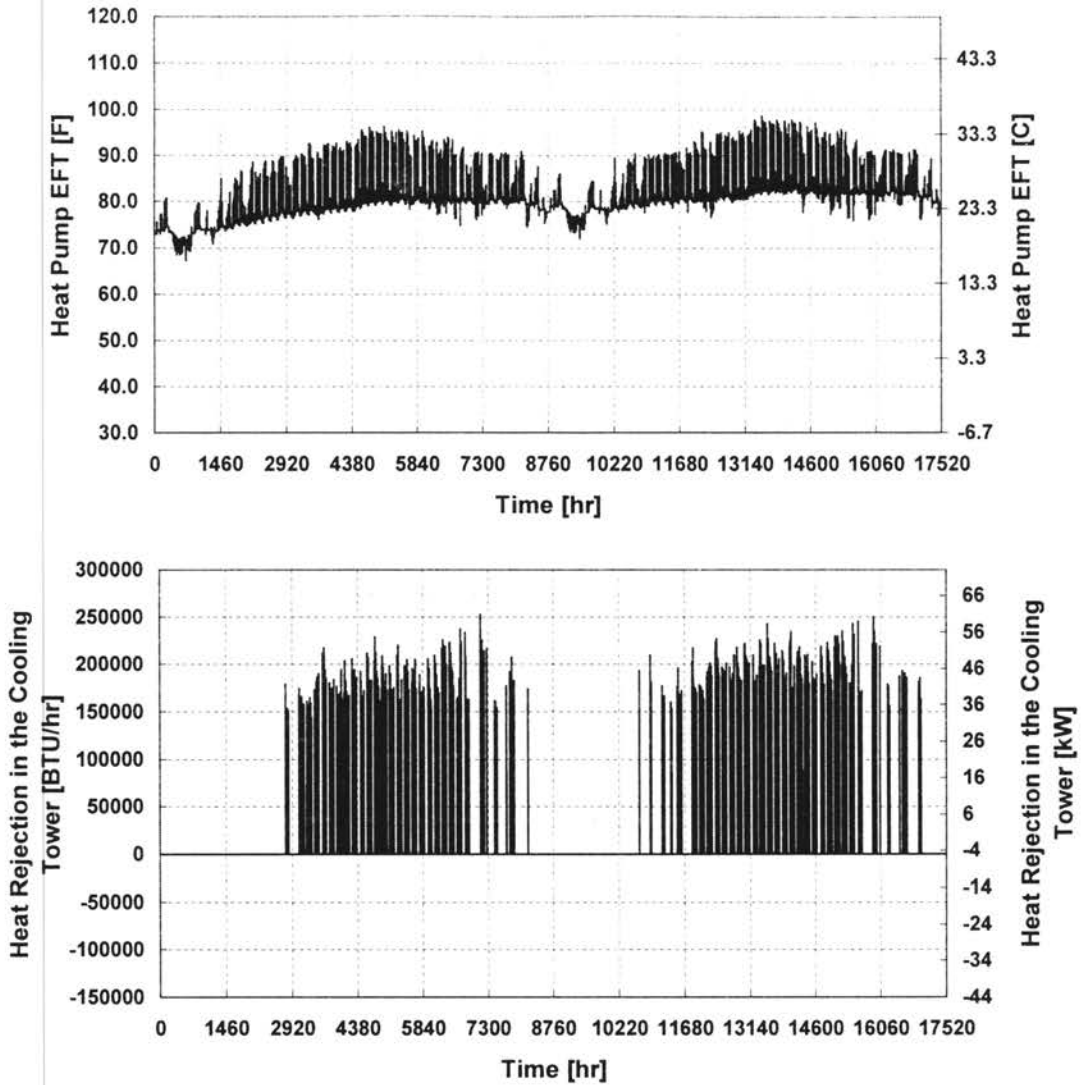


Figure 7.5 – Hourly entering fluid temperatures to the heat pump and heat rejection in the cooling tower for typical Houston, TX climatic conditions. 2-year simulation - Case 3a.

7.4.5.4. DIFFERENTIAL CONTROL FOR THE HEAT PUMP ENTERING AND EXITING FLUID TEMPERATURES (CASE 4)

An operating control strategy based on the difference between the heat pump entering or exiting fluid temperature and the ambient air wet bulb temperature is designed

to reject heat whenever the weather conditions are advantageous. The ambient air wet bulb temperature is preferred to the dry bulb temperature since the effectiveness of the cooling tower is based on the difference between the cooling tower inlet water temperature and the ambient air wet bulb temperature.

In this strategy, the cooling tower and the secondary loop water circulation pump are activated when the difference between EFT or ExFT and T_{WetBulb} are greater than the specified dead band high point (upper temperature difference). The cooling continues until this temperature difference falls below the dead band low point (lower temperature difference). For this analysis, a dead band low point of 2.7°F (1.5°C) is selected while two different dead band high points are used, 3.6°F (2.0°C) and 14.4°F (8.0°C) to investigate the effects of the size of the dead band. When the control strategy is based on the heat pump exiting fluid temperature a dead band with a low point of 2.7°F (1.5°C) and high point of 3.6°F (2.0°C) is defined.

Due to the higher cooling demand of the example building in Houston, a higher frequency for the cooling tower operation can be expected. The increased frequency for cooling tower operation strongly depends on the size of the borehole field as well as on the cooling demand of the building. The higher the cooling demand of the building and the smaller the borehole field, the more often will the cooling tower be operated.

Summaries of the simulation results for control strategies 4a, 4b and 4c are shown in Tables 7.5, 7.6 and 7.7.

For both climate regions, a general decrease in the annual operating hours of the cooling tower from the first year to the 20th year of system simulation is observed for the three control sub-strategies. This is because, on an annual basis, more heat is extracted than rejected. The hybrid system with this control strategy cools the ground rather than heats it on a long term basis. For Case 4b, the cooling tower runs significantly less hours than for Case 4a. An increase in the annual average time of operation is observed when the ExFT is used to establish the temperature differential for this control strategy (Case 4c). This was to be expected since, in the cooling mode, the ExFT is greater than EFT.

Unlike Case 3, in Cases 4a, 4b, and 4c, significant savings in the heat pump electricity consumption are realized. For the best case, 4c, 27% savings in heat pump electricity consumption are achieved in Houston, and 17% in Tulsa. In Houston, the overall savings in electricity consumption (37%) are significantly higher because of the reduced pumping requirements. In Tulsa, the overall savings are approximately the same as the heat pump savings because the reduced electricity consumption of the main circulating pump is offset by the electricity consumption of the cooling tower fan and secondary circulating pump.

TABLE 7.5
Hybrid System Simulation Summary for Control Strategy 4a

	HOUSTON, TX			TULSA, OK		
	1 st year	20 th year	20-year average	1 st year	20 th year	20-year average
Operation of the Cooling Tower [hr]	5,140	4,470	4,569	5,159	4,647	4,723
Power Consumption-Cooling Tower Pump [kWh]	311	270	276	312	281	286
Power Consumption-Cooling Tower [kWh]	1,901	1,653	1,690	1,908	1,719	1,747
Power Consumption-Heat Pump [kWh]	19,199	19,016	19,045	17,664	17,542	17,568
Power Consumption-Main Circulation Pump [kWh]	5,392	5,392	5,392	4,044	4,044	4,044
Total Power Consumption-[kWh]	26,804	26,333	26,405	23,929	23,587	23,646

TABLE 7.6

Hybrid System Simulation Summary for Control Strategy 4b

	HOUSTON, TX			TULSA, OK		
	1 st year	20 th year	20-year average	1 st year	20 th year	20-year average
Operation of the Cooling Tower [hr]	3,961	3,483	3,550	3,818	3,430	3,481
Power Consumption-Cooling Tower Pump [kWh]	239	210	215	231	207	210
Power Consumption-Cooling Tower [kWh]	1,465	1,288	1,313	1,412	1,269	1,288
Power Consumption-Heat Pump [kWh]	20,435	20,507	20,488	18,571	18,649	18,644
Power Consumption-Main Circulation Pump [kWh]	5,392	5,392	5,392	4,044	4,044	4,044
Total Power Consumption-[kWh]	27,533	27,399	27,409	24,260	24,170	24,188

TABLE 7.7

Hybrid System Simulation Summary for Control Strategy 4c

	HOUSTON, TX			TULSA, OK		
	1 st year	20 th year	20-year average	1 st year	20 th year	20-year average
Operation of the Cooling Tower [hr]	5,456	4,909	4,993	5,542	5,002	5,088
Power Consumption-Cooling Tower Pump [kWh]	330	297	302	335	302	308
Power Consumption-Cooling Tower [kWh]	2,018	1,816	1,847	2,050	1,850	1,882
Power Consumption-Heat Pump [kWh]	18,162	17,722	17,792	16,648	16,423	16,463
Power Consumption-Main Circulation Pump [kWh]	5,392	5,392	5,392	4,044	4,044	4,044
Total Power Consumption-[kWh]	25,903	25,229	25,335	23,078	22,621	22,699

Hourly entering fluid temperatures to the heat pump and the hourly heat rejection in the cooling tower of this control strategy are shown in Figure 7.6 for a 2-year simulation using the control strategy 4c for Houston TMY. The maximum entering fluid temperature is 80.5°F (26.9°C) occurring in the first month of the 20-year simulation, while the minimum EFT is 40.5°F (4.7°C) and occurs in the 20th month. The EFT's to the heat pump for the 20-year simulation is shown in Figure 7.7.

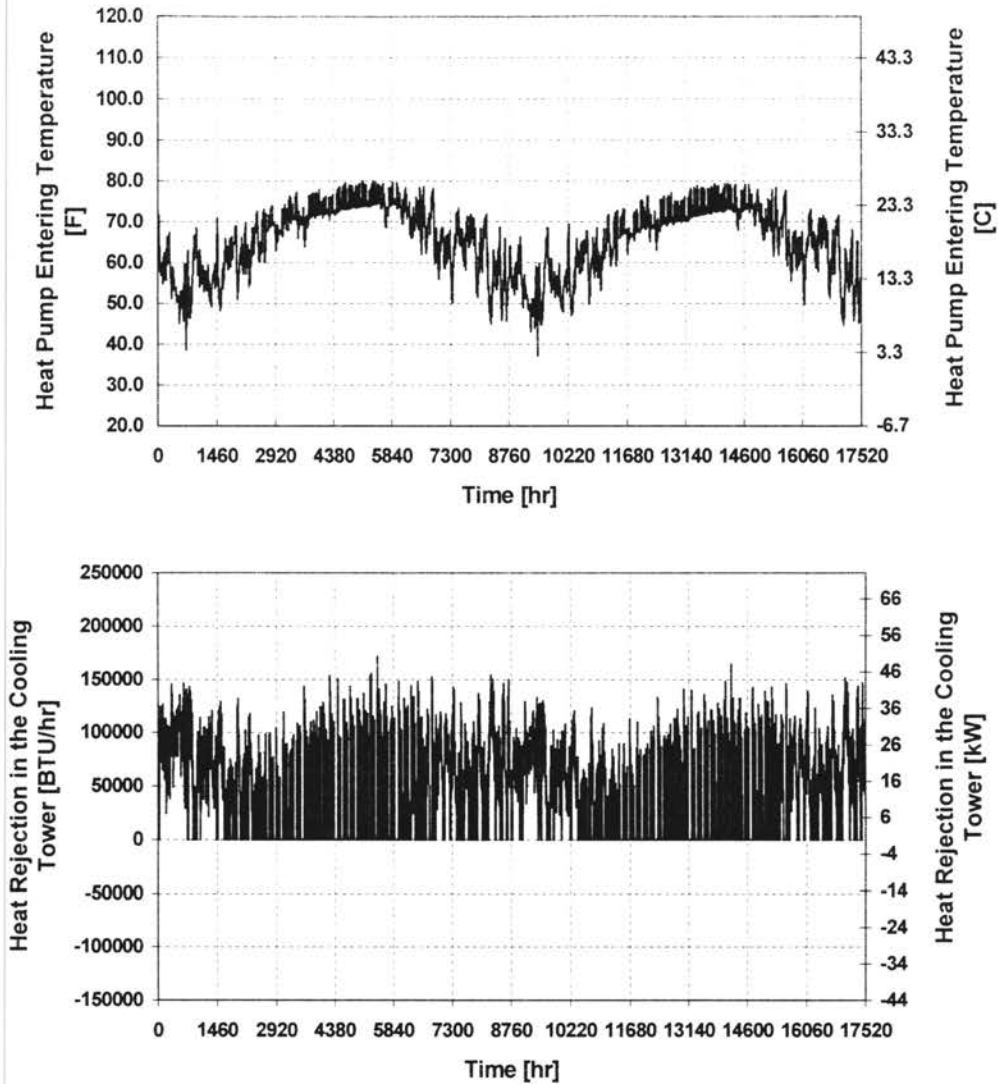


Figure 7.6 – Hourly entering fluid temperatures to the heat pump and heat rejection in the cooling tower for typical Houston, TX climatic conditions. 2-year simulation - Case 4c.

For cases 4a and 4b, the peak entering fluid temperatures to the heat pump are relatively close to each other for both climate regions (91.0°F [32.8°C] and 94.2°F [34.6°C] for Houston; 93.2°F [34.0°C] and 94.7°F [34.8°C] for Tulsa respectively). However, when the temperature dead band as in Case 4b is increased the system runs

'hotter', since the supplemental heat rejection occurs less often due to the larger dead band.

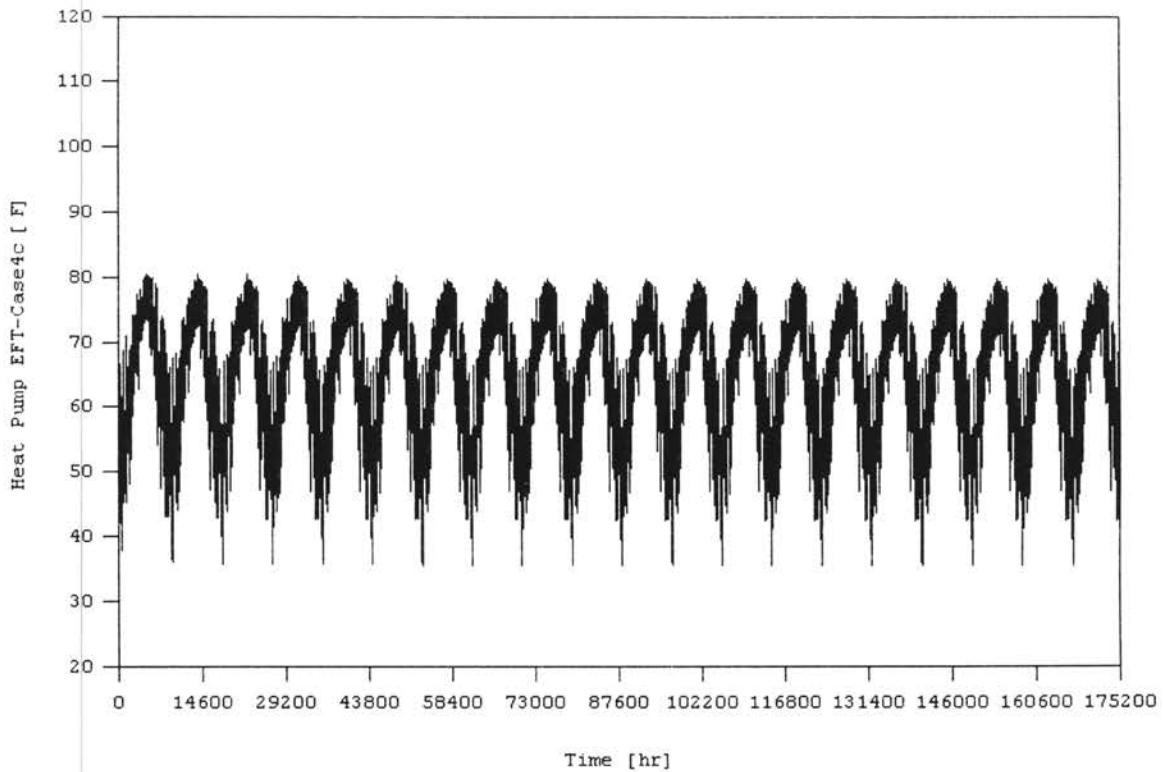


Figure 7.7 – *Hourly entering fluid temperatures to the heat pump for typical Houston, TX climatic conditions. 20 year simulation - Case 4c.*

7.4.5.5. SCHEDULED RECHARGE OF THE BOREFIELD (CASE 5)

In this case, excess heat is rejected by simply running the cooling tower and both circulating pumps at scheduled times (midnight to 6:00 a.m.) during the night. In addition, if the EFT to the heat pump exceeds 96.5°F (35.8°C). This has the advantage of simplicity of controls, since the cooling tower and pumps can be controlled with a timer. Tables 7.8, 7.9 and 7.10 show the operating hours of the cooling tower and the energy consumption of the hybrid system for each control sub-strategy for Houston and Tulsa

TMY conditions. Control strategies Case 5b and 5c are designed to compare seasonal effects of cool storage. Case 5b considers the winter months (ground recharge starts in January and runs through March) and Case 5c the summer months (ground recharge starts in June and runs through August).

TABLE 7.8
Hybrid System Simulation Summary for Control Strategy 5a

	HOUSTON, TX			TULSA, OK		
	1 st year	20 th year	20-year average	1 st year	20 th year	20-year average
Operation of the Cooling Tower [hr]	2,649	2,740	2,721	2,619	2,672	2,660
Power Consumption-Cooling Tower Pump [kWh]	160	165	164	158	161	161
Power Consumption-Cooling Tower [kWh]	980	1013	1006	969	988	984
Power Consumption-Heat Pump [kWh]	23,964	24,532	24,453	20,343	20,853	20,769
Power Consumption-Main Circulation Pump [kWh]	5,392	5,392	5,392	4,044	4,044	4,044
Total Power Consumption-[kWh]	30,497	31,105	31,018	25,515	26,048	25,959

The annual operating hours for the cooling tower in Case 5a remains relatively stable throughout the 20-year simulation period. Most of the hours of operation are scheduled, so the slight increase in run time is due to the set point condition being reached more often as the fluid temperatures increases. The power consumption due to the operation of the cooling tower fan and the secondary loop circulation pump account

for 3.8% of the total energy consumption for this strategy. The power consumption of the heat pump accounts for 78.8% of the total power consumption of the system, and is about 1.3% less than the power consumption as compared to the base case for Houston. Overall, the system uses about 25% less electricity than the base case, due substantially to the reduced pumping power requirements. In Tulsa, the overall electricity savings are only about 6%, since the pumping power requirements are not as strongly reduced.

Figure 7.8 shows the results of this operating strategy using Case 5a for Houston TMY. The entering fluid temperatures to the heat pump appear to remain at relatively stable levels throughout a 20-year simulation period. The maximum EFT to the heat pump is 96.0°F (35.6°C) and the minimum 54.1°F (12.3°C) both occurring in the first year of simulation. It may also be noted that there are a few hours when the cooling tower adds heat to the ground loop during the spring months. During this time, the ground loop is still relatively cold - while the ambient wet bulb temperature is higher, but the cooling tower is being operated based only on the operating schedule.

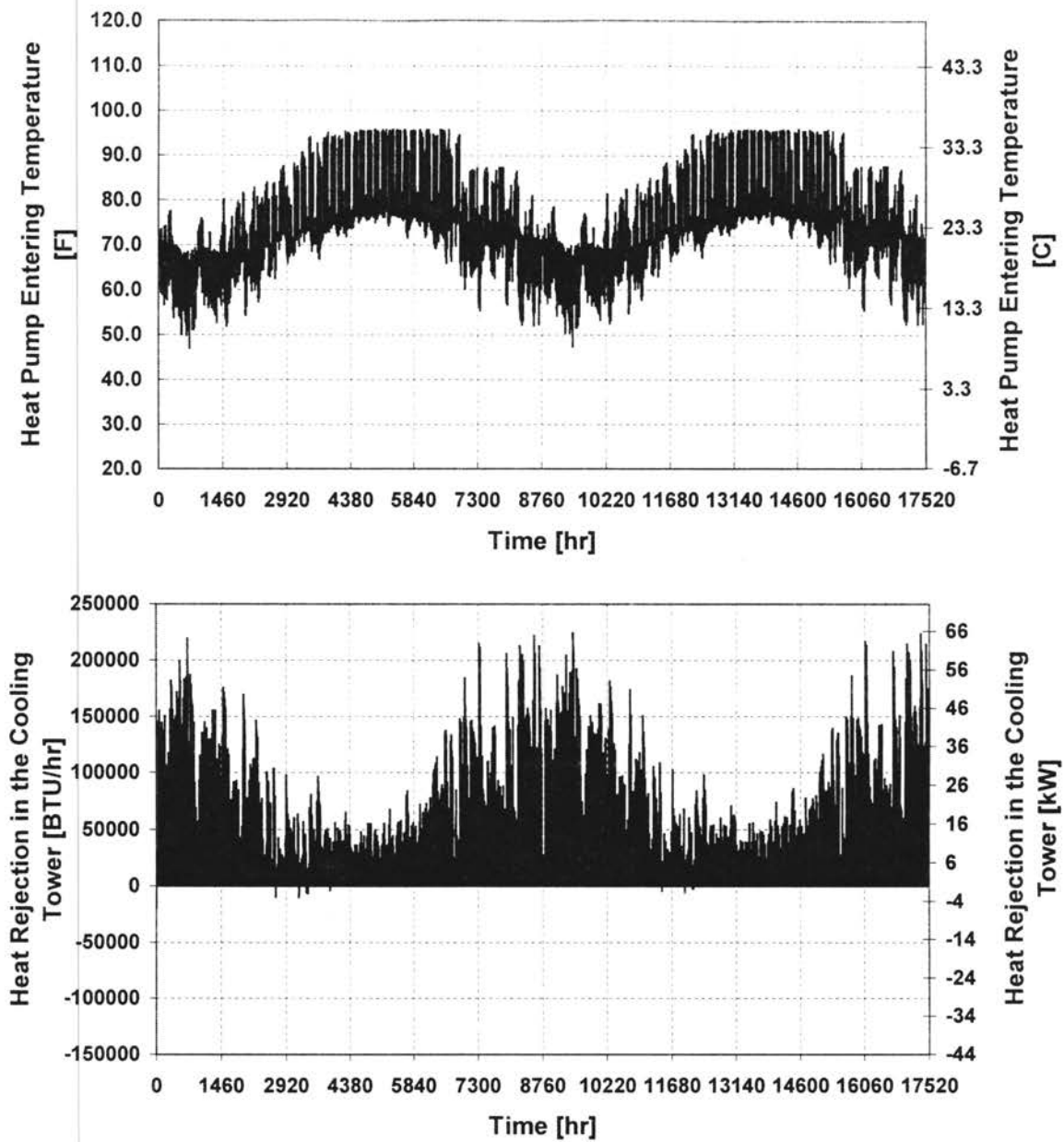


Figure 7.8 –Hourly heat pump entering fluid temperature and heat rejection in the cooling tower for Houston, TX typical weather conditions and using control strategy 5a for the first two years of simulation.

The hourly entering fluid temperatures and cooling tower heat rejection plots for Tulsa are qualitatively very similar to the ones for Houston.

TABLE 7.9

Hybrid System Simulation Summary for Control Strategy 5b

	HOUSTON, TX			TULSA, OK		
	1 st year	20 th year	20-year average	1 st year	20 th year	20-year average
Operation of the Cooling Tower [hr]	815	1,081	1034	710	865	834
Power Consumption-Cooling Tower Pump [kWh]	49	65	62	42	52	50
Power Consumption-Cooling Tower [kWh]	301	399	382	262	320	308
Power Consumption-Heat Pump [kWh]	24,587	25,886	25,696	20,735	21,876	21,664
Power Consumption-Main Circulation Pump [kWh]	5,392	5,392	5,392	4,044	4,044	4,044
Total Power Consumption-[kWh]	30,330	31,744	31,534	28,085	26,293	26,067

The maximum EFT's to the heat pump for Case 5b and 5c are only about 1.8°F (1.0°C) higher than Case 5a. As expected, the minimum EFT to the heat pump is higher for Case 5c than for Case 5b. In addition, an increase of about 9% is observed in the cooling tower operation time for Case 5c. Overall, the ground loop in Case 5b runs hotter than in Case 5a, and the ground loop in Case 5c runs hotter than in Case 5b.

Consequently, the savings in electricity consumption for Case 5b compared to the base case are 1-2% lower than for Case 5a. The savings in electricity consumption for Case 5c are 1-2% lower than for Case 5b. With this control strategy, it appears to increase in performance as more night run time is scheduled. However, only three schedules were considered and there may be a more optimal schedule that can be

implemented with a timer. In addition, the savings in electricity cost may be considerably different from the savings in electricity consumption if time-of-day rates apply.

TABLE 7.10
Hybrid System Simulation Summary for Control Strategy 5c

	HOUSTON, TX			TULSA, OK		
	1 st year	20 th year	20-year average	1 st year	20 th year	20-year average
Operation of the Cooling Tower [hr]	830	1148	1094	722	870	839
Power Consumption-Cooling Tower Pump [kWh]	50	69	66	43	52	50
Power Consumption-Cooling Tower [kWh]	307	424	405	267	321	310
Power Consumption-Heat Pump [kWh]	24,899	26,324	26,108	20,915	21,995	21,800
Power Consumption-Main Circulation Pump [kWh]	5,392	5,392	5,392	4,044	4,044	4,044
Total Power Consumption-[kWh]	30,649	32,221	31,972	25,270	26,414	26,205

7.5. COMPARISON OF CONTROL STRATEGIES-HYBRID SYSTEM

INSTALLATION AND OPERATING COST ANALYSIS

In order to compare the various cases, a cost analysis is conducted considering a system first and operating cost for a 20-year design period. The present value of the

predicted operating costs and the system first costs are calculated based on series of assumptions. The cost analysis makes the following assumptions:

- a) The cost of the ground heat exchanger is calculated at \$6.00 per foot of the borehole. (Kavanaugh 1998) This amount includes the horizontal runs and connections.
- b) The first cost of the cooling tower including the isolation plate heat exchanger is calculated at \$350.00 per ton (3.52 kW) of cooling tower capacity. (Means 1999) This amount includes other equipment and apparatus required for controls.
- c) The cost of auxiliary equipment and materials for the cooling tower and the plate heat exchanger is estimated to be about 10% of the first cost.
- d) The cost of electricity is assumed to be \$0.07 per kWh.
- e) A 6% annual percentage rate is used for the present value analysis. Annual compounding is used for the 20-year analysis.

It should be emphasized here this is a fairly simple approach; and it is no replacement for a detailed financial feasibility study of a specific building at a specific location with local climatic and ground conditions.

Consistent with the purpose of this analysis of demonstrating the use and power of a short time-step simulation model in building energy analysis, issues related to the maintenance of supplemental heat rejecters and related equipment were not included in this study. Nevertheless, it must be pointed out that failure to implement proper maintenance on supplemental heat rejecters (more so for cooling towers and fluid coolers than for surface heat rejecters) may at the end negate any economical benefits of hybrid ground source heat pumps. A strict maintenance program as suggested by ASHRAE (1996) must be considered for the proper operation of hybrid systems.

The results of the cost analysis are summarized for Houston and Tulsa TMY conditions in Tables 7.11 and 7.12. Figure 7.9 shows the cooling tower size that was selected to implement each control strategy based on the rate of heat transfer in the cooling tower at the time of peak entering fluid temperatures to the heat pump. The cooling tower size, as discussed previously, is specified at the design wet bulb condition. It can, of course, reject more heat when the wet bulb temperature is lower. Hence, the cooling tower may reject twice its rated capacity during cold winter hours. It should be noted that the control strategy with the least average operating hours per year for the supplemental heat rejection system does not necessarily represent the economically most beneficial approach. Attention must be paid to the size of the cooling tower with which a control strategy can be optimally implemented.

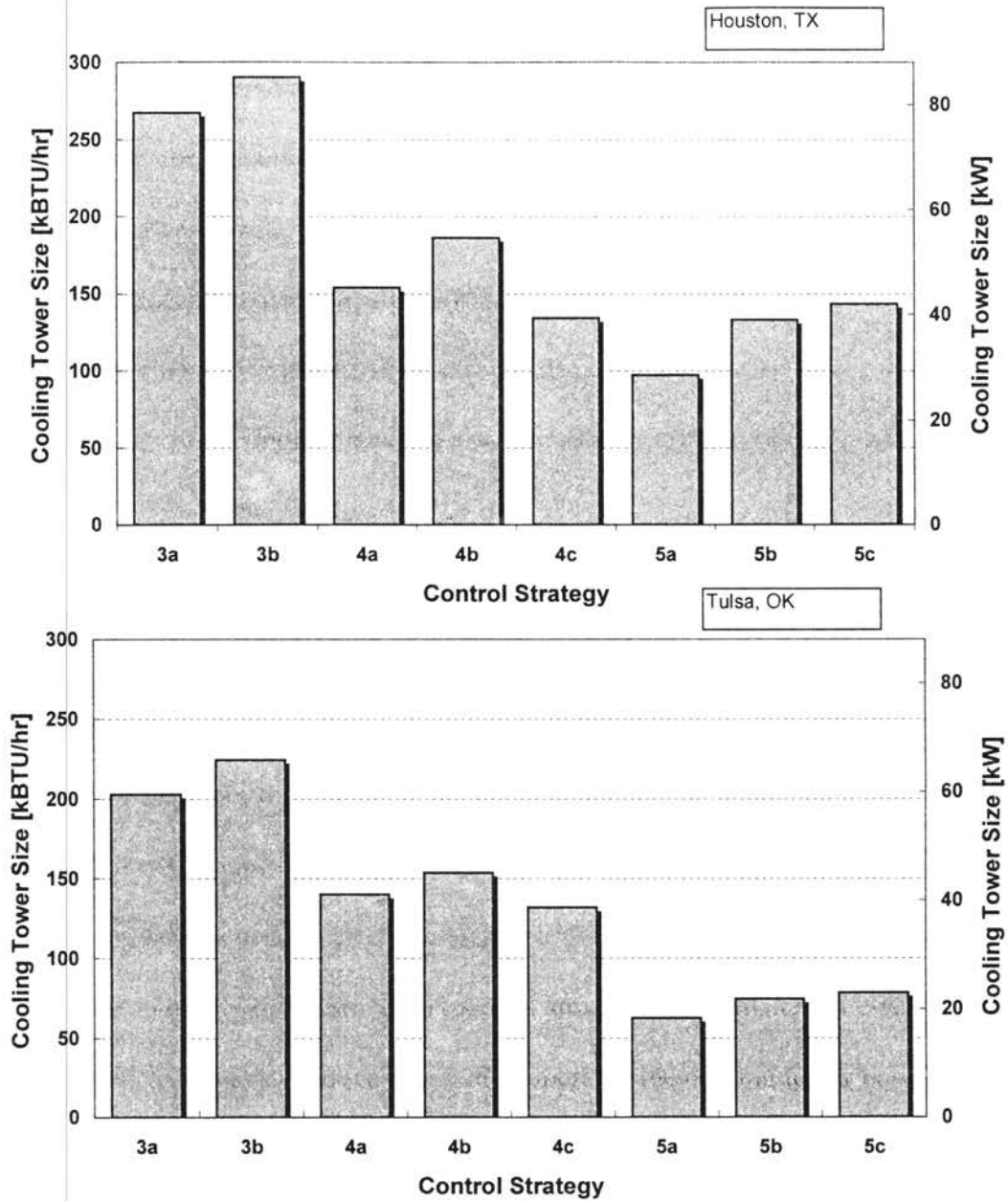


Figure 7.9 –Cooling tower size required for each control strategy.

Furthermore, this is a complex design problem with tradeoffs between ground loop heat exchanger size, cooling tower size, and control strategy. We have not attempted to optimize the design, but note that development of optimal design procedure is an excellent topic for further research.

TABLE 7.11

Cost Analysis Summary for each Control Strategy for Houston, TX

	BASE- 'optimum design'	Case-2	Case-3a	Case-3b	Case-4a	Case-4b	Case-4c	Case-5a	Case-5b	Case-5c
Number of Boreholes	6x6	3x4	3x4	3x4	3x4	3x4	3x4	3x4	3x4	3x4
Total Length of Loop installation [ft]	9000	2400	3000	3000	3000	3000	3000	3000	3000	3000
Total Cost of Loop Installation [\$]*	\$54,000	\$18,000	\$18,000	\$18,000	\$18,000	\$18,000	\$18,000	\$18,000	\$18,000	\$18,000
Savings in Boreholes and Loop Installation [\$]			\$36,000	\$36,000	\$36,000	\$36,000	\$36,000	\$36,000	\$36,000	\$36,000
Max. Heat Transfer in the Cooling Tower [BTU/hr]			267762	290280	154036	186268	134294	97763	133061	143365
Max. Heat Transfer in the Cooling Tower [tons of cooling]			22.31	24.19	12.84	15.52	11.19	8.15	11.09	11.95
Max. Flow Rate [gpm]	108	36	36	36	36	36	36	36	36	36
EWT max during 20 years of operation [F]	96.6	126.6	96.3	97.6	90.9	94.3	80.5	96.0	97.8	97.6
EWT min during 20 years of operation [F]	71.3	67.3	67.3	67.3	39.9	41.3	40.5	54.1	52.5	67.2
Design Capacity of the Cooling Tower [tons of cooling]	n/a	n/a	22.5	24.5	13.0	15.5	11.5	8.5	11.5	12.0
First Cost of Cooling Tower + Plate Heat Exchanger incl. Controls [\$] **	n/a	n/a	\$7,875	\$8,575	\$4,550	\$5,425	\$4,025	\$2,975	\$4,025	\$4,200
Cost of Auxilliary Equipment [\$]***	n/a	n/a	\$787	\$857	\$455	\$542	\$402	\$297	\$402	\$420
Total First Cost of Equipment [\$]	n/a	n/a	\$8,662	\$9,432	\$5,005	\$5,967	\$4,427	\$3,272	\$4,427	\$4,620
Present Value of 20 year operation (includes CT fan+Circ. Pump Elec. Cons. for Cases 3 through 5) [\$]****	\$32,062	n/a	\$23,671	\$24,841	\$21,224	\$22,013	\$20,375	\$24,874	\$25,248	\$25,592
Present Value of Total Cost[\$]	\$86,062	n/a	\$50,333	\$52,274	\$44,229	\$45,980	\$42,803	\$46,146	\$47,676	\$48,212

(*) - Estimated as \$6.00 per ft. of borehole including horizontal runs and connections

(**) - Estimated as \$350.00 per ton of cooling including controls

(***) - Estimated as 10% of the first cost

(****) – \$0.07 per kWh is assumed for cost of electricity. A 6% annual percentage rate is used for life cycle-cost analysis.

TABLE 7.12

Cost Analysis Summary for each Control Strategy for Tulsa,OK

	BASE- 'optimum design'	Case-2	Case-3a	Case-3b	Case-4a	Case-4b	Case-4c	Case-5a	Case-5b	Case-5c
Number of Boreholes	4x4	3x3	3x3	3x3	3x3	3x3	3x3	3x3	3x3	3x3
Total Length of Loop installation [ft]	3,840.00	2,160.00	2,160.00	2,160.00	2,160.00	2,160.00	2,160.00	2,160.00	2,160.00	2,160.00
Total Cost of Loop Installation [\$]*	\$23,040	\$12,960	\$12,960	\$12,960	\$12,960	\$12,960	\$12,960	\$12,960	\$12,960	\$12,960
Savings in Boreholes and Loop Installation [\$]			\$10,080	\$10,080	\$10,080	\$10,080	\$10,080	\$10,080	\$10,080	\$10,080
Max. Heat Transfer in the Cooling Tower [BTU/hr]			202942	224423	139962	153646	131825	62580	74631	78509
Max. Heat Transfer in the Cooling Tower [tons of cooling]			16.91	18.70	11.66	12.80	10.99	5.22	6.22	6.54
Max. Flow Rate [gpm]	48	27	27	27	27	27	27	27	27	27
EWT max during 20 years of operation [F]	96.4	121.8	96.9	98.2	93.2	94.7	79.0	97.9	98.5	97.7
EWT min during 20 years of operation [F]	50.2	39.9	39.8	39.9	24.3	24.5	24.2	39.2	38.8	39.9
Design Capacity of the Cooling Tower [tons of cooling]	n/a	n/a	17.0	19.0	12.0	13.0	11.0	5.5	6.5	7.0
First Cost of Cooling Tower + Plate Heat Exchanger incl. Controls [\$]**	n/a	n/a	\$5,950	\$6,650	\$4,200	\$4,550	\$3,850	\$1,925	\$2,275	\$2,450
Cost of Auxilliary Equipment [\$]***	n/a	n/a	\$595	\$665	\$420	\$455	\$385	\$193	\$228	\$245
Total First Cost of Equipment [\$]	n/a	n/a	\$6,545	\$7,315	\$4,620	\$5,005	\$4,235	\$2,118	\$2,503	\$2,695
Present Value of 20 year operation (includes CT fan+Circ. Pump Elec. Cons. for Cases 3 through 5) [\$]****	\$21,587	n/a	\$19,254	\$20,360	\$19,003	\$19,424	\$18,248	\$20,814	\$20,863	\$20,978
Present Value of Total Cost [\$]	\$44,627	n/a	\$38,759	\$40,635	\$36,583	\$37,389	\$35,443	\$35,892	\$36,325	\$36,633

(*) - Estimated as \$6.00 per ft. of borehole including horizontal runs and connections

(**) - Estimated as \$350.00 per ton of cooling including controls

(***) - Estimated as 10% of the first cost

(****) - \$0.07 per kWh is assumed for cost of electricity. A 6% annual percentage rate is used for life cycle-cost analysis

7.6. DISCUSSION OF THE RESULTS

The analysis provides a comparative study of several control strategies for the operation of a hybrid ground source heat pump systems used in a small office building. A simple cost analysis considering the first cost of the supplemental heat rejection, the first cost savings achieved through smaller ground heat exchangers and the system operating costs is conducted based on a 20-year period. The three control strategies might be broadly characterized as follows. In Case 3, the set point control runs the cooling tower only when necessary to avoid a high EFT to the heat pump. However, this generally occurs under the least advantageous weather conditions. In Case 4, the differential control strategy operates the cooling tower under the most advantageous weather conditions. Under this strategy, the ground loop temperatures are held to a much lower level, and, as a result, the cooling tower never needs to operate to avoid a high EFT under weather conditions that are not advantageous. In Case 5, the cooling tower is merely operated on a schedule. This strategy does not take particular advantage of weather conditions and wastes some energy by running the cooling tower during hours when little or no heat rejection may be performed. Specific conclusions are summarized below:

- i) For the example building, typical for small size office buildings, a hybrid ground source heat pump system does appear to be beneficial on both a first cost and an annual operating cost basis for relatively hot climates such as Houston, TX and for moderately warm climates such as Tulsa, OK. The analyses suggest that the higher the building cooling loads relative to the building heating loads, the more

first cost can be saved due to reduction in the ground heat exchanger size, and consequently, the more beneficial the hybrid ground source heat pump application. For the example building that is analyzed here, a hybrid application operated based on differential control scheme (Case 4c) appears to be the most beneficial choice. However, compared to the base case, a hybrid system implemented with any of the control strategies investigated appears to have significant economic benefits based on first cost and 20-year operating cost analysis (Tables 7.11 and 7.12).

- ii) For the small office building, the addition of a supplemental heat rejecter could not be justified for locations in relatively cold or moderately cold climates. However, buildings with different load profiles might be good candidates for hybrid ground source heat point systems.
- iii) Based on the limited study of control strategies investigated, the best control strategy investigated was 4c, which operated the cooling tower based on the difference between the fluid temperature exiting the heat pump and the outside wet bulb temperature. This control strategy had the lowest first cost and the lowest operating cost. It takes advantage of the storage capacity of the ground heat exchanger by “storing cold” in the ground during the winter. It also rejects heat when conditions are advantageous in the spring, summer, and fall.

- iv) In general, the control strategies which operated the cooling tower more hours gave more benefit than those which operated the cooling tower fewer hours. This is particularly true when the cooling tower was operated under advantageous conditions, as in Case 4. But it is also true that running the cooling tower at night in addition to running it when the EFT exceeds the setpoint (Case 5) is better than running it only when the EFT exceeds the set point, as in Case 3.

Just comparing Case 5 to Case 3, the additional hours that the Case 5 cooling tower runs allows the Case 5 cooling tower to be smaller, and thus have a lower first cost. However, because the Case 5 cooling tower runs indiscriminately, it has a slightly higher overall operating cost than the Case 3 cooling tower.

- v) The use of a hybrid ground source heat pump system resulted in significant land area savings. For the small office building, in Houston, the surface area of the borehole field was reduced from 3906 ft² (363.1 m²) to 937 ft² (87.1 m²), a 76% savings. In Tulsa, the area was reduced from 1296 ft² (120.5 m²) to 576 ft² (53.5 m²), a 55% savings. For commercial buildings located in areas where property costs are high, the savings on land costs might be considerable. They were not accounted for in this study.

- vi) The pumping cost associated with the circulation of the heat transfer fluid through the borehole field accounts for a significant share in total system operating costs. An additional benefit of hybrid applications is that through the reduction in

ground loop length the operating cost associated with pumping of the heat transfer fluid can also be reduced significantly. The need for smaller capacity pumps also reduces the system first cost, although this was not accounted for in our analysis.

Finally, the use of a short time-step ground loop heat exchanger simulation model in a component modeling environment proves to be a very powerful tool in assessing the behavior and dynamics of hybrid ground source heat pumps. It allows the implementation of sophisticated (based on hourly or less time intervals) operating and control strategies, previously not considered. Time-of-day electricity rates may also be considered, though we did do so in this study.

However, his study leaves open a number of areas for future research. These include:

- i. Optimization of the design procedure and control strategy. Hybrid ground source heat pump systems have many degrees of freedom; there are tradeoffs between the reduction in size of the ground loop heat exchanger, the size of the cooling tower, and the control strategy. This is a good candidate for development of an optimal design procedure, which could simultaneously optimize all of the parameters of interest.
- ii. Additional validation of the model, using data from a working system, would be useful.

- iii. A similar analysis of other supplemental heat rejecters, such as shallow ponds and pavement heating systems would be useful.

- iv. The interaction between the control strategies, design, and time-of-day electricity rates should also be considered. It is quite possible that the optimal solution in a case where electricity is much less expensive at night would involve running the cooling tower for the entire night.

8. MEASUREMENT OF GROUND'S THERMAL CONDUCTIVITY USING PARAMETER ESTIMATION TECHNIQUES

Determination of the ground's thermal conductivity is a significant challenge facing designers of ground source heat pump systems. The number of boreholes and the depth and cost of each borehole are highly dependent on the ground thermal properties. Hence, depending on the geographic location and the local drilling costs, the ground thermal properties strongly influence the initial cost to install a ground source heat pump system. This is particularly true for applications for commercial buildings.

For relatively large commercial ground source heat pump systems, an extensive effort is made to design the ground loop heat exchangers so that they are not too large (resulting in too high of a first cost) or too small (resulting in entering water temperatures to the heat pumps being too high or too low). The design tools used to size ground loop heat exchangers (Ingersoll 1954, Kavanaugh 1984, Eskilson 1987, Cane 1991, IGSHPA 1991 and Spitler et al. 1996) rely on some estimate of the ground thermal conductivity and volumetric specific heat. This estimate is critical to the design, yet it is very difficult to make. The required borehole depth or length is highly dependent on the thermal properties of the ground. This in turn strongly influences the cost of the system and its competitiveness with conventional systems.

The traditional approach to estimating the ground thermal properties has been to first ascertain the type (or types) of soil or rock that surrounds the borehole. Once the type of soil or rock is determined, its thermal conductivity can be estimated from tabulated data, such as that contained in the Soil and Rock Classification for the Design of Ground-Coupled Heat Pump Systems Field Manual (EPRI, 1989). For each rock type, a horizontal band is drawn to indicate the range of thermal conductivity expected. Considering one rock type, “Quartzose sandstone, wet”, the thermal conductivity varies from about 1.8 Btu/h-ft-°F (3.1 W/m-K) to about 4.5 Btu/h-ft-°F (7.8 W/m-K). This is a significant variation, and the prudent designer will probably choose the lower value of about 1.8 Btu/h-ft-°F (3.1 W/m-K), even though the extra borehole depth required may not allow the ground loop system to be competitive on either a first cost basis or a life cycle cost basis.

Therefore, a method for more accurately estimating the ground thermal conductivity is therefore highly desirable. The analysis presented in this study develops a procedure for predicting the ground thermal conductivity based on experimentally measured temperature responses using a test borehole. An experimental apparatus has been built that is capable of imposing a heat flux on a test borehole, and measuring its temperature response. The parameter estimation method used utilizes the downhill simplex minimization algorithm of Nelder and Mead (1965) to estimate the ground thermal conductivity. The transient, two-dimensional numerical finite volume model for the vertical borehole, as described in Chapter 4, is used to evaluate the performance of a ground loop heat exchanger for parameter estimation. The procedure is validated through

comparison of independent measurements of the soil conductivity test results using several test boreholes and a medium-scale laboratory experiment with model predictions. An uncertainty analysis of the thermal conductivity predictions is conducted to assess the error of the model predictions.

8.1. DESCRIPTION OF EXPERIMENTAL APPARATUS

The experimental apparatus is housed in a trailer that can be towed to the site and contains everything needed to perform a test – the apparatus, two generators, and a purge tank containing 80 gallons (304 l) of water. A simplified schematic of the test system is shown in Figure 8.1. Once connected to a U-tube that has been inserted into a borehole, and after the system has been purged, a heat flux is imposed on the borehole using the three in-line water heaters, and the temperature response (average of inlet and outlet fluid temperatures, which changes with time) of the borehole is measured. A brief description of the experimental apparatus follows. A more detailed description is available in Austin (1998).

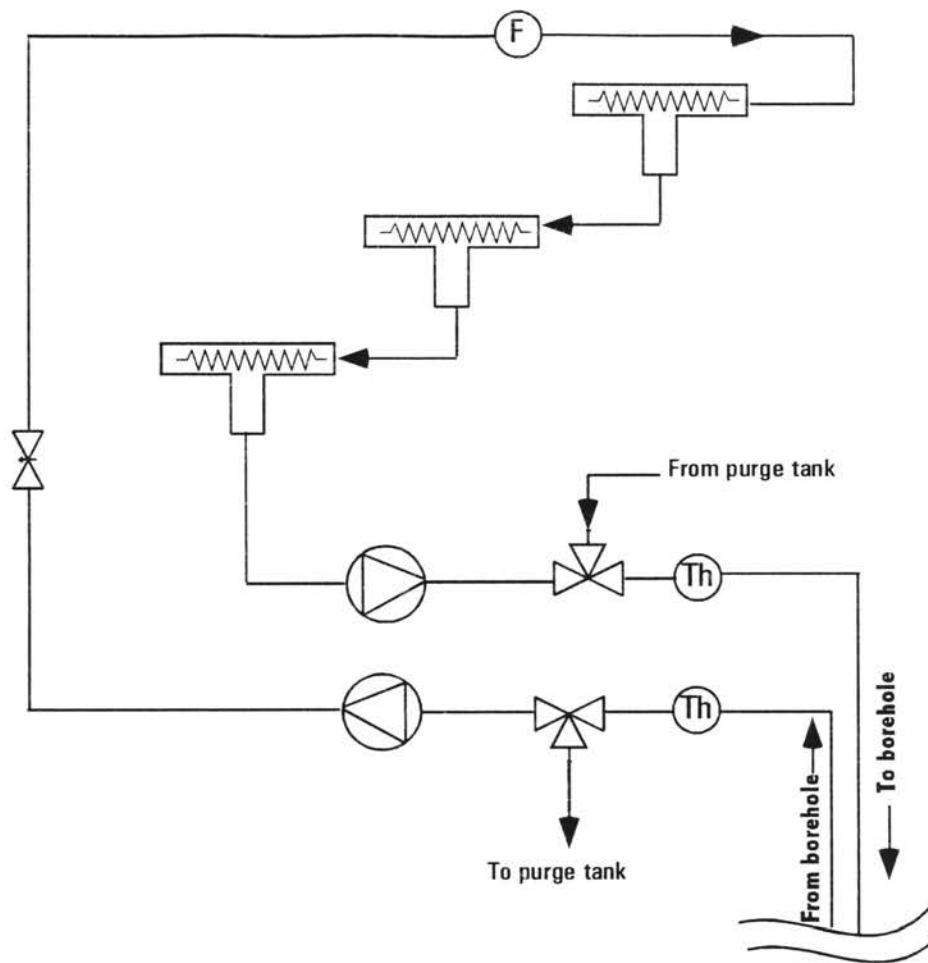
In addition to the components shown in Figure 8.1, a purge tank and two additional pumps are used to remove all air from the piping system before the heat pulse phase of the experiment begins. Also, when electricity is not otherwise available, two 7000 W capacity gasoline generators are used to power the experiment.

Once the system has been purged, the three-way valves shown in Figure 8.1 are turned to close the connection to the purge system. The following components are then used to impose a heat pulse on the borehole, and measure both the power and the temperature:

The circulating water inside the closed loop system is heated with (up to) three in-line water heaters shown schematically in Figure 8.1. The water heaters are ordinary water heating elements (typically used in residential water heaters) mounted in piping tees. The heater elements are rated at 1, 1.5, and 2 kW. The 2 kW water heater element is connected to an electronic power controller, so that by switching individual elements on or off, and by adjusting the controller, the power can be adjusted continuously between zero and 4.5 kW.

Two circulating pumps are used to circulate heated water through the U-tube in the borehole.

A needle valve is used to adjust the flow rate. Typically, a flow rate of approximately (2.50 gpm [0.16 l/s]) was used.



Symbols


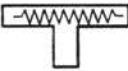




Needle valve		Tee with electric resistance element	
Circulating pump		Flow meter	
Three-way valve		Thermistor	

Figure 8.1 *In-situ thermal conductivity test system schematic*

All of the plumbing, inside and outside is insulated. The interior pipe insulation is fiberglass, about 1.5 inches (38.1 mm) thick. The tubing between the trailer and the borehole is insulated with three layers of insulation, a 0.5 inch (12.7 mm) thick foam rubber, and two layers of fiberglass duct insulation, 5 inches (127.0 mm) and 9 inches (228.6 mm) thick respectively.

The power consumption of the heaters and the circulating pumps is measured using a watt transducer.

Inlet and outlet temperatures are measured using two high accuracy thermistors, immersed in the circulating fluid.

The flow rate is measured using an in-line flow meter.

Experimental measurements are made every 2.5 minutes using a data logger, and the power input, the entering/exiting fluid temperatures of the loop and the volumetric flow rate are downloaded to an on-board computer.

8.2. OBJECTIVE FUNCTION

Parameter estimation involves minimizing the differences between experimentally obtained temperature responses and responses predicted by the numerical model of the borehole by adjusting inputs to the model. Some inputs to the model, such as time-varying power and borehole geometry will be fixed and other inputs, such as the thermal

conductivity of the ground formation and the thermal conductivity of the grout will be allowed to vary. By systematically varying the thermal conductivity of the ground formation and the thermal conductivity of the grout so that the minimum difference between the experimental results and the numerical model is sought, a best estimate of the thermal conductivities may be found.

The objective function algorithm will be using the following as inputs:

- i) power input in preset time intervals (obtained from experimental measurement)
average borehole temperatures in preset time intervals as a response to the power input (obtained from experimental measurement, determined by averaging the inlet and outlet temperatures of the loop)

- ii) undisturbed ground temperature (measured at beginning of the experiment by lowering a thermocouple into the U-tube legs along the borehole depth.)
geometry information: (pipe size, pipe wall thickness, borehole diameter, pipe spacing, borehole depth)

- iii) ground formation thermal properties (conductivity and volumetric specific heat)

- iv) grout thermal properties (conductivity and volumetric specific heat)

- v) pipe thermal properties (conductivity and volumetric specific heat)

vi) fluid properties (conductivity, volumetric specific heat, flow rate and viscosity)

Most of the inputs will be determined based on knowledge of the borehole installation. A few, however, will be treated as independent variables in an optimization. The objective function for the optimization is the sum of the squares of the errors (SSE) between the numerical model solution and the experimental results, specifically:

$$\text{SSE} = \sum_{n=1}^N (T_{\text{exp}} - T_{\text{num}})^2 \quad (8.1)$$

Where,

N = The total number of data points over the duration of the experiment.

T_{exp} = Average of the calibrated input and output temperature at the n^{th} data point.

T_{num} = Average fluid temperature at n^{th} data point as predicted by the numerical model.

SSE = Sum of the squares of the errors.

Although other methods Kuester (1973) could be used the optimization will be performed with a non-linear “downhill simplex” optimization technique of Nelder and Mead (1965). The estimated parameters for the optimization may be almost any of the inputs, although the obvious choices include the ground formation thermal properties, the grout thermal properties and the pipe spacing.

8.3. NELDER AND MEAD SIMPLEX OPTIMIZATION

This algorithm is a multidimensional minimization method suggested by Nelder and Mead (1965). Thus, it is capable of finding the minimum of a function of more than one independent variable. The method requires only objective function evaluations, no objective function derivatives. This is useful since it is quite costly in terms of computational effort and time to calculate derivatives of the objective function. The method uses a regular geometric figure – a simplex – consisting of $n+1$ points or vertices (thus the simplex in two dimensions is a triangle). The method adapts itself to the local landscape, using reflected, expanded and contracted points to locate the minimum. Unimodality is assumed and thus several sets of starting points should be considered. A step by step description of the Nelder-Mead simplex algorithm is provided below:

- i) The algorithm starts with the selection/guess of an initial point (first vertex of the simplex). A starting simplex is then constructed consisting of the starting point and additional n points ensuring that all $n+1$ points are not collinear.
- ii) Once the simplex is formed, the objective function is evaluated at each vertex of the simplex. This involves the computation of the sum of the squares error (SSE) between the experimental temperatures and the predicted temperatures using the two-dimensional, transient finite volume model described in Chapter 4.

- iii) The worst point (or the point with the highest SSE value) is then replaced with a new point through reflection. This new point is located by first determining the centroid coordinates of all points excluding the worst point and reflecting the worst point across the face of the simplex by a constant value.
- iv) If the reflected point has the worst objective function value of the current simplex vertices a contraction point is calculated between the worst point and the centroid point.
- v) If, however, the reflected point is better than the worst point but is not the best point, a contracted point is computed along the reflected point and the centroid.
- vi) The objective function is now computed at the contracted point. If an improvement is over the current points (vertices) is achieved the process is restarted. If there is no improvement, the process is only restarted after the vertices are moved one half distance towards the best point.
- vii) If the reflected point computed in step iii) is the best point, an expansion is computed along the centroid and the reflected point by constant value.

- viii) If then the expansion point is an improvement over the reflected point, the expansion point replaces the reflected point and the process is restarted.
- ix) If however the expansion point is not an improvement over the reflected point, the reflected point is retained and the process is restarted.
- x) The algorithm is terminated once a preset convergence criterion is satisfied.

Advanced features may also be incorporated into this algorithm so that after the simplex has converged, the algorithm may take small steps in all the directions and check whether the SSE values at those points are smaller than the current minimum. If yes, the algorithm can assume that point and restart itself. The algorithm, as implemented, is restarted at least once using the current minimum point as the starting point of the new (restarted) simplex to ensure that the algorithm was not stuck at the local minimum in the domain. The information flow diagram of the algorithm is shown in Figure 8.2.

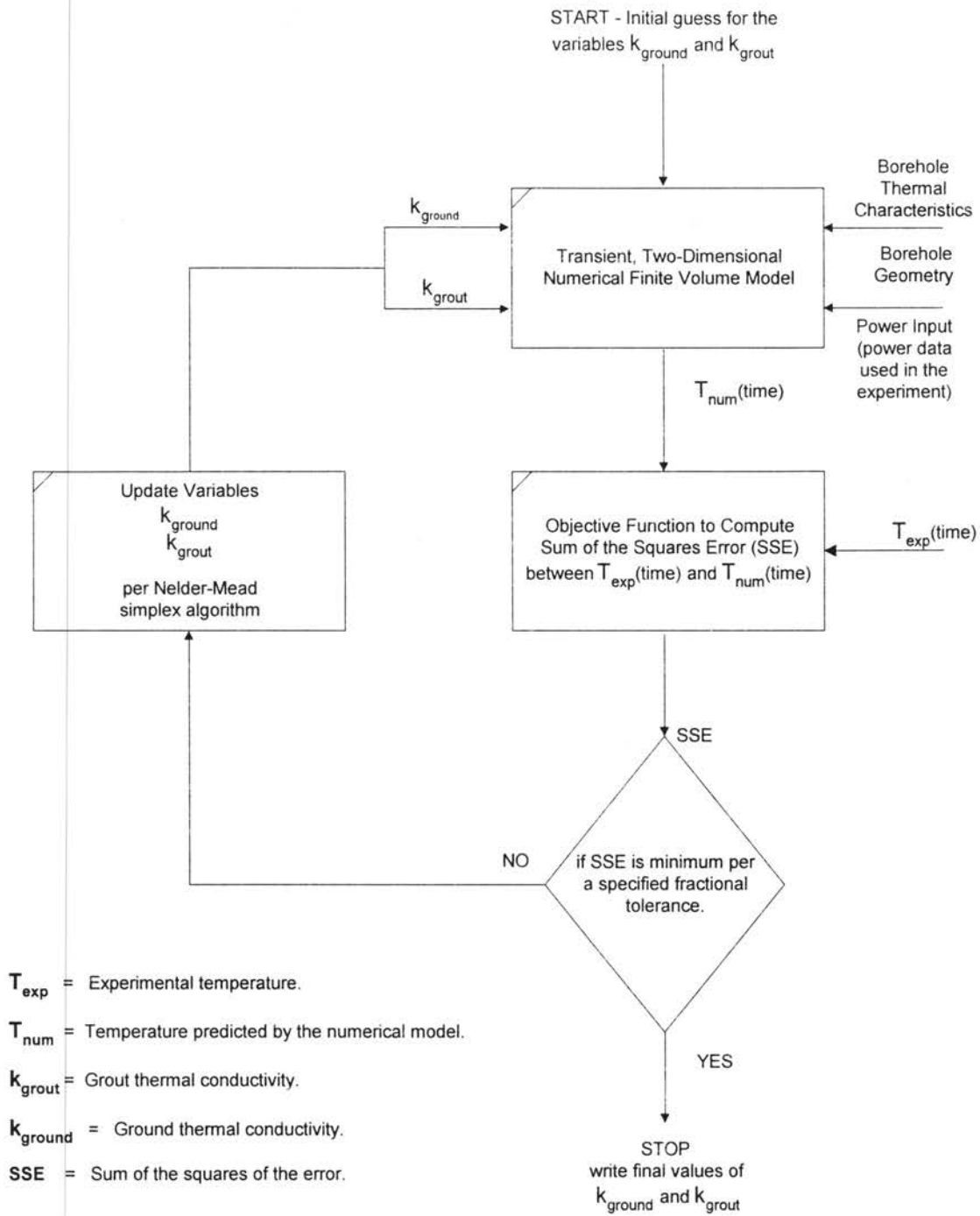


Figure 8.2. Information flow diagram for the parameter estimation algorithm.

8.4. PROCEDURE VALIDATION

A completely independent estimate of the ground thermal conductivity is required for validation of the parameter estimation model predictions. To accomplish this, several tests have been conducted where the ground conductivity was established independently.

One test was performed on a borehole that was drilled with a coring bit. The core samples were carefully preserved and the conductivity of 19 representative core samples was measured in a guarded hot plate apparatus (Smith 1998, Smith et al. 1999a, 1999b) to obtain an independent estimate for its thermal conductivity. Another test was performed using a medium-scale laboratory experiment where the geometry and thermal characteristics of a borehole are replicated under controlled conditions. The thermal conductivity of the soil material used in the experiment was determined independently with a calibrated soil conductivity probe.

Various other types of indirect confirmation have also been looked at to verify that the parameter estimation method works correctly. For example, measurements of thermal conductivity taken at nearby boreholes with different grout types and pipe types should give approximately the same value of thermal conductivity. Austin (1998) reports on extensive field experience obtained from a series of in-situ tests at various locations in Oklahoma. However, the results presented in this analysis focus on the tests with independent measurements of thermal conductivity.

8.4.1. CORED BOREHOLE

A series of test boreholes were drilled at an experimental field on the premises of the Oklahoma State University in Stillwater, Oklahoma (Test Site A). Core samples of the soil from one (Site A borehole #6) of the boreholes were obtained and analyzed using a modified guarded hot plate method as implemented by Smith (1998, 1999a, 1999b) to determine the effective thermal conductivity of the borehole core.

The guarded hot plate apparatus requires core samples 3.0 inches (76.2 mm.) in length and 3.0 inches (76.2 mm.) in diameter. A constant heat flux is imposed on one end of the sample, while the other end is cooled. The resulting temperature difference is used to determine the sample's thermal conductivity. The method has been validated on stainless steel samples, which have a thermal conductivity that is about 3 to 5 times higher than soil, with an error of about $\pm 1\%$.

Nineteen representative samples were analyzed. (Analysis of additional samples is ongoing, and may eventually result in an improved estimate of the average ground thermal conductivity surrounding the borehole.) The samples were chosen so that they represent identifiable layers. Since the thermal conductivity of the formational layers of the core sample varies, a thickness-weighted average thermal conductivity value is calculated. The resulting thermal conductivity then represents the effective thermal conductivity for the Test Site A #6 borehole.

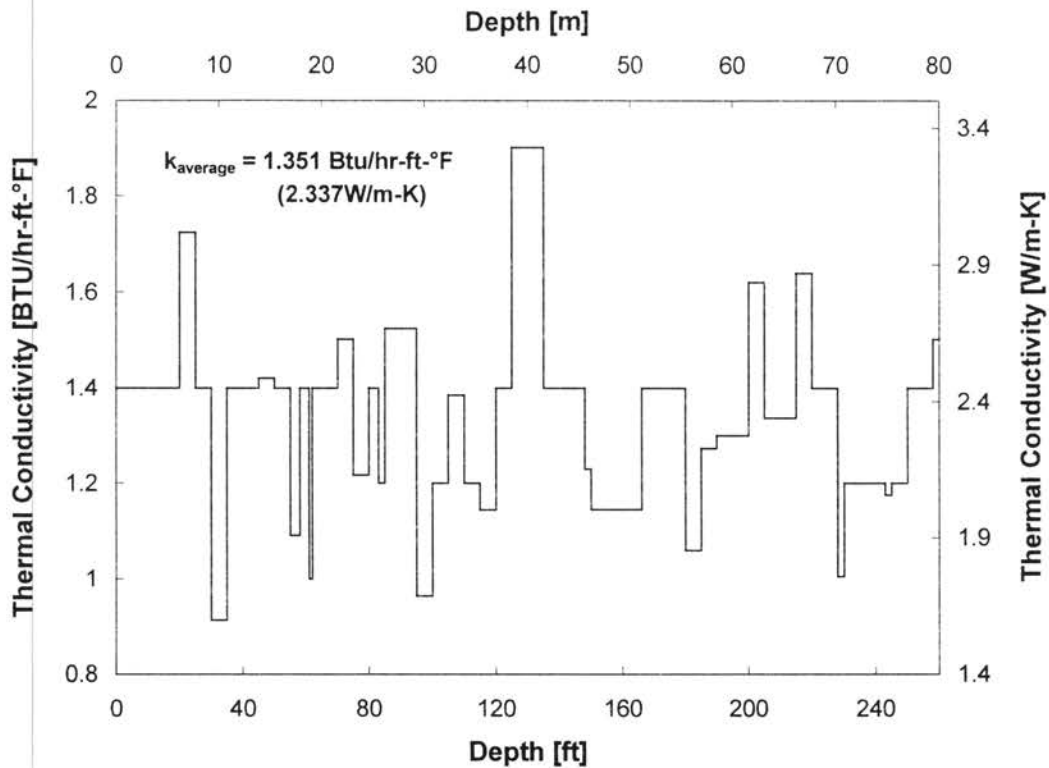


Figure 8.3. *Thermal conductivity vs. the cored borehole depth based on the guarded hot plate core experiments for Oklahoma State University site A #6 borehole.*

The results of the guarded hot plate tests are provided in Figure 8.3 (Smith 1998, 1999a, 1999b) where the measured ground conductivity for various layers of the borehole core is plotted against the depth of the borehole. The weighted average ground conductivity is calculated to be approximately 1.351 Btu/hr-ft-°F (2.337 W/m-K). The ground thermal conductivity varies between approximately 1.9 Btu/hr-ft-°F (3.3 W/m-K) and 0.9 Btu/hr-ft-°F (1.6 W/m-K). The strong variation in the thermal conductivity along the depth of a given borehole serves to reinforce the fact that the average thermal conductivity is really an “effective” thermal conductivity for the ground surrounding the borehole.

8.4.2. MEDIUM-SCALE LABORATORY EXPERIMENT

A medium-scale laboratory test where a homogeneous soil surrounds a simulated borehole was conducted to provide a validation for the in situ measurement procedure (Smith 1998, 1999a, 1999b). The flexible configuration of the simulated borehole allows for a series of borehole parameters such as the shank spacing of the U-tube and the exact geometry of the borehole to be controlled, as it is also easily modified for various grout and soil types for testing. The test apparatus utilizes its own data acquisition system, rather than the in situ apparatus described above.

The dimensions of the wooden structure that contains a homogenous soil (either dry or saturated sand) are 48.0 ft (14.6 m.) in depth, 4.0 ft (1.2 m) in width and height. The simulated borehole is created by placing a U-tube and bentonite-based grout inside of a horizontal 5.25-inch (133 mm) diameter aluminum pipe. The U-tube position inside the borehole is controlled with spacers, and the aluminum pipe is centered within the wooden structure.

Saturated and dry sands were tested. The thermal conductivity of the sands was independently determined using a 6 inch (150 mm) probe at various locations in the test apparatus. The thermal conductivity of the dry sand was determined to be between 0.142 Btu/hr-ft-°F (0.246 W/m-K) and 0.155 Btu/hr-ft-°F (0.268 W/m-K) based on five different measurement locations with an average of 0.149 Btu/hr-ft-°F (0.258 W/m-K).

Similarly, the thermal conductivity of the saturated sand was measured to be between 1.272 Btu/hr-ft-°F (2.201 W/m-K) and 1.565 Btu/hr-ft-°F (2.708 W/m-K) with an average of 1.353 Btu/hr-ft-°F (2.341 W/m-K). The dry and saturated sands were chosen for the medium scale laboratory tests since they represent a relatively wide range of ground thermal conductivities in addition to being relatively homogenous and readily available. The dry sand, however, is representative of extremely low ground conductivity.

The length of the tests was limited to between 46 and 50 hours to avoid edge effects. The far-field temperature of the ground was estimated to be the average initial temperature of the sand at five different locations at different radial distances from the center of the borehole. The temperature at the outer domain boundary of the wooden structure was observed throughout the experiment and the numerical simulation to insure that the domain temperature was unchanged from the initial 'far-field' temperature.

8.5. OVERVIEW OF THE PARAMETER ESTIMATION RESULTS

There are a number of ways that the parameter estimation might be approached. Specifically, one, two, or more parameters might be estimated simultaneously. Although a number of approaches were tried, including estimating up to five parameters (soil conductivity, grout conductivity, soil volumetric specific heat, grout volumetric specific heat, and shank spacing,) simultaneously, only the most promising approach is presented in this analysis.

The approach involves simultaneous estimation of both soil conductivity and grout conductivity. This has the advantage of allowing for an approximate accounting for several borehole-related parameters: grout conductivity, shank spacing and even borehole diameter. (The borehole will not necessarily be exactly the diameter of the drill bit.) The estimated grout conductivity might be considered as effective grout conductivity in this case.

Austin (1998) first attempted a single variable approach, involving only the estimation of the soil conductivity. This has the advantages of simplicity and computational speed, since only one parameter is varied for each function evaluation. The disadvantage of using only one variable is that all of the other inputs must be “correct”: shank spacing, grout conductivity, and grout volumetric specific heat, etc. While the grout conductivity and grout volumetric specific heat might be independently determined, the actual location of the U-tube in the borehole and the effective shank spacing cannot be determined with typical installation techniques. Although it is possible to control some of the parameters such as the shank spacing and the U-tube spacing in the borehole, further investigation is needed to determine its practicality.

Nevertheless, parameter estimation of only one variable cannot adequately account for uncertainties in the tube placement, grout conductivity and the exact borehole geometry. Although the ground thermal conductivity will obviously still be one of the estimated variables, a second variable is needed to be estimated to account for these

uncertainties in the borehole. In this respect, the grout conductivity as the second independent variable is a good surrogate for the other borehole parameters.

As discussed by Austin (1998), other approaches that involved estimation of additional parameters often gave very good fits to the experimental data. Unfortunately, some of the estimated parameters, especially the volumetric specific heats, were outside of what might be considered physically possible. Also, as more simultaneous parameters are estimated, more computational time is required.

Furthermore, simultaneous estimation of both soil conductivity and soil volumetric specific heat is problematic. In a transient conduction heat transfer problem, the governing equation is often written with only the thermal diffusivity, the ratio of the thermal conductivity to the volumetric specific heat. From this, one might conclude that it is impossible to estimate conductivity and volumetric specific heat simultaneously, as there are an infinite number of combinations that represent the same value of diffusivity. However, the boundary condition at the wall of the pipe is an imposed heat flux, and therefore $\left(k_{\text{Grout}} \frac{\partial T}{\partial n} \right)$ is fixed at any point in time. This does allow simultaneous estimation of thermal conductivity and volumetric specific heat, even if the results are not always satisfactory.

Consequently, the recommended procedure expects that the engineer analyzing the test will estimate the volumetric specific heat based on knowledge of the rock/soil

formation and treat it as a known value. The effect of this assumption on the thermal conductivity prediction is discussed in Chapter 8.6.

A summary of the two-dimensional parameter estimations on the simulated borehole and the cored borehole configurations is provided in Table 8.1 along with the independently measured values of the thermal conductivities. The parameter estimations used between 46 and 50 hours of measured data, as discussed in section 8.6.1.

TABLE 8.1.

Thermal conductivity estimations for the cored borehole and the simulated borehole configuration.

	Okla. State University SiteA6		Experiment - Dry Sand		Experiment - Saturated Sand	
	predicted	indep. measured	predicted	indep. measured	predicted	indep. measured
k_{ground} Btu/hr-ft-°F (W/m-K)	1.379 (2.386)	1.351 (2.337)	0.152 (0.263)	0.149 (0.258)	1.336 (2.311)	1.353 (2.341)
k_{grout} Btu/hr-ft-°F (W/m-K)	0.758 (1.311)	0.850 (1.471)	0.540 (0.934)	0.430 (0.744)	0.496 (0.858)	0.430 (0.744)
Avg. Error of the Fit °F (°C)	0.11 (0.06)	N/A	0.23 (0.13)	N/A	0.22 (0.12)	N/A
Iterations	47	N/A	72	N/A	83	N/A

A comparison shows a very reasonable agreement between the predicted values of thermal conductivities using the parameter estimation method based on the downhill simplex algorithm with the numerical model of the borehole and the known and/or measured values for the same. A maximum deviation of about 2.1% is observed (cored borehole Okla. State Univ. Site A6) while the simulated borehole with dry sand and the simulated borehole with saturated sand display a deviation of only about 2.0% and 1.3% respectively. As expected, the errors associated with the predictions of the thermal

conductivity of the grout are greater since the second independent parameter is used as a surrogate to account for uncertainties in the borehole.

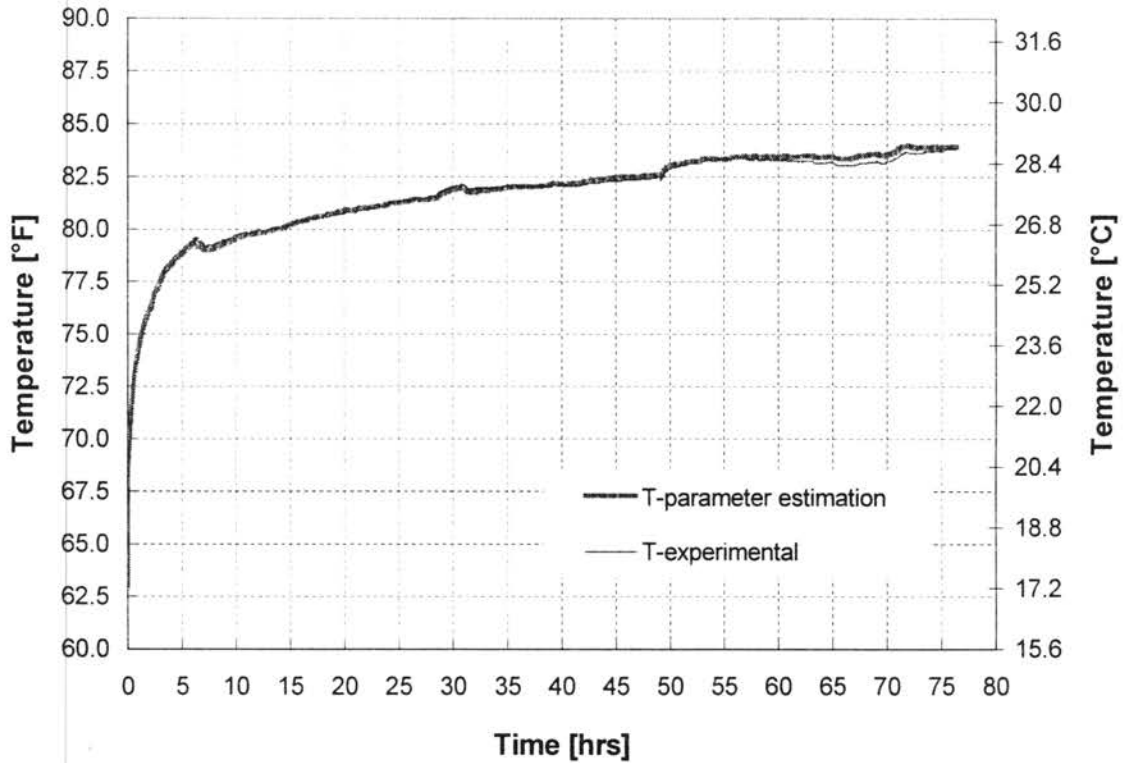


Figure 8.4. Comparison of in-situ experimental temperatures to predicted temperatures using the numerical function evaluation model based on the estimated parameters (k_{soil} and k_{grout}) using the Nelder-Mead simplex minimization. Oklahoma State University site A #6 borehole.

The absolute average error of the predicted temperatures using the estimated parameters ranges from about 0.11°F (0.06°C) to about 0.23°F (0.13°C). Figure 8.4 shows a typical comparison between the in-situ measured temperatures and the predicted temperatures with the numerical finite volume model using estimated ground and grout thermal conductivities. The temperature versus time plot in Figure 8.4 is provided for the cored borehole (OSU Site A #6). Although fluctuating power input was observed from

the in-situ test, the parameter estimation method was capable of predicting the ground conductivity within about $\pm 2\%$ of the measured value.

8.6. SENSITIVITY AND ERROR ANALYSIS

A series of sensitivity analyses have been performed to evaluate the influence of a number of input parameters that cannot be determined exactly, but estimated with some uncertainty. (The term “input parameters” refers here to parameters that are not estimated with the parameter estimation procedure, e.g. far-field temperature, volumetric specific heats, shank spacing, etc.) The uncertainty in the input parameters has a corresponding uncertainty in the estimated ground thermal conductivity. The sensitivity analyses are used to assess the impact of the input parameter uncertainty on the ground thermal conductivity.

In current practice, the spacing between the two legs of the U-tube is not consistently controlled over the entire depth of the borehole. Typically, the U-tube insertion into the borehole will not yield a perfectly centered U-tube with constant shank spacing. It is quite possible that after the installation is completed the U-tube legs may be touching each other at some borehole depths while spread apart at other borehole depths. Also, boreholes will often deviate from a perfectly straight path. Nevertheless, there will be an “effective” shank spacing value over the borehole that will be used in ground loop heat exchanger borehole models. The sensitivity to this “effective” shank spacing is examined below.

The volumetric specific heat of the ground varies with the type of the ground, but its value for most common soil types falls within a range from 20 Btu/ft³-°F (1340 kJ/m³-K) to about 50 Btu/ft³-°F (3350 kJ/m³-K). As discussed above, an estimate of the volumetric specific heat must be made.

Since the borehole temperature response to an imposed heat flux is sensitive to the undisturbed far field temperature of the ground, the value of the far field temperature has a significant impact on the estimated ground thermal conductivity. There are several maps (IGSHPA 1991) available that provide a general idea of the undisturbed ground temperatures for the continental U.S. using well water isotherms. However, such maps cannot possibly yield locally accurate information. Although several experimental procedures have been tried for obtaining the undisturbed ground temperature, the best procedure seems to be lowering a thermocouple (or other calibrated temperature sensor) down the U-tube and measuring the temperature of the heat transfer fluid along the borehole depth before each test. Even then, there is some uncertainty in the measurement. Although the ground thermal conductivity predictions will be strongly affected by variations in the assumed far field temperature, the impact on the borehole design is mitigated as long as the design value and the value used for the parameter estimation are the same.

Under field conditions, it is usually not feasible to tightly control the drilled borehole geometry as it pertains to borehole radius and depth. The borehole diameter

may vary. Parts of the borehole may have a diameter larger than the drill bit due to high-pressure drilling fluid washing out unconsolidated material. Other parts may have a diameter smaller than the drill bit due to local collapses in the borehole. Also, the borehole may not be a straight, vertical hole. Similarly, the borehole depth itself may also deviate from the desired depth, although it can be easily measured after the U-tube has been inserted. Therefore, sensitivity analyses are performed to assess the impact of uncertainties in the borehole radius and borehole depth on the estimated ground thermal conductivity.

In addition to uncertainties related to input parameters, uncertainties may be introduced through experimental errors. These primarily include uncertainties in the measured power-input and uncertainties due to mis-calibration of the temperature sensors. Sensitivity analyses have been conducted to assess the impact of such errors on the predicted ground thermal conductivity by artificially introducing errors into thermistor calibration and into power-input readings.

Finally, the duration of the test has an impact on the results. The accuracy of the estimated thermal conductivity was found to increase with the length of the test. However, it is highly desirable that the test be conducted in as short a time as possible. Therefore, the sensitivity of the results to the length of test is described below. Because all of the other uncertainties depend on the length of test, it is described first.

8.6.1. LENGTH OF IN-SITU TESTING

One of the most commonly asked questions about in situ testing is “How long does the test need to be?” One of the best approaches available for answering this question may be to run long tests, and to observe the sensitivity of the ground thermal conductivity estimations to the length of the data used. As the duration of data used increases, there should be a point in time beyond which the estimated value of the ground thermal conductivity does not change very much.

Field experience suggests that the estimate of the ground thermal conductivity reaches convergence between 80 and 100 hours. To illustrate the point, Figure 8.5 shows the typical dependency of the ground thermal conductivity on the test duration observed for three test boreholes (Oklahoma State University site A#1 and A #2 boreholes and a test borehole located in Chickasha, Oklahoma). The total duration of the in-situ test on the site A#2 borehole was slightly longer than 170 hours while the in-situ tests on site A#1 borehole and the Chickasha borehole were each about 100 hours long. For each data set, the ground thermal conductivity is estimated for various data lengths starting from the 20th hour. The data sets shorter than 170 hours have been logarithmically extrapolated up to the 170th hour for comparison. The estimated ground thermal conductivity values appear to converge after about 80 to 100 hours from which time on no significant changes are observed.

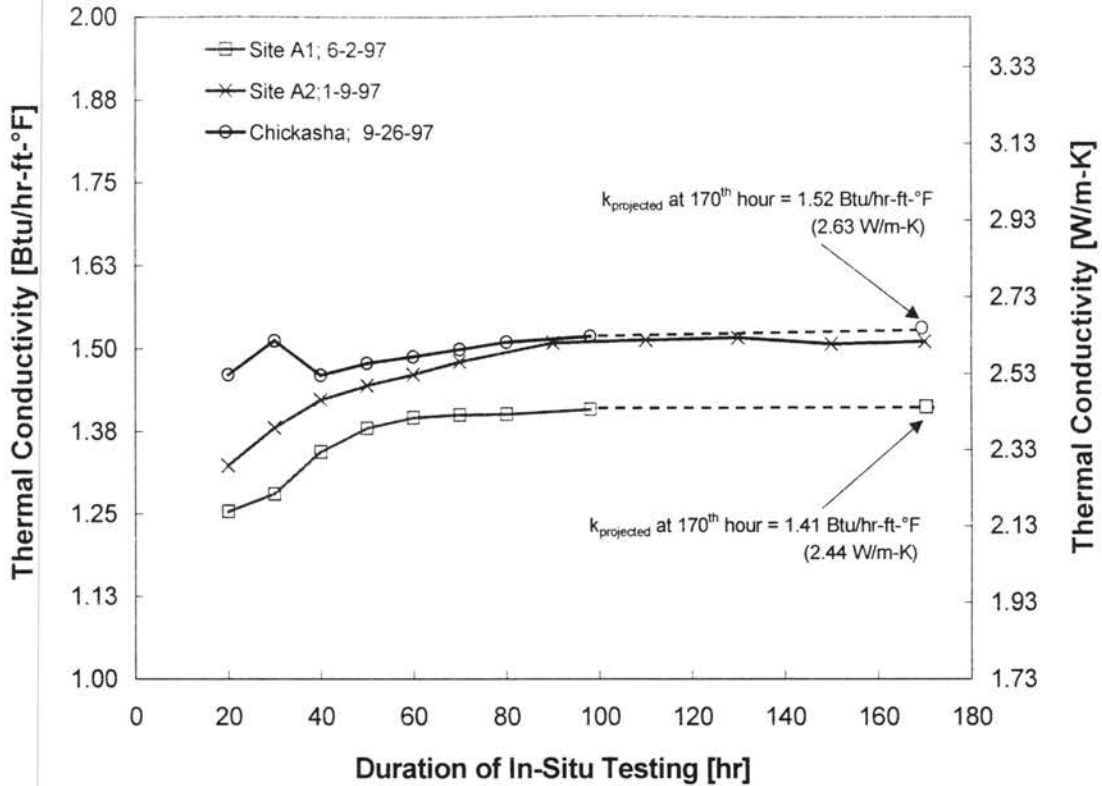


Figure 8.5. Ground thermal conductivity estimation vs. in-situ test duration. Oklahoma State University site A #1 and #2, and Chickasha test boreholes. (Dotted lines indicate logarithmic extrapolations.)

It is often not feasible to conduct a test of this length. Therefore, a significant effort has been made to find a suitable compromise between test length and test accuracy. Although the choice is somewhat subjective, the authors have settled on a test length of 50 hours based on analyses conducted on the current in-situ test data and field experience (Austin 1998). With in-situ tests shorter than 50 hours, the error in the ground thermal conductivity prediction can be significant. This error is quantified in Table 8.2 where the thermal conductivity estimations and associated errors from the converged value for the Oklahoma State University Site A#1, #2 and Chickasha test boreholes are provided. The

deviation between the ground thermal conductivity estimation of the 20-hour test and the estimations of the 170-hour test for the site A#2 borehole is approximately 14.2%. The absolute error diminishes rapidly as the length of data is increased. It is about 4.6% by the 50th hour. A very similar trend is observed on the site A#1 and Chickasha test boreholes where the absolute errors at the 50th hour from the converged estimations are observed to be about 2.2% and 2.8% respectively.

TABLE 8.2.
Thermal conductivity estimations and associated errors from the converged value for the Okla. State University Site A#1, #2 and Chickasha test boreholes.

Duration of In-Situ Testing [hr]	Okla. St. Uni.; Site A1; 6-2-97		Okla. St. Uni.; Site A2; 1-9-97		Chickasha; 9-26-97	
	k_{ground} Btu/hr-ft-°F (W/m-K)	Error [%]	k_{ground} Btu/hr-ft-°F (W/m-K)	Error [%]	k_{ground} Btu/hr-ft-°F (W/m-K)	Error [%]
20	1.254 (2.169)	12.48	1.323 (2.289)	14.20	1.461 (2.528)	4.04
30	1.280 (2.214)	10.15	1.381 (2.389)	9.46	1.513 (2.618)	0.49
40	1.344 (2.325)	4.93	1.423 (2.462)	6.18	1.460 (2.526)	4.10
50	1.380 (2.387)	2.20	1.445 (2.500)	4.60	1.478 (2.557)	2.81
60	1.396 (2.415)	1.00	1.461 (2.528)	3.43	1.488 (2.574)	2.15
70	1.400 (2.422)	0.70	1.480 (2.560)	2.08	1.499 (2.593)	1.40
80	1.401 (2.424)	0.64			1.510 (2.612)	0.65
90			1.509 (2.611)	0.15		
100	1.409 (2.438)	0.08			1.519 (2.628)	0.07
110			1.514 (2.619)	0.15		
130			1.517 (2.624)	0.36		
150			1.508 (2.609)	0.24		
170	1.410 (2.439)*	0.00	1.511 (2.614)	0.00	1.520 (2.630)*	0.00

(*) Projected

A series of in-situ tests on other nearby boreholes at the Oklahoma State University test site A were performed. Although one additional long-term test (longer than 100 hours) was conducted, the majority of the tests were about 70 hours. Analysis of the 100+ hour tests and the 70 hour tests indicated that the estimated ground thermal conductivity values, based on 50-hour test length, were typically within $\pm 6.5\%$ of the converged value, although about half of the long tests had values within $\pm 2.5\%$. On the

shorter (approximately 70 hours) tests, it was not always possible to determine the converged value. Therefore, it is possible that the uncertainty associated with the thermal conductivity estimates at the 50th hour might be somewhat greater, although current field experience appears to bound its range within $\pm 6.5\%$.

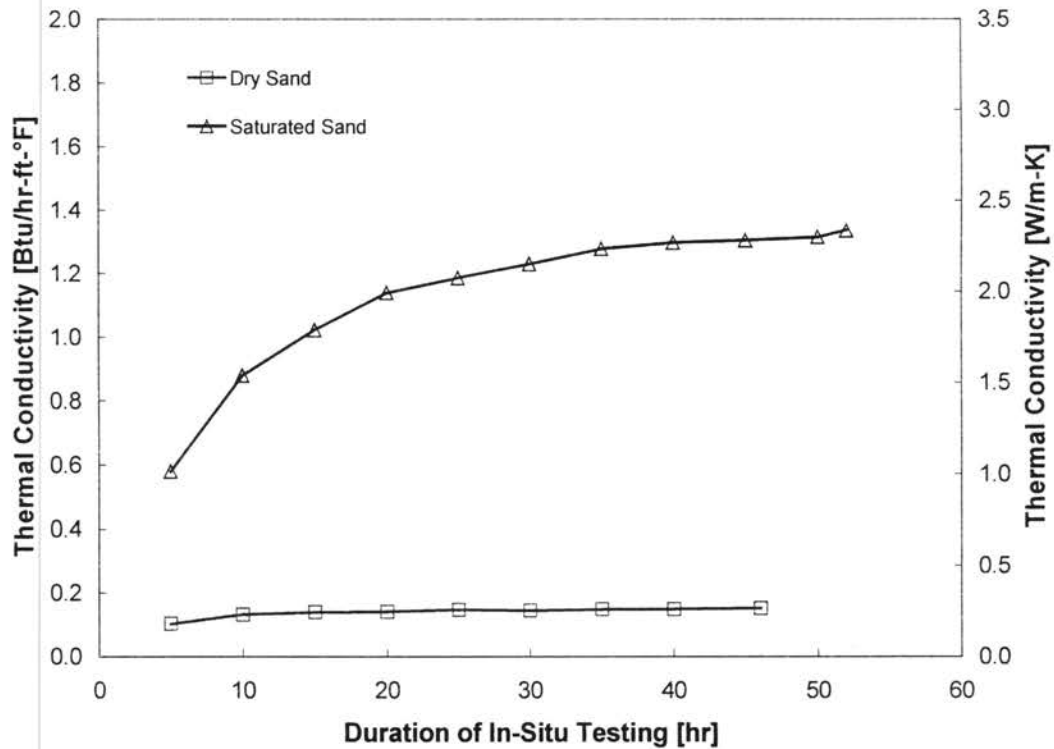


Figure 8.6. *Thermal conductivity estimation vs. duration of in-situ testing. Simulated borehole.*

In addition, there appears to be a correlation between the ground thermal conductivity and the required length of in-situ testing. Figure 8.6 illustrates that the dry sand with low conductivity and low diffusivity converges significantly faster than the saturated sand with higher conductivity, while in each test case identical grout of thermal conductivity of 0.43 Btu/hr-ft-°F (0.74 W/m-K) was used. As shown in Figure 8.6, the

simulated borehole tests with dry sand estimates the converged conductivity within $\pm 8\%$ with only 15 hours of in-situ test data, while the simulated borehole test with saturated sand requires about 35 hours of in-situ test data to achieve the same accuracy.

8.6.2. UNDISTURBED FAR-FIELD GROUND TEMPERATURE

The sensitivity of the parameter estimation model to the uncertainties in the measurement of the undisturbed far-field ground temperature can be seen in Figures 8.7 and 8.8 for the cored borehole and the simulated borehole in the medium-scale laboratory tests.

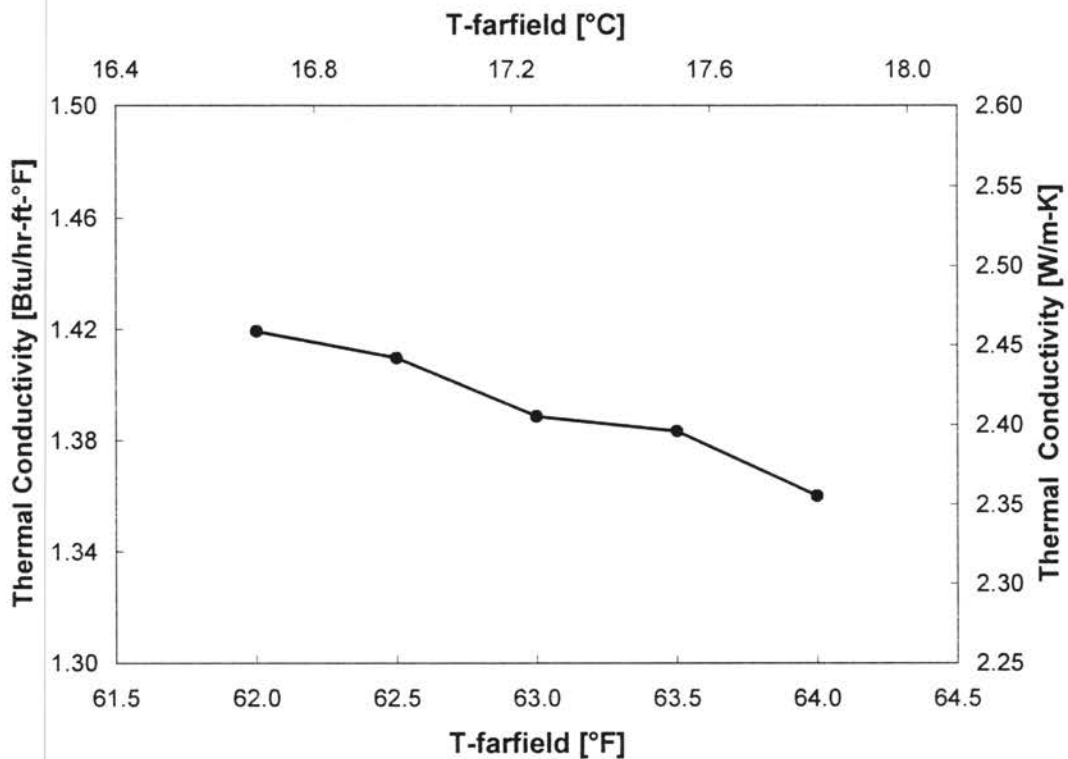


Figure 8.7. Ground thermal conductivity estimation vs. the undisturbed far-field ground temperature. Oklahoma State University site A #6 borehole.

For one particular experimental data set, five different far-field temperatures were used as input parameters. The analyses demonstrate the ground thermal conductivity prediction sensitivity based on a ± 1.0 °F (± 0.6 °C) error range. For each far-field temperature point, all other input parameters were kept constant.

Figures 8.7 and 8.8 show that the parameter estimation model is very sensitive to the estimate of the ground far-field temperature. It is also observed that this sensitivity is stronger for high thermal conductivity soils than for low thermal conductivity soils. As expected, the predicted ground thermal conductivity decreases with increasing far-field temperature, since, for unchanged series of heat transfer rates the temperature differences between the average borehole temperatures and the far-field temperature becomes larger. The analyses based on the simulated and cored boreholes show that if the ground far-field temperature can be determined within ± 1.0 °F (± 0.6 °C) the associated error in the thermal conductivity estimation will be limited to about $\pm 4.9\%$.

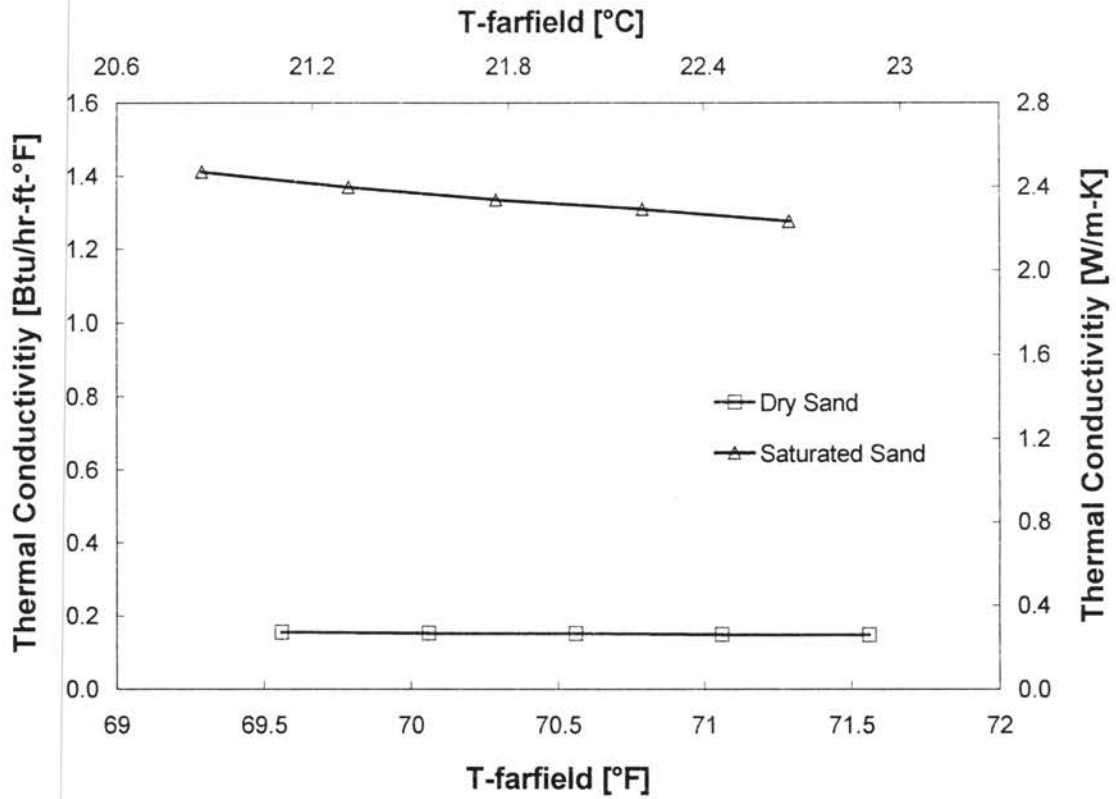


Figure 8.8. *Thermal conductivity estimations vs. the undisturbed far-field temperature. Simulated borehole.*

8.6.3. U-TUBE SHANK SPACING

The sensitivity of the ground thermal conductivity estimations to uncertainties in the shank spacing (the distance between the two pipes from pipe outer wall to pipe outer wall of a U-tube) is presented in this section. Since it is difficult in practice to control the shank spacing, this parameter was varied to examine its sensitivity to the ground thermal conductivity estimations.

Figure 8.9 shows the results obtained from the cored borehole and the simulated borehole tests. In each of these cases, five different shank spacing values that would not violate the borehole geometry were used. Since the inclusion of the second independent variable (k_{grout}) in the parameter estimation is expected to act as a surrogate for the uncertainties in the shank spacing, the sensitivity analyses have shown that even significant uncertainties (errors in the initial estimate) in the U-tube shank spacing only yield small changes in the ground conductivity predictions. A $\pm 40\%$ change in the ‘effective’ shank spacing only causes a $\pm 1.6\%$ change in the ground thermal conductivity estimation.

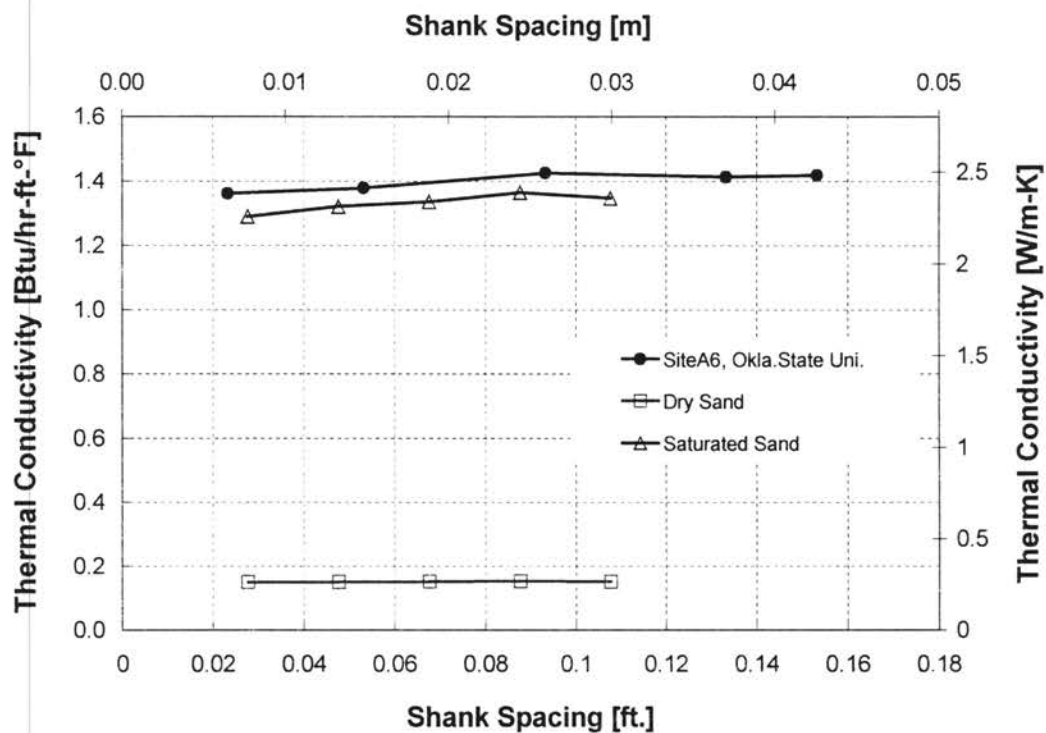


Figure 8.9. Thermal conductivity vs. the shank spacing of the U-tube. Oklahoma State University site A #6 borehole, and the simulated borehole in the medium-scale test unit with dry and saturated sand.

Although there is a strong correlation between the grout thermal conductivity estimates and the shank spacing values, the ground thermal conductivity is affected only slightly. The simulated borehole tests with dry and saturated sands suggest that very low thermal conductivity sand is significantly less sensitive to uncertainties in the shank spacing than saturated sand with higher thermal conductivity.

8.6.4. VOLUMETRIC SPECIFIC HEAT OF GROUND FORMATION

Since the transient conduction heat transfer problem depends strongly, but not solely, on the thermal diffusivity, it is inevitable that the estimated thermal conductivity will be dependent on the assumed value of the volumetric specific heat of the ground.

In order to determine the sensitivity, the effect of volumetric specific heat values ranging from 20 Btu/ft³-°F (1340 kJ/m³-K) to 50 Btu/ft³-°F (3350 kJ/m³-K) have been investigated. This range of volumetric specific heat, as reported by EPRI (1989) represents almost the entire practical range for commonly occurring soil types. In order to accommodate the medium-scale laboratory test cases involving dry sands with very low diffusivity, a relatively low volumetric specific heat value of 14 Btu/ft³-°F (938 kJ/m³-K) is also investigated.

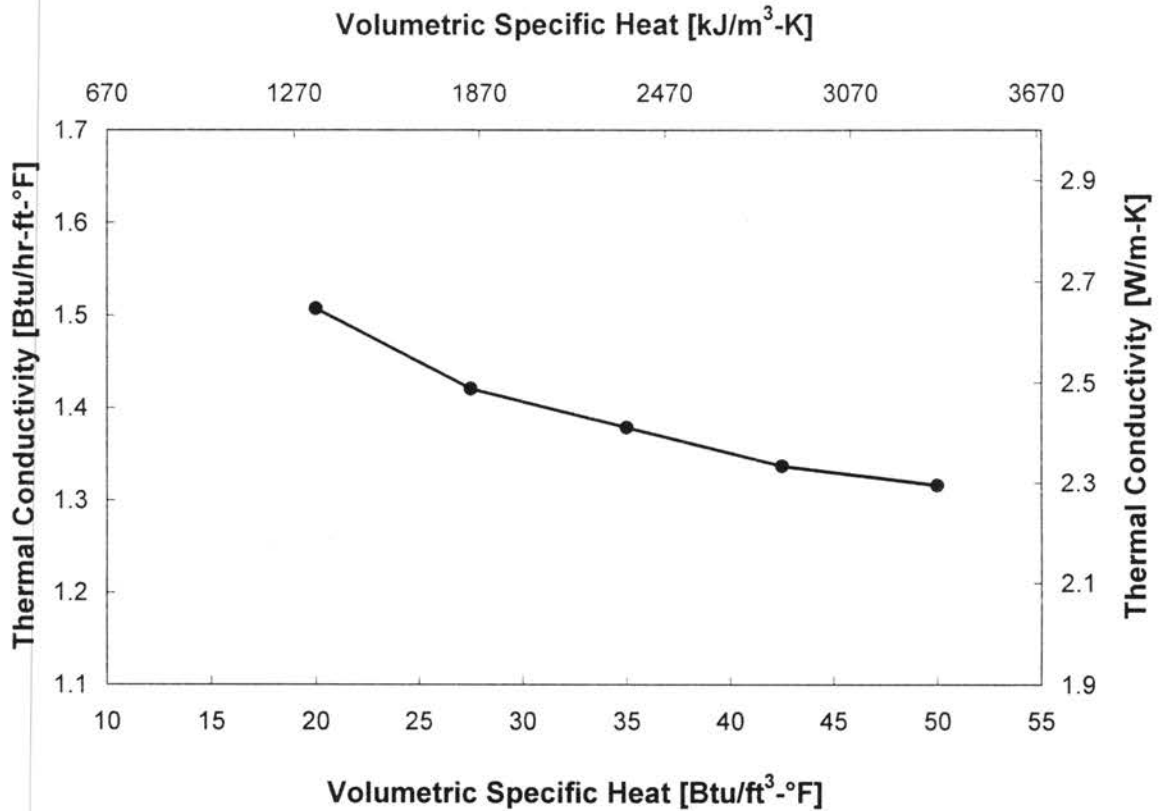


Figure 8.10. *Ground thermal conductivity estimation vs. the ground's volumetric specific heat. Oklahoma State University site A #6 borehole.*

Figure 8.10 shows the results of the sensitivity analyses for the cored borehole, and Figure 8.11 for the simulated borehole tests. A relatively strong correlation is observed between ground thermal conductivity and ground volumetric specific heat. The ground thermal conductivity estimations decrease as the volumetric specific heat of the ground increases, although this trend is not as strong in the case of the saturated sand as it is for soils with very low thermal conductivities. The low thermal conductivity soils appear to be more sensitive to uncertainties in the soil's volumetric specific than higher conductivity soils that are typical for soil types encountered in practice.

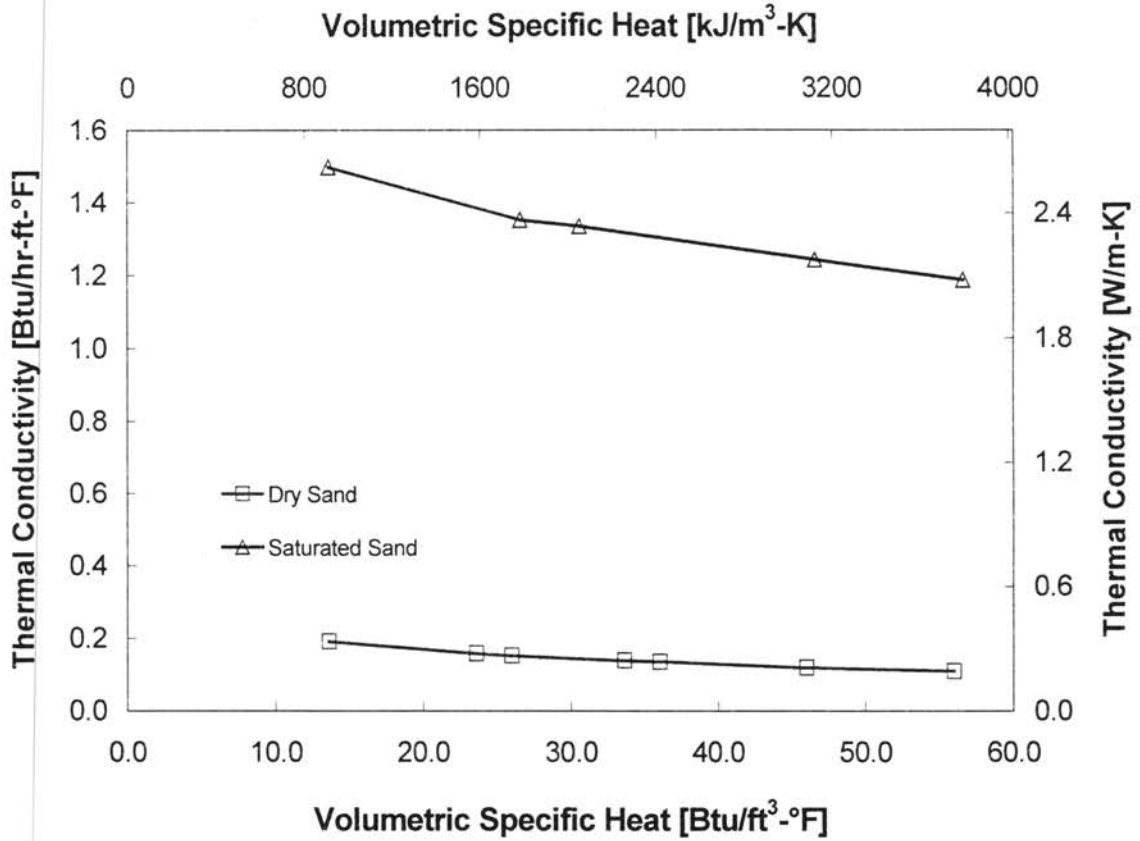


Figure 8.11. *Thermal conductivity estimations vs. the volumetric specific heat.*

Simulated borehole.

However, the analyses show that, if the volumetric specific heat of the ground can be estimated within ± 5 Btu/ft³-°F (± 335 kJ/m³-K), which represents about 10% to 25% of the practical range for commonly occurring soil types, the ground thermal conductivity estimations vary by about $\pm 2.6\%$ for the cored borehole and the simulated borehole with saturated sand while it varies by about $\pm 6.3\%$ for very dry sand.

8.6.5. POWER INPUT AND TEMPERATURE CALIBRATION

Errors due to improperly calibrated instrumentation can affect the in-situ test data. This may manifest itself in the form of incorrect power-input (errors on the watt transducer) and/or entering and exiting loop temperature readings (errors in temperature sensor calibration). Therefore, an error estimate for the experimentally collected data is required to investigate the sensitivity of the ground thermal conductivity predictions to uncertainties in power and/or temperature measurements

In order to accomplish this, artificial errors were introduced to the power and temperature sensor calibrations. For the temperature data, the slope of the sensor calibration curve was increased by 2% for both the borehole entering and exiting fluid temperatures. The experimental average borehole temperature was then ‘re-computed’ based on the artificially adjusted loop temperatures. The ground thermal conductivity estimations were then obtained based on the actual power-input data and the modified temperature response data. The results are reported in Table 8.3.

The sensitivity analysis of the ground thermal conductivity to uncertainties in the power-input measurements is implemented by an artificial modification of the power-input values. The power-input values for each time step were increased by 5% while the corresponding temperature responses to the changes in power were unchanged. The results of the power sensitivity analyses are also reported in Table 8.3.

The analyses for the specific cases investigated show an almost linearly proportional relationship between an increase of the calibration curve slope of the temperature sensors used or the increase in the power input, and the predicted thermal conductivity values for the cored and the simulated borehole cases.

TABLE 8.3.
Change in ground thermal conductivity Btu/hr-ft-°F (W/m-K) estimations
based on changes in power input and temperature measurement

	Base	Power up 5%	Change [%]	Base	Temp. Calib. Coeff. up 2%	Change [%]
$k_{\text{ground-OSU SiteA6}}$	1.379 (2.386)	1.445 (2.500)	4.79	1.379 (2.386)	1.400 (2.422)	1.52
$k_{\text{ground - Dry Sand}}$	0.152 (0.263)	0.160 (0.277)	5.26	0.152 (0.263)	0.154 (0.266)	1.32
$k_{\text{ground - Sat. Sand}}$	1.336 (2.311)	1.428 (2.470)	6.89	1.336 (2.311)	1.364 (2.360)	2.10

In summary, a $\pm 2\%$ change in the slope of the thermistor calibration curve causes an estimated uncertainty of about $\pm 2\%$. However, based on a simple statistical analysis of the sensor calibration, the uncertainty in the slope is expected to be less than $\pm 0.12\%$. This will cause a negligible uncertainty in the ground thermal conductivity estimate.

The watt transducer used in the experimental apparatus has an accuracy of approximately $\pm 1.5\%$ for the conditions encountered during in-situ tests. Based on this, the resulting uncertainty in the thermal conductivity estimations is projected to be about $\pm 1.5\%$.

8.6.6. BOREHOLE GEOMETRY

The drilling of boreholes under field conditions introduces uncertainties due to drilling processes used and the ground conditions at the field. The actual borehole diameter may be both larger than the drill bit in some places, and smaller than the drill bit in other places. Since it is not feasible that these occurrences be controlled (and are not controlled in typical practice) a series of sensitivity analyses are required to assess the impact of uncertainties introduced through inaccurate borehole depth and radius.

These uncertainties are analyzed only for the cored borehole. The borehole radius was varied between 0.149 ft (0.045 m) and 0.229 ft (0.070 m), a range that is within $\pm 20\%$ of the nominal borehole radius. Again, for each estimation, all other input parameters were kept constant.

Figure 8.12 illustrates the dependency of the ground thermal conductivity estimations on the uncertainty of borehole radius for the cored borehole. As the radius of the borehole becomes larger the estimated ground conductivity increases due to increased borehole resistance. This is expected, since, as the borehole resistance increases through the larger borehole diameter, the estimates for the ground conductivity have to increase to adjust for the unchanged average borehole temperatures. However, analyses suggest that, if the borehole radius can be determined within ± 0.04 ft (± 0.012 m), the uncertainty in estimating the ground thermal conductivity is reduced to about $\pm 3.6\%$.

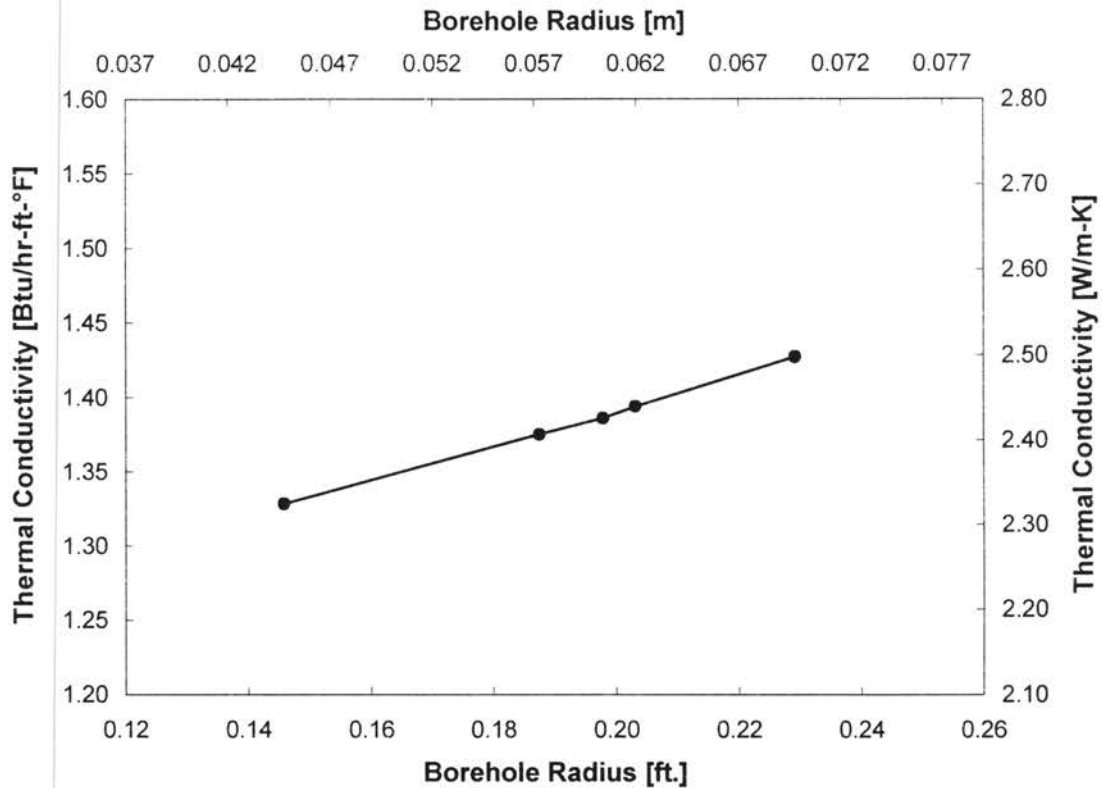


Figure 8.12. *Ground thermal conductivity estimation vs. the borehole radius. Cored borehole Oklahoma State University site A#6.*

The sensitivity of the estimated ground thermal conductivity to uncertainties in the depth of the borehole was also investigated. The estimated conductivity decreases with increasing depth, since, in the analyses, the total amount of heat transferred over the borehole is unchanged. Consequently, for shorter borehole depths, the amount of heat transferred per unit borehole depth increases while the average borehole temperatures and other input parameters are kept unmodified, resulting in higher ground thermal conductivity estimations. Similarly, lower ground thermal conductivities are estimated for increased borehole depths. The analyses indicate that the uncertainty in the ground thermal conductivity due to a ± 0.5 ft (0.15 m) uncertainty in the borehole depth is

$\pm 0.15\%$ for a 250 ft (76.2 m) deep borehole. This uncertainty is negligible when added in quadrature with the other uncertainties.

In addition to the uncertainties discussed above, the numerical finite volume model of the borehole also represents a source of uncertainty in the estimation of the ground's thermal conductivity. Yavuzturk et al. (1999) provides detailed discussion on the numerical model and its validation against an analytical solution using six different test cases that simulate a typical range of heat flux, model geometry and thermal properties. However, the analytical solution does not correspond exactly to the borehole geometry with differing ground and grout conductivities. Therefore, it is difficult to determine the exact impact of the uncertainties in the numerical model on the estimate of the ground conductivity. It appears, but probably cannot be proven, that the inaccuracies in the numerical model are reflected in the estimate of the grout conductivity. Accordingly, a heuristic estimate of the impact of the uncertainty in the numerical model on the ground conductivity is made. The $\pm 1.2\%$ uncertainty corresponds to the error in the numerical model results at 12 hours.

8.7. DISCUSSION

A summary of the sources of uncertainties and their effect on the ground thermal conductivity estimation is given in Table 8.4. Since the uncertainties described in Table 8.4 pertain to parameters that are all independent or nearly independent from each other they may be added in quadrature. Thus, the total estimated uncertainty of the ground

thermal conductivity estimations falls within a range of about 9.6% - 11.2% depending on the level of the estimated thermal conductivity, since very low conductivity sands appear to be more sensitive to the estimate of the volumetric specific heat. The overall uncertainties compare very well with the range of values that was obtained from other tests in nearby locations (Austin 1998). (Uncertainties smaller than 0.2 % have been ignored, as their contribution to the overall uncertainty is negligible.)

TABLE 8.4.

Summary of primary sources of uncertainties in the estimation of thermal conductivity of the ground.

Source	Estimated uncertainty in predicted k_{ground}
Length of Test – approx. 50 hours	$\pm 6.5\%$
Power Measurement. ($\pm 1.5\%$ uncertainty.)	$\pm 1.5\%$
Estimate of the volumetric specific heat of the ground. ($\pm 5 \text{ Btu/ft}^3\text{-}^\circ\text{F}$ [$\pm 335 \text{ kJ/m}^3\text{-K}$])	$\pm 2.6\%$ (average soils) or $\pm 6.3\%$ (extremely dry soils)
Estimate of the borehole radius. (± 0.5 inches [12.7 mm])	$\pm 3.6\%$
Estimate of the shank spacing. ($\pm 40\%$)	$\pm 1.6\%$
The numerical model.	$\pm 1.2\%$
Estimate of the far-field temperature. (± 1 $^\circ\text{F}$ [± 0.6 $^\circ\text{C}$])	$\pm 4.9\%$
TOTAL ESTIMATED UNCERTAINTY	$\pm 9.6\% - 11.2\%$

It is obvious that the estimated uncertainty is somewhat higher than the errors found when the parameter estimation procedure was applied to the validation test cases.

It should be noted that, for these cases, a number of the input parameters, e.g. far field temperature, volumetric specific heat, borehole radius, and shank spacing were determined more accurately than what might be feasible under typical field conditions.

Specific conclusions and recommendations regarding the design of the in-situ test apparatus and experimental procedure are discussed in detail by Austin (1998).

Additional conclusions and recommendations related to the length of in-situ test and the parameter estimation procedure, and overall accuracy of the estimates are as follows:

The length of test should be no less than 50 hours to obtain a value of ground conductivity that would be within about $\pm 6.5\%$ of that obtained with a much longer tests. Preliminary analyses suggest that the ground thermal conductivity to be estimated may have a significant influence on the length of in-situ testing. It appears that low thermal conductivity soils require less time to converge than higher thermal conductivity soils.

An error analysis suggests that with data measured by the experimental apparatus, the two-variable parameter estimation procedure can be expected to predict the ground thermal conductivity within a range of about $\pm 9.6\%$ and $\pm 11.2\%$.

Validation test cases using saturated and dry sands under laboratory conditions and the cored borehole show that the two-variable parameter estimation model estimates the ground thermal conductivity within a maximum range of $\pm 2.1\%$. As noted, the errors here are smaller than the general error estimate because several of the input

parameters were estimated more accurately than what might be feasible under typical field conditions.

It is obviously desirable that the required time for the in situ test and parameter estimation be reduced. To that end, the following recommendations for further investigation are offered:

In order to quantify the relationship between the required length of in-situ tests and the ground's thermal conductivity, further research is suggested utilizing test data from an even wider range of ground thermal conductivities.

Since the duration of the test depends on the desired accuracy, any improvement in accuracy of the method may allow for a shorter test. Accordingly, methods for reducing the uncertainty of the input parameters should be investigated. In particular, methods for more accurately estimating the far-field temperature, the average borehole radius (perhaps by measuring the total grout volume), and the ground volumetric specific heat should be pursued.

The current recommended duration of the in situ test is 50 hours. In practice, it is highly desirable to be able to do the test in a significantly shorter amount of time. One possible approach for this is to improve the model's accuracy in the first few hours. This might be done by extending the numerical model to 3 dimensions and/or more closely matching the actual geometry by using a boundary-fitted coordinate grid. Presumably,

any improvements made in the first few hours will help allow for a shorter test (This has been demonstrated to have potential in a recent article by Spitler, Rees and Yavuzturk [1999]). At the same time, it will probably be useful to physically control the position of the U-tube in the borehole. Whether the reduced test time will be worth the increased computational time for the parameter estimation remains to be seen.

The parameter estimation algorithm is a computationally intensive procedure. For acceptable estimation accuracy, about 50-80 objective function evaluations are typically required, with each one requiring a simulation using the detailed numerical model of the borehole. In order to reduce the computational time, a better initial guess for the conductivities may be made by using a simple analytical model in conjunction with the parameter estimation procedure. This estimate can be made very quickly, and used to reduce the number of objective function evaluations made with the detailed numerical model

In order to reduce the time from the start of the experiment to final parameter estimation results, the parameter estimation may be performed simultaneously (on-line) instead of subsequently (off-line). The suitability of on-line parameter estimation methods, such as recursive and/or adaptive techniques should be investigated. This could also have the advantage of being able to tell the operator when the experiment is “done”, rather than running a predetermined number of hours.

9. SUMMARY

This thesis is organized so that detailed conclusions are given for each aspect of the work in Chapters 4-8. Therefore, this section provides a brief summary of the work and the most important conclusions and recommendations. A detailed literature survey is conducted on the design and simulation tools for modeling ground source heat pump systems that use vertical, closed-loop ground heat exchangers. The literature survey also includes currently used methods for the determination of ground formation thermal conductivity (Chapter 2).

A transient, two-dimensional finite volume model is developed and validated for the calculation of heat transfer in and around the borehole of a vertical U-tube ground loop heat exchanger (Chapter 4). The numerical model is developed for use in two applications that require the prediction of the short time scale thermal response of the borehole field. The first application is to provide the thermal response of ground loop heat exchangers on shorter time scales (hourly or less time intervals) for heat exchanger design purposes and component-based building energy analysis. The second application is the development of a procedure that is based on the short-term response for in-situ ground thermal conductivity measurements. In this case, the numerical model of the borehole is used to solve the inverse heat transfer problem associated with estimating ground and grout thermal conductivity from in-situ test data (Chapter 8).

The short time-step response factors are developed and used in a short time step model in conjunction with a load aggregation algorithm to improve computational

efficiency. The model is also cast as a TRNSYS component model (Chapter 5). Two example applications for the model are provided via simulations based on the loads of actual buildings (Chapters 5 and 7). Experimental validation for the short time step model is provided using operating data collected at the Maxey elementary school in Lincoln, NE (Chapter 6).

A detailed discussion of the results of the various sections of this study and recommendations for further research are given at the end of previous chapters. The following conclusions and recommendations for further research may be made as the final summary of this study:

- i) The transient, two-dimensional finite volume model of the ground heat exchanger borehole is a significant improvement over the currently available analytical (line source or cylinder source models) and numerical modeling approaches. It provides a significantly more accurate representation of the ground heat exchanger borehole by separately modeling the individual borehole components. The thermal effects of U-tube pipes, the backfill grout, soil and the heat transfer fluid can be accounted for as separately interacting entities. The errors that are associated with the numerical model are acceptably small.
- ii) Because of the pie-sector representation of the U-tubes, the average borehole temperature predictions of the two-dimensional numerical model become

somewhat less accurate for early times (less than 1 hour) of simulations. An improvement of the temperature predictions for these early times may be achieved by either more accurately adjusting the shape of the pie-sector representation or by adopting a boundary-fitted coordinates approach should be investigated. Nevertheless, for the objectives of this study, the numerical model, as suggested in Chapter 4, models the short time temperature response of ground heat exchangers reasonably well for time steps as small as one hour. However, there is a point of diminishing returns. The computational effort required to improve the accuracy of the two-dimensional numerical model may not justify the additional effort considering the sensitivity of its applications (Chapters 5, 6 and 7). However, for the estimation of the ground thermal conductivity, a more detailed model may be beneficial (Chapter 8).

- iii) The non-dimensional, short time-step response factors are a very useful extension of the long time-step response factors developed by Eskilson (1987). The short time step response factors allow for an hour-by-hour or shorter time-step evaluation of system energy consumption and electrical demand. A more accurate and detailed assessment of the short-term behavior of ground-coupled heat pump systems can thus be made for the design of ground loop heat exchangers, energy analysis of ground source heat pump systems, and design and dynamic behavior of hybrid ground source systems. For hybrid ground source heat pump applications, the model allows the implementation of sophisticated system operating and control strategies for

which there were previously no simulation tools available. Development of an optimal design procedure for hybrid ground source heat pump systems, incorporating the short time step response factor model, is a promising topic for future research..

- iv) In conjunction with the transient, two-dimensional finite volume model of the borehole, a parameter estimation procedure is developed to predict effective thermal conductivity of ground formations surrounding ground heat exchanger boreholes. The in-situ procedure utilizes inverse heat transfer techniques and is capable of predicting effective ground thermal conductivities within a range of about $\pm 9.2\%$ to $\pm 11.2\%$ based on a 50 hour in-situ test length. Further research utilizing test data from even a wider range of ground thermal conductivities is recommended. Although the recommended in-situ test duration is 50 hours, it is highly desirable to shorten this time. Since the duration of the in-situ testing is presumably related to the accuracy of the borehole model, increasing the accuracy of the numerical borehole model by extending to the 3rd dimension and/or using a boundary-fitted coordinate grid should be investigated. Another area of further research may be that the parameter estimation procedure is performed simultaneously (on-line) with the in-situ borehole thermal response test instead of subsequently (off-line). The suitability of on-line parameter estimation methods based on recursive and/or adaptive techniques should also be investigated.

BIBLIOGRAPHY

Abramowitz, M., 1970. Handbook of Mathematical Functions. Dover Publications, New York.

Allen, J. R., 1920. Theory of Heat Losses from Pipes Buried in the Ground, ASHVE Transactions, Vol. 26.

American Society for Testing and Materials. 1963. Thermal Conductivity of Materials by Means of a Guarded Hot Plate. ASTM Specifications C177-63.

Andrews, J. W., 1985. Optimized Ground Coupled Heat Pump Design Phase 1 Final Report. Brookhaven National Laboratory, 38869.

Arpaci, V. S., 1966. Conduction Heat Transfer. Reading Mass., Addison Wesley Publishing Co.

ASHRAE Handbook. 1985. Handbook of Fundamentals, New York.

ASHRAE. 1995b. Commercial/Institutional Ground-Source Heat Pumps Engineering Manual. Caneta Research Inc., American Society of Heating, Refrigerating and Air-Conditioning Engineers.

ASHRAE. 1996. *ASHRAE Handbook-Systems and Equipment*. Chapter 36, American Society of Heating, Refrigerating and Air-Conditioning Engineers.

ASHRAE. 1997. (Kavanaugh, S.P. and K. Rafferty, Authors) *Ground Source Heat Pumps- Design of Geothermal Systems for Commercial and Institutional Building*

Austin, W. A. 1998. *Development of an In-Situ System for Measuring Ground Thermal Properties*. Master's thesis. Oklahoma State University. Stillwater, Oklahoma. (Also available at http://www.mae.okstate.edu/Faculty/spitler/Austin_thesis.pdf)

Austin, W. A., C. Yavuzturk, J. D. Spitler., 2000. *Development of an In-Situ System and Analysis Procedure for Measuring Ground Thermal Properties*. Submitted to ASHRAE Transactions.

Ball, D. A., Fisher, R. D., Hodgett, D. L. 1983. *Design Methods for Ground Source Heat Pumps*. ASHRAE Transactions Vol.89.

Beck J. V., K. J. Arnold. 1977. *Parameter Estimation in Engineering and Science*. New York: Wiley.

BLAST. 1986. *BLAST (Building Loads and System Thermodynamics)*. University of Illinois, Urbana-Champaign.

Bose, J. E., Parker, J. D. 1983. "Ground Coupled Heat Pump Research", ASHRAE Transactions Part 2B.

Bose, J. E., 1984. "Closed Loop Ground Coupled Heat Pump Design Manual", Engineering Technology Extension Oklahoma State University.

Bose, J. E., Ledbetter, C. W., Partin, J. R., 1979. "Experimental Results of a Low-Cost Solar-Assisted Heat Pump System Using Earth Coil and Geothermal Well Storage", Proceedings of the 4th Annual Heat Pump Technology Conference.

Bose, J. E., Ledbetter, C. W., Partin, J. R., 1980. "Earth Coupled and Solar Assisted Heat Pump Systems", Proceedings of the 5th Annual Heat Pump Technology Conference.

Bose, J. E., 1982. "Earth Coil /Heat Pump Research at the Oklahoma State University", Proceedings of the 6th Annual Heat Pump Technology Conference.

Bose, J. E., Parker, J. D., 1984. "A Report on the ASHRAE Project to Develop a Design Data Manual for Ground Coupled Heat Pumps", Proceedings of the 7th Annual Heat Pump Technology Conference.

Bose, J. E., 1981. "Design and Testing of Solar Assisted Earth Coils", Final Report to DOE, EM-78-S-01-4257.

Cane, R. L. D., Forgas, D. A., 1991. "Modeling of Ground Source Heat Pump Performance", ASHRAE Transactions

Caneta Research Inc. 1995. Operating Experiences with Commercial Ground Source Heat Pump. ASHRAE Research Project 863. Atlanta: American Society of Heating Refrigerating and Air-Conditioning Engineers. Cited by Kavanaugh (1998).

Carslaw, H. S., 1921. "Introduction to the Mathematical Theory of Heat in Solids", 2nd Edition, Macmillan.

Carslaw, H. S., and J. C. Jaeger. 1947. Conduction of Heat in Solids. Oxford, U.K.: Clarendon Press.

Claesson, J., Eskilson, P., 1987. "Simulation Model for Thermally Interacting Heat Extraction Boreholes", Lund University, Sweden.

Claesson, J., Eskilson, P., 1987. "Conductive Heat Extraction by a Deep Borehole", Lund University, Sweden.

Deerman, J. D., Kavanaugh, S. P. 1991. "Simulation of Vertical U-Tube Ground Coupled Heat Pump Systems Using the Cylindrical Heat Source Solution". ASHRAE Transactions 97(1): 287-295.

Department of Energy. 1981. Engineers Manual, Version 2.1A, Energy and Environment Division Building Energy Simulation Group. Lawrence Berkeley Laboratory, University of California, November.

De Vries, D. A., 1974. Heat Transfer in Soils. In Heat and Mass Transfer in Biosphere. 1. Transfer Processes in Plant Environment (D. A. De Vries and N. H. Afgan Eds.). New York: John Wiley & Sons Inc., Halsted Press. Cited by Farouki (1986).

De Vries, D. A., A. J. Peck, 1958. On the Cylindrical Probe Method of Measuring Thermal Conductivity with Special Reference to Soils. Austr. Journal of Physics. Vol. 11, p. 225-271 and p. 409-423. Cited by Farouki (1986).

Dobson, M.K., O'Neal, D. L., 1992. "A Non-Dimensional Analysis of Vertical-Configuration Ground-Coupled Heat Pump Start-Up." Solar Engineering, Vol. 1, ASME.

Edwards, J. A., Vitta, P. K., 1983. "Heat Transfer from Earth-Coupled Heat Exchangers- Experimental and Analytical Results", ASHRAE Transactions, Part 1, pp. 70-80.

Eklof, C. and S. Gehlin. 1996. TED – A Mobile Equipment for Thermal Response Test. Master's Thesis 198E. Lulea University of Technology, Sweden.

EPRI. 1989. (Bose, J.E., Editor) Soil and Rock Classification for the Design of Ground-Coupled Heat Pump Systems—Field Manual. Electric Power Research Institute Special Report, EPRI CU-6600.

Eskilson, P. 1987. Thermal Analysis of Heat Extraction Boreholes. Doctoral Thesis, University of Lund, Department of Mathematical Physics. Lund, Sweden.

Farouki, O. T., 1986. Thermal Properties of Soils. Series on Rock and Soil Mechanics Vol. 11. Trans Tech Publications. Clausthal-Zellerfeld, Germany.

Gehlin, S. and B. Nordell. 1998. Thermal Response Tests of Boreholes – Results from In Situ Measurements. Paper submitted to The Geothermal Project at Richard Stockton College Conference. March 16-17.

Gilbreath, C. S. 1996. Hybrid Ground Source Heat Pump Systems for Commercial Applications. Master's Thesis. University of Alabama, Tuscaloosa, Alabama.

Grober, H. S., Grigull, U., 1961. Fundamentals of Heat Transfer, New York, McGraw-Hill.

Hackner, R. J., Hughes, P. J., O'Neil, R. A., 1987. Design of ECHP Systems in Northern Climates, ASHRAE Transactions, Vol.93.

Hackner, R. J., 1986. Earth Coupled Heat Pump Demonstration for Commercial Building Applications, Niagara Mohawk Power Corp.

Hackner, R. J., Hughes, P. J., Fleming, W. S., 1986. Materials, Design and Installation Techniques, I.E.A. ground Source Heat Pump Workshop, Albany, NY.

Hart, D. P., Couvillion, R., 1986. Earth Coupled Heat Transfer, Publication of the National Water Well Association.

Hellstrom, G. 1989. Duct Ground Heat Storage Model: Manual for Computer Code. University of Lund, Department of Mathematical Physics. Lund, Sweden.

Hellstrom, G. 1991. Ground Heat Storage. Thermal Analysis of Duct Storage Systems: Part I Theory. University of Lund, Department of Mathematical Physics. Lund, Sweden.

Hughes, P. J., 1987. Residential Ground Source Heat Pump Demonstration: Phase 3 Final Report, N.Y. State Energy Research and Development Authority.

Hughes, P.J., Hackner, R.J., 1988. Field Performance Validation of an Advanced Design Earth-Coupled Heat Pump System” U.S. Department of Energy Office of Buildings and Community Systems, ORNL/Sub/85-22035/1.

Hellstrom, G. 1989. Duct Ground Heat Storage Model. Manual for Computer Code.
University of Lund, Department of Mathematical Physics. Lund, Sweden.

Hellstrom, G. 1991. Ground Heat Storage. Thermal Analysis of Duct Storage Systems.
Part I Theory. University of Lund, Department of Mathematical Physics. Lund, Sweden.

Hellstrom, G. 1991. Bedrock Heat Store in Lulea. Numerical Simulations 1983-1988.
University of Lund, Department of Mathematical Physics. Lund, Sweden.

Hellstrom, G. 1998. Personal Communications.

IGSHPA. 1991. (Bose, J.E., Editor) Design and Installations Standards. Stillwater,
Oklahoma: International Ground Source Heat Pump Association.

Ingersoll, L.R. and H.J. Plass. 1948. Theory of the Ground Pipe Heat Source for the Heat
Pump. Heating, Piping & Air Conditioning. July. pp. 119-122.

Ingersoll, L. R., O. J. Zobel, and A. C. Ingersoll. 1954. Heat Conduction with
Engineering, Geological, and Other Applications. New York: McGraw-Hill.

Ingersoll, L. R., Plass, H. J., 1948. Theory of the Ground Pipe Heat Source for the Heat
Pump, Transactions of Amer. Soc. Of Heating and Ventilating Engineers, 47.

Incropera, F. P., DeWitt, D. P., 1980. Fundamentals of Heat Transfer, New York, John Wiley and Sons.

Jakob, M., 1956. Heat Transfer, John Wiley & Sons, New York.

Kalman, M. D., 1980. Earth Heat Exchangers for Ground Source Heat Pumps, MS Thesis, Georgia Institute of Technology.

Kavanaugh, S.P. 1985. Simulation and experimental verification of vertical ground-coupled heat pump systems. Ph.D. dissertation. Stillwater, Oklahoma: Oklahoma State University.

Kavanaugh, S. P., 1992. "Field Test of a Vertical Ground Coupled Heat Pump in Alabama", ASHRAE Transactions

Kavanaugh, S. P., Falls, R. S., Parker, J. K., 1994. "A Variable Speed Ground Source Heat Pump", ASHRAE Transactions

Kavanaugh, S. P., C. S. Gilbert. 1995. Cost Containment for Ground-Source Heat Pump Systems. Final Report to the Tennessee Valley Authority, Chattanooga. Cited by Kavanaugh (1998).

Kavanaugh, S. P., K. Rafferty. 1997. *Ground Source Heat Pumps: Design of Geothermal Systems for Commercial and Institutional Buildings*. Atlanta: .. American Society of Heating, Refrigerating and Air-Conditioning Engineers.

Kavanaugh, S. P., 1998. A Design Method for Hybrid Ground-Source Heat Pumps. ASHRAE Transactions 104(2).

Kelvin, Sir W. Thomson. 1882. *Mathematical and Physical Papers*, II, p.41,ff., cited by Ingersoll, et al. (1954).

Kersten, M. A., 1949. *Thermal Properties of Soils*. University of Minnesota Engineering Experiment Station Bulletin No. 28. Cited by Farouki (1986).

Klein, S. A., et al.. 1996. *TRNSYS Manual, a Transient Simulation Program*. Madison: Solar Engineering Laboratory. University of Wisconsin-Madison.

Komor, P. 1997. Space Cooling Demands from Office Plug Loads. ASHRAE Journal December 1997: 41-44.

Kutatelzadeh, S. S., 1963. *Fundamentals of Heat Transfer*, Academic Press, New York.

Kusuda, T., Achenbach, P. R., 1965. Earth Temperature and Thermal Diffusivity at Selected Stations in the U.S. ASHRAE Transactions Vol. 71.

Kusuda, T., 1969. Thermal Response Factor for Multi-Layer Structures of Various Heat Conduction Systems ASHRAE Semi-Annual Meeting, Chicago, Ill., Jan. 27-30.

Kuester, J. L. and J. H. Mize. 1973. Optimization Techniques with FORTRAN. McGraw-Hill Book Company.

Klein, S. A., et al. 1996. TRNSYS Manual, a Transient Simulation Program. Madison: Solar Engineering Laboratory. University of Wisconsin-Madison.

Means. 1994. Means Facilities and Repair Cost Data. Kingston Mass.: R. S. Means Co.

Means. 1997. Means Mechanical Cost Data. Kingston Mass.: R. S. Means Co.

Mei, V. C., Fisher, S. K., 1983. Vertical Concentric Tube Ground Coupled Heat Exchangers. ASHRAE Transactions, Part 2B.

Mei, V. C., Fisher, S. K., 1984. A Theoretical and Experimental Analysis of Vertical Concentric Tube Ground Coupled Heat Exchangers. Oak Ridge National Labs. / CON-153.

Mei, V. C. and C.J Emerson. 1985. New Approach for Analysis of Ground-Coil Design for Applied Heat Pump Systems. ASHRAE Transactions 91(2):1216-1224.

Mei, V. C., 1986. "Heat Pump and Ground Coil Analysis with Thermal Interference", ASME Winter Annual Meeting, WA/SOL-6.

Mei, V. C., Baxter, V. D., 1986. Performance of a Ground Coupled Heat Pump with Multiple Dissimilar U-Tube Coils in Series. ASHRAE Transactions, Part 2A.

Mei, V. C., 1991 Heat Transfer of Buried Pipe for Heat Pump Applications. Journal of Solar Energy Engineering, Feb.

Metz, P. D., Ground Coupled Heat Pump System Experimental Results. Brookhaven National Laboratory, 33540, 1983.

Metz, P. D., A simple Computer Program to Model Three Dimensional Underground Heat Flow with Realistic Boundary Conditions", ASME Transactions Vol.105, 1983.

Metz, P. D. ,Andrews, J. W. , Saunders, J. H., 1984. A Refined Computer Program for the Transient Simulation of Ground Coupled Heat Pump Systems., Brookhaven National Laboratory, 34818.

Mikhailov, M. D., Ozisik, M. N., 1991. Heat Transfer Solver. Prentice-Hall, Englewood Cliffs, NJ.

Mochlinski, K., 1964. Some Industrial Measurements of Thermal Properties of Soils. International Study Group on Soils. Lectures at meetings in Cambridge, England, July 12-26, p168-178. Cited by Farouki (1986).

Mogensen, P. 1983. Fluid to Duct Wall Heat Transfer in Duct System Heat Storages. Proceedings of the International Conference on Subsurface Heat Storage in Theory and Practice. Document D16:1983. Swedish Council for Building Research. June 6-8.

Muraya, N. K., 1995. Numerical Modeling of the transient thermal interference of vertical U-tube heat exchangers. Ph.D. Thesis, Texas A&M University, College Station, TX.

Muraya, N. K., D. L. O'Neal and W. M. Heffington 1996. Thermal Interference of Adjacent Legs in a Vertical U-Tube Heat Exchanger for a Ground-Coupled Heat Pump. ASHRAE Transactions 102(2):12-21.

Myers, G. E., Ceylan, A., 1980. Long-Time Solutions to Heat Conduction Transients with Time Dependent Inputs, Journal of Heat Transfer, Vol. 102.

Myers, G. E., 1971. Analytical Methods in Conduction Heat Transfer. McGraw-Hill, New York.

- Nelder, J. A., and R. Mead. 1965. A Simplex Method for Function Minimization. *Computer Journal* 7(1): 308-313.
- National Rural Electric Cooperative Association, Oklahoma State University, International Ground Source Heat Pump Association. 1988. Closed Loop Ground Source Heat Pump Systems Installation Guide.
- Ozisik, N. M. 1980. *Heat Conduction*. New York, John Wiley & Sons.
- Paul, N. D. 1996. The Effect of Grout Thermal Conductivity on Vertical Geothermal Heat Exchanger Design and Performance. Master of Science Thesis. South Dakota State University.
- Patankar, S. V. 1980. *Numerical Heat Transfer and Fluid Flow*. Hemisphere, New York, NY.
- Patankar, S. V. 1991. *Computation of Conduction and Duct Flow Heat Transfer*. Innovative Research Inc. Maple Grove, MN.
- Phetteplace, G. and W. Sullivan. 1998. Performance of a Hybrid GCHP System. *ASHRAE Transaction* 104(1).

Rottmayer, S. P., W. A. Beckman, and J. W. Mitchell. 1997. Simulation of a Single Vertical U-Tube Ground Heat Exchanger in an Infinite Medium. ASHRAE Transactions 103(2): 651-659.

Sauer, H. J., Howell, R. H., 1983. Heat Pump Systems, John Wiley and Sons.

Schneider, P. J., 1955. Conduction Heat Transfer, Addison-Wesley, Reading Mass.

Scott, R. F., 1964. Heat Exchange at the Ground Surface CRREL Cold Regions Science and Engineering Monograph II-A1, AD 449434. Cited by Farouki (1986).

Seem, J. E., Klein, S. A., Beckman, W. A., Mitchell, J. W., 1989. Transfer Functions for Efficient Calculation of Multidimensional Transient Heat Transfer, Journal of Heat Transfer, Vol.111.

Shannon, W. L., and W. A. Wells, 1947. Tests for Thermal Diffusivity of Granular Materials. Proceedings, American Society for Testing and Materials. 47:1044-1055. Cited by Farouki (1986).

Shonder J.A., J. V. Beck. 1999. Determining Effective Soil Formation Thermal Properties from Field Data Using Parameter Estimation Technique. ASHRAE Transactions 105(1).

Simonson, J. R., 1955. Engineering Heat Transfer, The Macmillan Press, London.

Singh, J. B., G. Foster. 1998. Advantages of Using the Hybrid Geothermal Option. The Second Stockton International Geothermal Conference. The Richard Stockton College of New Jersey. (<http://styx.geophys.stockton.edu/proceedings/hybri/singh/singh.PDF>)

Shonder J.A. 1999. Personal Communications. Oak Ridge National Laboratory, Oak Ridge, Tenn.

Smith, M. 1998. Personal Communications. International Ground Source Heat Pump Association. Stillwater, Oklahoma: Oklahoma State University. Division of Engineering Technology.

Smith, M.D., K. Belanus, R.L. Perry, W.A. Holloway. 1999a. Development of Models for Improved Thermal Property Data from Core Samples. Research Update Report for the Department of Energy. Stillwater, Oklahoma: Oklahoma State University. Division of Engineering Technology.

Smith, M.D., R.L. Perry, W.A. Holloway. 1999b. Development of a System for Verification of Transient In-Situ Testing Models and Development of a Testing Standard. Research Update Report for the Department of Energy. Stillwater, Oklahoma: Oklahoma State University. Division of Engineering Technology.

Spitler, J. D., 1995. Advanced Indoor Environmental System Class Notes MAE 5873, Spring Semester 1995, Oklahoma State University.

Spitler, J.D., C. Marshall, R. Delahoussaye, M. Manicham. 1996. Users Guide of GLHEPRO, School of Mechanical and Aerospace Engineering, Oklahoma State University, Stillwater, OK.

Spitler, J.D., S. Rees, C. Yavuzturk 1999. "More Comments on In-Situ Borehole Thermal Conductivity Testing" The Source, International Ground Source Heat Pump Association (IGSHPA) Newsletter, March/April, Stillwater, Oklahoma.

Stephenson, D. G., Mitalas, G. P., 1967. "Cooling Load Calculations by Thermal Response Factor Method", ASHRAE Transactions, Vol. 73.

Sunderland, J. E., Johnson, K. R. 1964. Shape Factors for Heat Conduction Through Bodies with Isothermal or Convective Boundary Conditions, ASHRAE Transactions 10:237-241.

Thornton, J. W., T. P. McDowell, J. A. Shonder, P. J. Hughes, D. Pahud, G. Hellstrom. 1997. Residential Vertical Geothermal Heat Pump System Models: Calibration to Data. ASHRAE Transactions 103(2): 660-674.

Thomas, L. C., 1993. Heat Transfer: Professional Version, Prentice Hall, Englewood Cliffs, NJ.

Wintercorn, H. F., 1961. Discussion on Water and its Conduction in Soils. UK Highway Research Board Bulletin 287:81-82. Cited by Farouki (1986).

Yavuzturk, C. and J. D. Spitler. 1999. A short time step response factor model for vertical ground loop heat exchangers. ASHRAE Transactions 105(2).

Yavuzturk, C., J. D. Spitler, S. J. Rees. 1999. A Transient two-dimensional Finite Volume Model for the Simulation of Vertical U-Tube Ground Heat Exchangers. ASHRAE Transactions 105(2).

APPENDIX A

Discussion of Cooling Tower Sizing Procedure

The initial size of the cooling tower is determined for each control strategy in both locations using the proprietary sizing procedure of Pioneerair Quite Module cooling towers as follows (available at <http://www.pioneerair.com/product/cool/capac.htm>).

First, a larger-than-necessary cooling tower is selected with the following procedure:

- i) Select the maximum design wet bulb temperatures for Tulsa, OK (78°F) and Houston, TX (80°F).
- ii) Set the cooling range (the difference between the entering and exiting fluid temperatures of the cooling tower) at the design conditions. This was set at 10°F for both locations.
- iii) Set the approach temperature (the difference between the exiting fluid temperature of the cooling tower and the design wet bulb temperature). This was set assuming a fluid temperature of 85°F exiting the cooling tower under design conditions.
- iv) Specify the required fluid flow rate (this was set equal to the heat transfer fluid flow rate in the ground heat exchanger loop).
- v) Choose a “cooling tower selection factor” from a table produced by the cooling tower manufacturer based on the design wet bulb temperature, the approach temperature and the cooling range.

- vi) Look up the cooling tower model/capacity in terms of volumetric flow rate, and the “cooling tower selection factor”. Each cooling tower model also has a set airflow rate.
- vii) The volumetric flow rate of the air through the cooling tower is one of the input parameters to the TRNSYS cooling tower component model. The hourly simulations of the hybrid ground source heat pump system assume a counter-flow, single cell cooling tower with a fixed volumetric flow rate. The sump temperature of the cooling tower is stipulated to be equal to the ambient air wet bulb temperature. The amount of heat rejection through a cell of the cooling tower is determined with

$$q_{\text{cell}} = \varepsilon_a \dot{m}_a (h_{w,i} - h_{a,i}) \quad (\text{A-1})$$

with ε_a = air-side heat transfer effectiveness defined as

$$\varepsilon_a = \frac{1 - e^{-NTU(1-m^*)}}{1 - m^* e^{-NTU(1-m^*)}} \quad (\text{A-2})$$

$$NTU = c \left[\frac{\dot{m}_w}{\dot{m}_a} \right]^{1+n} \quad (\text{A-3})$$

where

$h_{w,i}$ = enthalpy of the entering fluid temperature to the cooling tower

$h_{a,i}$ = enthalpy of the entering air temperature to the cooling tower

\dot{m}_a = mass flow rate of the air drawn through the cooling tower

\dot{m}_w = mass flow rate of the cooling water through the cooling tower

$$\dot{m}^* = \frac{\dot{m}_a C_s}{\dot{m}_{w,i} C_{pw}}$$

C_{pw} = constant water specific heat

C_s = saturation specific heat (the average slope of the saturation enthalpy with respect to the temperature curve).

n, c = mass transfer correlation coefficients.

Then, for each control strategy in both locations, the system was simulated with the large cooling tower, sized as described above. The cooling tower heat rejection rate that coincided with the peak entering fluid temperature to the heat pump for a 20-year simulation period was used to size the cooling tower as follows:

- i) Select the maximum design wet bulb temperatures for Tulsa, OK (78°F) and Houston, TX (80°F). Note that this inherently oversizes the cooling tower because the maximum design wet bulb temperature is not likely to coincide with the peak entering fluid temperature.

- ii) Set the cooling range (the difference between the entering and exiting fluid temperatures of the cooling tower) at the design conditions. This was set at 10°F for both locations.
- iii) Set the approach temperature (the difference between the exiting fluid temperature of the cooling tower and the design wet bulb temperature). This was set assuming a fluid temperature of 85°F exiting the cooling tower under design conditions.
- iv) Adjust the required fluid flow rate based on the required cooling tower capacity:

$$\dot{m}_{\text{Water}} = \frac{\dot{q}}{c_p \Delta T_{\text{Cooling Range}}} \quad (\text{A-5})$$

- v) Choose a “cooling tower selection factor” from a table produced by the cooling tower manufacturer based on the design wet bulb temperature, the approach temperature and the cooling range.
- vi) Calculate a new cooling tower capacity by linearly interpolating the air volumetric flow rate and the “cooling tower selection factor”. This yields a new air volumetric flow rate through the cooling tower that is based on the maximum heat rejection at the time interval where the maximum EFT occurs.

The hourly simulations are then re-run on TRNSYS with the new volumetric flow rate of air drawn through the cooling tower to determine system-operating cost.

Estimates of first cost are based on actual size with $(\frac{\$350}{\text{ton}} \times \frac{\dot{q}}{12000 \text{ BTU/hr}})$.

As noted above, the cooling tower is somewhat oversized due to the design procedure. This is especially noticeable for case 4c, where the peak EFT to the heat pump only reaches 80.5 °F (26.9 °C). As a future research topic, it would be interesting to develop a design procedure which optimally sizes the cooling tower for this control strategy.

VITA

Cenk Yavuzturk

Candidate for the Degree of

Doctor of Philosophy

Thesis: MODELING OF VERTICAL GROUND LOOP HEAT EXCHANGERS FOR GROUND SOURCE HEAT PUMP SYSTEMS.

Major Field: Mechanical and Aerospace Engineering.

Biographical:

Education: Received the degree of Diplom-Ingenieur in Energy and Processing Engineering from the Technical University of Berlin, Germany in November 1988. Completed the requirements for the Doctor of Philosophy degree with a major in Mechanical and Aerospace Engineering at Oklahoma State University in December 1999.

Experience: Worked for Aydin ElectroFab in Croydon, PA from 1989 to 1991 as a process engineer. Worked for Aydin Corporation from 1991 to 1994 as HVAC project engineer. Employed by the Oklahoma State University from 1995-1999 as teaching assistant and research associate. Currently assistant professor at the University of Wyoming.

Professional memberships: American Society of Heating, Ventilating and Air-Conditioning Engineers (ASHRAE), International Ground Source Heat Pump Association (IGSHPA), The Association of Energy Engineers.